

Fabrication and Characterization of Nanometer Thin Films for Low-Voltage DEAs

Inauguraldissertation

zur

Erlangung der Würde eines Doktors der Philosophie

vorgelegt der

Philosophisch-Naturwissenschaftlichen Fakultät
der Universität Basel

von

Florian Micha Weiss

aus Sulz bei Laufenburg, Schweiz

Basel, 2016

Originaldokument gespeichert auf dem Dokumentenserver der Universität Basel
edoc.unibas.ch

Genehmigt von der Philosophisch-Naturwissenschaftlichen Fakultät auf Antrag von:

Prof. Dr. Bert Müller, Fakultätsverantwortlicher
Prof. Dr. Anne Ladegaard Skov, Koreferentin

Basel, den 23. Februar 2016

Prof. Dr. Jörg Schibler, Dekan

Contents

Summary	v
Zusammenfassung	ix
List of Publications	xiii
1 Introduction	1
1.1 Dielectric elastomer actuators	2
1.2 Compliant metal electrodes	3
1.3 Elastomer deposition	3
1.3.1 Electro-spray deposition	3
1.3.2 Molecular beam deposition	5
2 Results	7
2.1 Impact of electrode preparation on the bending of asymmetric planar electro-active polymer microstructures	7
2.2 Electro-spraying nanometer-thin elastomer films for low-voltage dielectric actuators	17
2.3 Thin film formation and morphology of electro-sprayed polydimethylsiloxane	33
2.4 Molecular beam deposition of high-permittivity polydimethylsiloxane for nanometer-thin elastomer films in dielectric actuators	42
3 Conclusions and Outlook	53
Bibliography	54
Acknowledgments	57
Curriculum Vitae	59

Summary

Nanometer-thin films are the essential components of a low-voltage dielectric elastomer actuator (DEA). Comprising of two electrodes sandwiching a dielectric elastomeric material DEAs have evoked versatile materials research. Before choosing the materials used to manufacture low-voltage DEAs one should carefully consider the targeted application. This project aims at finding new techniques to realize nanometer-thin films to obtain low-voltage DEAs with possible future application as artificial muscle to treat urinary incontinence. Therefore, the materials used should be highly biocompatible. Two promising materials are gold and polydimethylsiloxane (PDMS) both show high biocompatibility due to their inherent chemical inertness. Additionally, their physical properties exhibit most of the desired qualities such as for example high electric conductivity for gold and high elasticity for the PDMS.

To deposit metal electrodes with nanometer scale thickness, the most frequently used techniques are radio frequency (RF) magnetron sputtering, thermal- or electron beam evaporation, chemical vapor deposition (CVD) methods and electrochemical deposition. Deposition from the liquid/dissolved state by applying a potential between the conducting substrate and a counter electrode, as done in electrochemical techniques, is not applicable for DEA production since the metal has to be deposited on the dielectric elastomer. Regarding the listed deposition methods from the gaseous phase only the physical vapor deposition (PVD) was considered with focus on thermal evaporation and RF magnetron sputtering. The electromechanical properties of simple one layer DEAs with either sputtered or evaporated gold electrodes were investigated taking advantage of the bending of asymmetric planar DEA structures on a flexible substrate. The bending of these cantilever-like structures is induced by applying a voltage. It was found that the actuation at the same voltage was up to 39 % higher for the RF magnetron sputtered actuator compared to the thermally evaporated one. This finding will have a big impact on the stiffness of future multi-stack actuators (cp. Section 2.1).

Considering the fabrication of elastomeric nanometer-thin films two methods were established and proven to lead to obtain the targeted nanometer scale in film thickness. Both methods, electro-spray deposition (ESD) and organic molecular beam deposition (OMBD), have advantages and disadvantages regarding the applicable materials, deposition rates, costs and up scaling. In the following sections each method and the corresponding findings will be discussed in more detail.

The in house built electro-spray deposition system, which can be coupled to a spectroscopic ellipsometer (SE) to acquire inter alia real time data of film growth, was evaluated as a possible method for the creation of nanometer-thin elastomeric PDMS films. Therefore, the appropriate deposition mode, solvent and pre-polymer had to be identified. Since the aim was to fabricate multi-stack actuators it had to be considered that the conducting substrate needed for direct current (dc) experiments could not be assured throughout the whole manufacturing process. Therefore, it

was decided on using the alternating current mode (ac). This mode, according to literature, prevents surface charge accumulation on non-conducting substrate due to neutralization by incoming opposite charged species. As a solvent ethyl acetate was chosen since it dissolves PDMS pre-polymer chains and it is not poisonous to humans. Considering the pre-polymer the commonly used two components PDMS Elastosil 745 A/B was first applied. After deposition and subsequent heat treatment for curing the Elastosil was still a viscous liquid. This finding was attributed to the reduction/oxidation of the Pt catalyst by the applied electric field of ± 5 kV (18 Hz). At this point it was decided to use vinyl-terminated PDMS which has been approved to work with UV curing in OMBD. Having determined the fundamentals to obtain a stable electro-spray and a curing process to manufacture PDMS films, investigations on deposition parameters towards optimization of the resulting films were conducted. First of all the influence of the deposition rate on the resulting film morphology was studied applying in-situ SE, atomic force microscopy (AFM) and interferometry. The results revealed that the surface roughness of the deposited films increases with increasing deposition rate but smoothed to values in the same range by UV irradiation for all deposition rates. The obtained surface roughnesses vary between 0.20 and 0.28 nm determined by atomic force microscopy on areas of $25 \mu\text{m}^2$ and between 2 and 20 nm on an area of 0.72 mm^2 as obtained by interferometry for deposition rates between 0.02 to 5.54 nm/s. With thicknesses in the scale of a few hundreds of nanometer to micrometer these films qualify for use in DEA manufacturing (cp. Section 2.2).

In a further study of the electro-spray deposition the focus was put on the film growth mechanism of the deposited droplets/islands. This investigation was based on quasi-dynamic observations of the deposited and subsequently cured PDMS islands. Techniques used to evaluate the film growth ranged from AFM images to select appropriate pre-polymer molecular weight, optical micrograph segmentation to spectroscopic ellipsometry. The most convenient pre-polymer molecular weight, from the four investigated in this study, turned out to be 6,000 g/mol. Furthermore, studies of the deposited and cured islands of this pre-polymer revealed an average height of 30 nm. During the early stages of deposition a 3D growth is observed which eventually, with increasing deposition time, turns into a 2D growth. With a flow rate of 267 nL/s and an average deposition time of 155 s a confluent layer with a thickness of about 91 nm, which still exhibits a rough surface, can be obtained. Prolonging the deposition time will smoothen the surface to a scale of a few nanometers (cp. Section 2.3).

OMBD deposition, possible after assembling a small ultra-high vacuum (UHV) chamber, was applied to get a proof of concept for thermal evaporation, deposition and UV curing of PDMS pre-polymer chains. In a later stage a more elaborate UHV chamber was assembled with e.g. a mounted SE to conduct sophisticated investigations. Based on the structure of a standard (DMS-V05) pre-polymer, approved for thermal evaporation, a new pre-polymer was synthesized. The new poly((chloropropyl)methylsiloxane-co-dimethylsiloxane) copolymer showed higher dielectric permittivity and higher break down strength in liquid state. Therefore, a comparison study of film growth with in-situ curing as well as their resulting films after post deposition cure was conducted. The results suggest the use of the new copolymer for low-voltage DEA application since it has enhanced dielectric and elastic properties. Due to the inherent higher polarity a different growth mode during

the early deposition stages could be detected by real time SE. The resulting films showed an increased surface roughness by a factor of two but still in the subnanometer scale for an area of $5\ \mu\text{m} \times 5\ \mu\text{m}$ as determined by AFM (cp. Section 2.4). These results show that a major step towards low-voltage DEA has been accomplished with this work.

Zusammenfassung

Nanometer-dünne Filme sind essenzielle Komponenten von dielektrischen Elastomer-Aktuatoren (DEA) die mit tiefen Spannungen betrieben werden. Bestehend aus zwei Elektroden, welche ein elastisches Material einklemmen, hat diese Technologie zu breiter Materialforschung angetrieben. Bevor man aber das Material wählt um einen solche Aktuator herzustellen, sollte man sich bewusst sein für welche Applikation dieser eingesetzt wird. In diesem Projekt war es das Ziel neue Methoden zu finden um nanometer-dünne Schichten zu realisieren welche für den Einsatz oben genannter Aktuatoren geeignet sind. Solche Dünnschicht-Aktuatoren könnten in der Zukunft zum Beispiel, als künstliche Sphinktermuskeln zur Behandlung von Harninkontinenz verwendet werden. Deswegen ist es wichtig biokompatible Materialien zu verarbeiten. Gold und Polydimethylsiloxan (PDMS) sind zwei Materialien die sich gut dafür eignen würden da sie beide chemisch inert sind. Zusätzlich zeigen auch beide gewünschte Eigenschaften auf wie z.B. hohe elektrische Leitfähigkeit oder hohe Elastizität.

Die gängigsten Methoden nanometer-dicke metallische Elektroden herzustellen sind Magnetron sputtern, thermisches verdampfen, Elektrodenstrahl Verdampfung, chemische Gasphasen Abscheidung oder elektrochemische Methoden. Deposition aus der flüssigen oder gelösten Phase mittels angelegtem potential zwischen dem leitenden Substrat und einer Gegenelektrode, wie es bei den elektrochemischen Verfahren der Fall ist, kann wegen des nicht leitenden Substrates nicht angewendet werden. Hier werden nur die thermische Verdampfung und der Sputterprozess näher betrachtet und verglichen. Die erhaltenen Resultate von elektromechanischen Messungen von Aktuatoren mit gesputterten und thermisch aufgedampften Elektroden zeigen einen Unterschied von bis zu 39 % in der Auslenkung. Das heisst die gesputterten Elektroden haben einen geringeren Effekt auf die Versteifung des Aktuators, was eine wichtige Erkenntnis ist, wenn man mehrere tausend nanometer-dünne Aktuatoren aufeinander stapeln muss um gewünschte Leistungen zu erhalten (siehe Kapitel 2.1). Für die Herstellung von elastischen nanometer-dünnen Filmen wurden im Rahmen dieser Arbeit zwei neue Methoden entwickelt. Beide Methoden, Elektrospray Deposition (ESD) und organische Molekularstrahldeposition (OMBD), führen zu diesen Dünnschichten. Bezüglich benutzbaren Materialien, Depositionsraten, Kosten und Hochskalierung für Industrielle Zwecke haben beide Methoden Vorteile wie auch Nachteile. In den folgenden Abschnitten werden diese detaillierter diskutiert.

Das selbst gebaute Elektrospray System, welches mit einem spektroskopischen Ellipsometer gekoppelt werden kann, wurde als mögliche Methode um elastische Dünnschichten im Nanometermassstab herzustellen geprüft. Zuerst mussten dafür die entsprechenden Parameter wie Depositionsmodus, Lösungsmittel und Polymer identifiziert werden. Mit dem Ziel mehrlagige Aktuatoren herzustellen, ist es nicht möglich im Gleichstrommodus zu arbeiten, da nicht über den ganzen Prozessverlauf ein leitendes Substrat gewährleistet werden kann. Deswegen musste man auf den Wechselstrommodus ausweichen. Im Wechselstrommodus ist es den auftreffenden Partikeln

möglich sich gegenseitig zu neutralisieren da sie abwechselnd mit positiver oder negativer Ladung aufgeladen werden. Als Lösungsmittel wurde Ethylacetat gewählt, weil es im Gegensatz zu anderen Lösungsmitteln, die PDMS lösen können, für Menschen am ungefährlichsten ist. Oft wird zur Herstellung der Silikonfilme für die Aktuatoren ein Zweikomponenten System verwendet. Ein solches Zweikomponenten Silikon System (Elastosil 745 A/B) wurde anfänglich auch hier getestet. Diese Systeme werden meistens durch Wärmeeinwirkung mittels Metallkatalysator vernetzt. Jedoch wurde durch die Einwirkung des elektrischen Wechselfeldes von ± 5 kV (18 Hz) der Katalysator reduziert bzw. oxidiert und somit unbrauchbar gemacht. Deswegen wurde auf ein bewährtes Polymer zurückgegriffen welches für die organische Molekularstrahldeposition schon verwendet wurde. Hierbei handelt es sich um ein kurzkettiges, Vinyl-terminiertes PDMS Polymer welches mit UV-Strahlung vernetzt werden kann. Nachdem die grundsätzlichen Parameter identifiziert wurden, konnte man weitere Untersuchungen durchführen wie z.B. den Einfluss der Durchflussrate von der fünfprozentigen Polymerlösung auf die Oberflächenmorphologie der entstehenden Filme. Durch die Möglichkeit spektroskopische Messungen während des Depositionsprozesses zu machen, konnte man zum einen die Depositionsraten und zum andern die Oberflächenbeschaffenheit des noch flüssigen Filmes bestimmen. Es hat sich gezeigt, dass mit zunehmender Depositionsrate auch die Oberflächenrauigkeit des Films zunimmt. Wird der Film danach der UV-Strahlung ausgesetzt nimmt die Rauigkeit wieder ab und konvergiert zu ähnlichen Werten. Mittels atomarer Kraftmikroskopie (AFM) wurden Werte zwischen 0.20 und 0.28 nm für eine Fläche von $25 \mu\text{m}^2$ für alle Depositionsraten ermittelt. Für eine grössere Fläche von 0.72mm^2 liegen die Rauigkeitswerte zwischen 2 und 20 nm welche mit einem Interferometer ermittelt wurden. Die benutzten Depositionsraten lagen zwischen 0.02 und 5.54 nm/s. Diese Filme, deren Dicke mehrere hundert Nanometer beträgt, sind geeignet für die Herstellung der Dünnschicht Aktuatoren (siehe Kapitel 2.2).

In einer folge Studie wurde der Fokus zum einen auf die Morphologie der entstanden einzelnen Inseln und zum andern auf den Wachstum des Films gerichtet. Dazu wurden erst Proben von einzelnen Inseln mit zunehmender Kettenlänge hergestellt und mit AFM untersucht und analysiert um eine geeignete Grösse des Ausgangspolymers zu bestimmen. Wie sich heraus stellte, ist dies das Polymer mit einem Molekulargewicht von 6000 g/mol. Für die Untersuchung des Filmwachstums wurde dann nur die fünfprozentige Lösung mit diesem Polymer verwendet. Die bestimmte Durchschnittshöhe der Inseln beträgt 30 nm. Ausserdem konnte man in den Anfangsstadien der Deposition ein 3D Wachstum feststellen, welches mit zunehmender Depositionszeit allmählich in ein 2D Wachstum überging. Mit einer Durchflussrate von 267 nL/s kann man nach einer Depositionszeit von 155 s einen schliessenden Film mit erhöhter Rauigkeit erwarten. Mit fortschreitender Depositionszeit nimmt die Oberflächenrauigkeit zunehmend ab (siehe Kapitel 2.3).

Für die OMBD wurde erst eine kleine Ultrahochvakuum (UHV) Kammer aufgebaut um das Konzept der thermischen Verdampfung von PDMS polymeren zu überprüfen. Nach ersten erfolgreichen Experimenten wurde eine grössere und komplexere UHV Anlage zusammengestellt, mit welcher auch in-situ spektroskopische Ellipsometrie während des Wachstums möglich wurde. Um noch ein Schritt weiter zu gehen wurde ein neues kurzkettiges Polymer (Poly((chloropropyl)methyl-co-dimethylsiloxan)) synthetisiert, welches eine ähnliche Struktur wie unser Standard DMS-V05 Polymer hat. Der einzige Unterschied liegt darin, dass das neue Polymer einige polare Sei-

tengruppen enthält. Die schon bekannte Synthese des neu verwendeten Polymers wurde so optimiert, dass die Kettenlänge in etwa der entspricht, von dem bereits verdampften Polymer DMS-V05. Durch die erhöhte Polarität hat das neue Polymer eine grössere dielektrische Konstante und Durchschlagsspannung. Des weiteren kann anfangs der Deposition des synthetisierten Polymers ein 3D Wachstum beobachtet werden. Dieser geht aber mit fortschreitender Zeit in ein 2D Wachstum über. Das Standardpolymer hingegen zeigt von Anfang an ein 2D Wachstum. Obwohl die Rauigkeit des synthetisierten Polymers etwa um einen Faktor zwei grösser ist, liegt sie trotzdem für beide Filme im Sub-Nanometer Bereich. Mit den verbesserten Eigenschaften zeigt das neu verwendete Material eine Gütezahl die 4.6 mal grösser ist als die des Standards (siehe Kapitel 2.4). Aufgrund dieser Resultate wurde ein grosser Fortschritt für die Herstellung von Dünnschichtaktuatoren erzielt.

List of Publications

- F. Weiss**, T. Töpfer, B. Osmani, H. Deyhle, G. Kovacs, B. Müller, “Thin film formation and morphology of electro-sprayed polydimethylsiloxane.” (2016) submitted.
- F. Weiss**, T. Töpfer, B. Osmani, S. Peters, G. Kovacs, B. Müller, “Electro-spraying nanometer-thin elastomer films for low-voltage dielectric actuators.” *Advanced Electronic Materials* (2016) accepted.
- B. Osmani, T. Töpfer, **F. Weiss**, F. Wohlfender, V. Leung, C. Bippes, B. Müller, “Nanomechanical characterization of polydimethylsiloxane films.” *European Cells and Materials* **30** Supplement 1, 56 (2015)
- T. Töpfer, B. Osmani, **F. Weiss**, B. Müller, “Viscoelastic properties of Polydimethylsiloxane studied by cantilever bending.” *European Cells and Materials* **30** Supplement 1, 68 (2015).
- T. Töpfer, **F. Weiss**, B. Osmani, C. Bippes, V. Leung, B. Müller, “Siloxane-based thin films for biomimetic low-voltage dielectric actuators.” *Sensors and Actuators A* **233** 32-41 (2015). (doi:10.1016/j.sna.2015.06.014)
- T. Töpfer, B. Osmani, **F. Weiss**, C. Winterhalter, F. Wohlfender, V. Leung, B. Müller, “Strain-dependent characterization of electrode and polymer network of electrically activated polymer actuators.” *Proceedings of SPIE* **9430** 94300B (2015). (doi:10.1117/12.2084595)
- B. Osmani, T. Töpfer, C. Deschenaux, J. Nohava, **F. Weiss**, V. Leung, B. Müller, “Micro- and nanostructured electro-active polymer actuators as smart muscles for incontinence treatment.” *AIP Conference Proceedings* **1646** 91-100 (2015). (doi:10.1063/1.4908588)
- F. Weiss**, T. Töpfer, B. Osmani, C. Winterhalter, B. Müller, “Impact of electrode preparation on the bending of asymmetric planar electro-active polymer microstructures.” *Proceedings of SPIE* **9056** 905607 (2014). (doi:10.1117/12.2045152)
- F. M. Weiss**, X. Zhao, P. Thalmann, H. Deyhle, P. Urwyler, G. Kovacs, B. Müller, “Measuring the bending of asymmetric planar EAP structure.” *Proceedings of SPIE* **8687** 86871X (2013). (doi:10.1117/12.2009355)
- F. Weiss**, H. Deyhle, G. Kovacs, B. Müller, “Designing micro- and nanostructures for artificial urinary sphincters.” *Proceedings of SPIE* **8340** 83400A1 (2012). (doi: 10.1117/12.914649)

Publications not directly related to the present thesis

F. Weiss, F. Schmidli, M. Jungo, B. Müller, “Incompatibility of dental alloys: Evaluation by ec-pen corrosion measurements.” *European Cells and Materials* **30** Supplement 1, 70 (2015).

T.M.T. Huynh, **F. Weiss**, N.T.M. Hai, W. Reckien, T. Bredow, A. Fluegel, M. Arnold, D. Mayer, H. Keller, P. Broekmann, “On the role of halides and thiols in additive-assisted copper electroplating.” *Electrochimica Acta* **89** 537-548 (2013). (doi:10.1016/j.electacta.2012.10.152)

N.T.M. Hai, J. Furrer, F. Stricker, T.M.T. Huynh, I. Gjuroski, N. Luedi, T. Brunner, **F. Weiss**, A. Fluegel, M. Arnold, I. Chang, D. Mayer, P. Broekmann, “Polyvinylpyrrolidones (PVPs): Switchable Leveler Additives for Damascene Applications.” *Journal of the Electrochemical Society* **160** D3116–D3125 (2013). (doi:10.1149/2.019312jes)

1 Introduction

Prevalence rates for urinary incontinence (UI) are higher in women than in men and range between 4.5 to 53 % and 1.6 to 24 %, respectively.¹ The number of patients suffering from UI increases with age. The actual number of people suffering from incontinence is said to be even larger since it is often unuttered. Furthermore, it is likely to increase in future due to demographic changes especially in the western world. The inability to properly hold back the urinary flow influences the quality of life because it limits sportive activities and can even lead to social isolation. Hitherto, there are various approaches to treat incontinence both non-invasive and invasive. For patient suffering from a moderate urinary incontinence non-invasive treatment such as nervous stimulation or specific exercise of the pelvic floor muscles can be sufficient. Also medication or insertion of absorbing materials (especially for women) is applied. In severe cases on the other hand, operative actions can be taken. Depending on the severity different approaches are chosen. For stress urinary incontinence (SUI), e.g. induced by coughing or Valsalva maneuver, sling procedures are often the method of choice.^{2,3} Sling procedures describe the incorporation of a synthetic or natural sling that supports/pulls up the urethra or the bladder neck in order to avoid leakage by stress induced pressure increase. In case the patient is suffering from severe incontinence not only induced by stress, artificial sphincter implants can be inserted. The most known is the AMS 800™ (American Medical Systems, Minnetonka, Minnesota, USA). This is a mechanically driven implant that connects a fluid filled reservoir with a cuff placed around the urethra. To close the urethra the fluid is pumped from the reservoir through a valve into the cuff. This squeezes the urethra and restores continence. Pressing the valve causes the liquid to flow back to the reservoir and thus, opens up the urethra for urine release. The downside of this implant is its high revision rate. Up to 50 % have to be removed within the first five years due to atrophy, tissue erosion or lacking perfusion.⁴

Alternatively, smart designs and technologies with much improved properties should be used in future to substitute such implants. Electroactive polymer (EAP) technology, which can be divided into two main groups, seems to be a promising approach. One group consists of the ionic EAPs which are operated at low driving voltages (1 - 2 V).⁵ Since they depend on the diffusion of ions they have rather long response times (seconds). Additionally they need electrolytes to operate which complicates their application in sensitive environments such as in human tissue. The second group are the dielectric EAP actuators, which exhibit millisecond response time.⁶ They are usually driven at voltages above several 100 V.⁵ As the artificial muscles need reasonable power, the necessary currents cannot be neglected. The application of such currents in combination with the high voltages is incompatible with physiological surroundings. Consequently, the dielectric EAPs have to be modified to low-voltage DEA for medical applications.

1.1 Dielectric elastomer actuators

Actuators based on the EAP technology, also called dielectric elastomer actuators (DEAs), have the same set up as a capacitor. They consist of two electrodes sandwiching a dielectric material, but differ in the sandwiched materials used. It is essential for DEAs to have an elastic dielectric material in order to allow for contraction and relaxation back to its original state. Applying a voltage, loading the electrodes with opposite charges, a contraction is induced. The contraction is due to the so called Maxwell pressure p_{el} . This is a physical quantity describing the amount of force acting on a defined area of a DEA related to a certain applied driving voltage U (cp. formula (1.1)).

$$p_{el} = \epsilon_0 \epsilon_r \left(\frac{U}{d} \right)^2 = \epsilon_0 \epsilon_r E^2 \quad (1.1)$$

Furthermore, formula (1.1) relates the Maxwell pressure to the relative dielectric constant ϵ_r and the layer thickness d of the elastomeric material. The vacuum permittivity is represented by ϵ_0 . The applied voltage divided by the elastomeric layer thickness can also be written as the electric field E between the two electrodes. Dividing the Maxwell pressure by the Young's modulus Y the maximal possible strain in z direction for a specific material and applied voltage can be obtained using formula (1.2)

$$s_z = \frac{p_{el}}{Y} = \frac{\epsilon_0 \epsilon_r E^2}{Y} \quad (1.2)$$

The elastomeric material is assumed to be incompressible meaning its volume must remain constant. Hence, the compression in z direction has to be compensated by an expansion in x - and y - direction. This is the origin of one of the limiting factors in DEA technology. If the surface area enlarges in x - and y - direction, the electrode has to be compliant in order to guarantee proper function. Researchers came up with different approaches to solve this problem which will be further discussed at a later stage in this introduction.

To approach low-voltage DEAs formulas (1.1) and (1.2) should be reconsidered. One of the keys towards low-voltage application is to tune the elastomeric material properties. According to formula (1.1) increasing the permittivity and according to formula (1.2) decreasing the Young's modulus will enhance the performance. These terms both linearly depend on the resulting Maxwell pressure. The second and more effective approach, due to its quadratic dependence on the Maxwell pressure (cp. formula (1.1)), is to decrease the thickness of the dielectric elastomer. Inherently by decreasing the layer thickness the maximal possible contraction in z direction and the force decreases thus, multi-stack DEAs have to be built to obtain strains comparable to e.g. few tens of micrometer thick elastomeric layers in DEAs

In this work, both aspects are addressed to make a step further towards low-voltage actuators for medical applications such as artificial muscles to treat incontinence. The materials of choice in this work are: polydimethylsiloxane (PDMS), an elastomer well-established in EAP technology as well as in medical applications and gold which is known for the high electric conductivity and its chemical inertness.

1.2 Compliant metal electrodes

As pointed out above it is essential to have compliant electrodes in order to maintain functionality of DEA structures. Materials from metal to graphite, composites,⁷ graphene,⁸ and conducting polymers⁹ have been investigated and evaluated. In this work the focus is put on metal electrodes since they still have the highest conductivities and are therefore capable to charge the whole surface area in an appropriate time scale. This allows for fastest response times as desired for artificial sphincter implants. Nevertheless it should be considered that metals itself only allow for strains between 1 and 2 %¹⁰ and have a great impact on the stiffening especially of nanometer thin multi-stack DEAs.

The three most common methods to create metal electrodes for DEAs are magnetron sputtering, thermal evaporation and ion implantation. In contrast to the first two techniques, ion implantation does not lead to confluent metal films, but rather to PDMS/metal composites and is thus not further discussed.

It has been observed that thermal evaporation as well as magnetron sputtering induce surface corrugation on PDMS films. This effect occurs due to the heat energy transferred from the metal source and/or from the atoms to the surface of the PDMS film.¹¹ The heated PDMS reacts with thermal expansion during the deposition and enlarges its surface area, which is simultaneously covered by metal. After deposition the PDMS starts to shrink back towards its original state but the deposited stiffer metal film hinders a full recovery. The compromise of these events is the wrinkle formation where the interface eventually reaches an equilibrium state. Unfortunately the corrugation does not show an anisotropic behavior thus the wrinkles are not aligned but are rather randomly distributed. A parallel alignment of the wrinkles would increase the compliance of the electrode in direction of the wrinkle wavelength. Approaches applying a unidirectional pre-strain during deposition have been shown to yield aligned wrinkle formation.¹²

Taking an even closer look at the metallic film formation, it is known that the morphology of thermally evaporated and magnetron sputtered films differs.¹³ Hence, the influence of the preparation method on the actuation was investigated within this work. To this end asymmetric bending bar measurements were conducted and atomic force microscopy images of the surfaces were taken.

1.3 Elastomer deposition

After treating some aspects of compliant metal electrodes the focus is put on the elastomeric material sandwiched between the electrodes. Hitherto, there has not been much effort to improve techniques to manufacture thin films especially in the nanometer scale. In the following sections two methods are introduced which will potentially bring the nanometer-thin film production of PDMS to the laboratories.

1.3.1 Electro-spray deposition

This technique has been shown to be very effective for homogeneous nanoscale film or particle formation especially for inorganic materials¹⁴ or polymers.^{15,16} There are two main modes electro-sprays can be operated. The much more common direct current

(dc) electro-spray is well established, whereas the second mode, the alternating current (ac), is much less explored.

Here the well described mechanism of dc electro-spray will be roughly introduced. A solution with a very low concentration of the deposit is introduced to a nozzle with an inner radius in the sub-millimeter range. The nozzle itself is attached to a voltage source whereas the substrate, which is conducting, is usually grounded. If a voltage is applied to the nozzle a directed electric field is generated. The charges applied to the nozzle will ionize the solvent or the ions/molecules dissolved. Charged species move along the directed electric field and concentrate at the meniscus of the nozzle. This meniscus at the nozzle tip will form a characteristic Taylor cone if there is a critical pressure on the solvent towards the nozzle tip (induced by gravity or syringe pump) and a critical applied electric field. The charged particles at the meniscus tip eventually accumulate to a critical number and will be repelled from the tip as a single drop. The drop, consisting of mainly solvent, will decrease its volume due to evaporation of the solvent until the volume to charge ratio reaches a critical value where the drop will explode into smaller droplets with a homogeneous size distribution. This event is called a coulomb explosion.¹⁷ This process will be repeated for several times and thus, the droplets impinging onto the substrate can be as small as a few tens of nanometer and are in a narrow size distribution resulting in homogeneous nanoscale films or nano-particles.

The electro-spray deposition is sensitive to set-up parameters like the nozzle substrate distance (electric field) and the flow rate, but also to the physical properties of the solution such as the electrical conductivity, surface tension, vapor pressure and viscosity.¹⁸

As mentioned above, the dc mode depends on a conductive substrate which is grounded in order to dissipate the charges arriving. If this is not the case the charges accumulate on the surface and will eventually repel the incoming particles with the same charge. If the substrate is not conducting the ac mode, which has an analog set up to dc ESD, is applied. This is more convenient since the incoming particles are of opposite charge and therefore neutralize each other. With alternating charging an additional parameter, the frequency, can be altered but also induces instability to the system. The instability arises from the temporal opposite charging of the solution at the nozzle tip. By accumulating, for example, negative charge at the meniscus at the nozzle tip and then switching to positive charge, the negative charged species will instantaneously be retracted from the meniscus, which can cause a jet break up. This process shows great dependence on the frequency applied.

To manufacture nanometer thin elastomeric films for multi-stack DEAs by ESD, the ac mode is most appropriate since only the first electrode may be grounded but not the following. This is because only the first electrode which may be deposited onto a conducting substrate is still grounded. Subsequent electrodes will not be grounded because of the dielectric elastomeric layers in-between. In this work first evaluations and investigations on nanometer-thin PDMS films deposited by ac ESD were conducted using optical- and atomic force microscopy as well as spectroscopic ellipsometry (SE).

1.3.2 Molecular beam deposition

Molecular beam deposition (MBD) emerged from semiconductor research¹⁹ and is a physical deposition from the gas phase, well-known for its well-defined and controllable growth. Depositions are conducted in ultra-high vacuum (UHV) conditions ($\leq 10^{-8}$ mbar) where the deposited material is evaporated from e.g. effusion cells. Bringing the deposit in gas phase in this manner the atoms/molecules are directed towards the substrate in such a way that there is no interaction between each other nor with other molecules of the surrounding atmosphere until they reach the substrate. Hence, their mean free path, defined as the average distance atoms or molecules travel before interacting with another species, is in the km range.²⁰ This is the major key to have highest control of the deposition process. Therefore, to obtain nanometer thin films with high homogeneity MBD is often the method of choice.

In the last decades it has been shown that also organic molecules can be deposited using this technique.²¹ Nevertheless, there are limitations for organic MBD (OMBD) since the molecules mostly do not have high thermal stability and decompose before brought in the gaseous phase.²²

In literature it has been shown that it is possible to deposit short PDMS polymers to fabricate DEAs by OMBD and subsequent UV irradiation of the deposit.²³ Based on this finding an improved PDMS polymer, exhibiting increased dielectric constant, dielectric breakdown and lower Young's modulus, has been synthesized and characterized. Additionally its deposition and subsequent curing has been investigated applying AFM and SE. The obtained results of this investigation show that there still is potential to optimize materials and methods for further steps towards low-voltage DEAs for e.g. medical applications.

2 Results

2.1 Impact of electrode preparation on the bending of asymmetric planar electro-active polymer microstructures

Comparing measurements of EAP structures under actuation with gold electrodes prepared by thermal evaporation and radio frequency magnetron sputtering reveal better actuation for the ones prepared by sputtering.

Published in Proceedings of SPIE

Impact of electrode preparation on the bending of asymmetric planar electro-active polymer microstructures

Florian M. Weiss^{*a,b}, Tino Töpfer^a, Bekim Osmani^a, Carla Winterhalter^a and Bert Müller^a

^aBiomaterials Science Center, University of Basel, c/o University Hospital, 4031 Basel, Switzerland;

^bSwiss Federal Laboratories for Materials Science and Technology, Überlandstrasse 129, 8600 Dübendorf, Switzerland.

ABSTRACT

Compliant electrodes of microstructures have been a research topic for many years because of the increasing interest in consumer electronics, robotics, and medical applications. This interest includes electrically activated polymers (EAP), mainly applied in robotics, lens systems, haptics and foreseen in a variety of medical devices. Here, the electrodes consist of metals such as gold, graphite, conductive polymers or certain composites. The common metal electrodes have been magnetron sputtered, thermally evaporated or prepared using ion implantation. In order to compare the functionality of planar metal electrodes in EAP microstructures, we have investigated the mechanical properties of magnetron sputtered and thermally evaporated electrodes taking advantage of cantilever bending of the asymmetric, rectangular microstructures. We demonstrate that the deflection of the sputtered electrodes is up to 39 % larger than that of thermally evaporated nanometer-thin film on a single silicone film. This difference has even more impact on nanometer-thin, multi-stack, low-voltage EAP actuators. The stiffening effect of many metallic electrode layers is expected to be one of the greatest drawbacks in the multi-stack approaches, which will be even more pronounced if the elastomer layer thickness will be in the sub-micrometer range. Additionally, an improvement in voltage and strain resolution is presented, which is as low as 2 V or 5×10^{-5} above 10 V applied.

Keywords: Compliant electrodes, asymmetric planar electro active polymers, Young's modulus, thermal evaporation, magnetron sputtering, cantilever bending, polyetheretherketone, polydimethylsiloxane.

1. INTRODUCTION

Metal coatings of low weight, low cost and compliant materials gain increasing interests in areas as packaging industry and microelectronics [1-4]. Thus, metal deposition onto polymer materials has been a subject of research. Investigations concerning the bi-layer systems of relatively soft polymer bulk material and rather rigid thin-layered coatings have been published. Here, the diffusion of metals into the bulk [5-7] and barrier materials [7], the wettability [8], as well as the conductivity have been considered [1-4, 9-13]. Further, investigations on the surface reactivity, activation and modification were conducted suggesting the formation of a third interfacial metal/polymer composite layer, when subject to cold ion plasma sputtering [2, 4, 9, 10, 12, 13].

For dielectric elastomer actuators (DEA) the choice of the electrode material including the preparation is of key importance. Especially for multi-stack DEA's compliant electrodes, which do not dominate the stiffness of the entire structure, have to be identified. The use of nanometer-thin metallic films as electrodes is a widespread approach. It is well known that the compliance of metals is usually not given and only allows for strains between 1 and 2 % [14]. There are examples of ultra-thin noble metal films on polymers including polydimethylsiloxane (PDMS), which give rise to strains well above 10 % [14]. Nevertheless, the impact of the Young's modulus from the metal onto the effective modulus of the entire EAP structure cannot be neglected, although the electrodes are much thinner than the polymer layer. The stiffening effect is pronounced in multi-stack actuators [14, 15].

For the optimization of ultra-thin metal layer electrodes in DEA's we hypothesize that the film preparation, for example by thermal evaporation and by magnetron sputtering, has a significant impact on the actuation of DEA-microstructures. Our instrument to evaluate this impact is based on a matured technique used in a broad range of applications [16-22] and has been introduced as a method to evaluate EAP microstructures with high resolution at low voltages [23, 24].

*florian.weiss@unibas.ch; phone 41 61 265 9618; fax 41 61 265 9699; www.bmc.unibas.ch

Electroactive Polymer Actuators and Devices (EAPAD) 2014, edited by Yoseph Bar-Cohen, Proc. of SPIE Vol. 9056, 905607 · © 2014 SPIE · CCC code: 0277-786X/14/\$18 · doi: 10.1117/12.2045152

Proc. of SPIE Vol. 9056 905607-1

2. EXPERIMENTAL

2.1 Electrically activated polymer microstructures

Figure 1 displays the procedure for preparing the asymmetric planar structure. The measured asymmetric EAP microstructures were built on polyetheretherketone (PEEK) substrates (APTIV 2000, Victrex, Lancashire, UK) with a thickness of 25 μm . The PEEK films were cut to the shape of 3-inch wafers. These substrates were rinsed in acetone (Merck KGaA, Darmstadt, Germany) to clean the surface. Subsequently, gold (Lesker, East Sussex, United Kingdom) was either thermally deposited or magnetron sputtered on the rough side of the PEEK film, mean surface roughness about 0.8 μm , under vacuum conditions at room temperature. The related sputtering conditions in the Balzers Union SCD 040 system (Balzers, Lichtenstein) corresponded to 0.05 mbar Ar-atmosphere (Carbagas AG, Gümliigen, Switzerland) and a constant working current of 30 mA. The thickness was measured using a quartz crystal microbalance (QSG 301, Balzers, Balzers, Lichtenstein). A Baltec MED 020 (Leica Microsystems, Wetzlar, Germany) was used to thermally evaporate the gold at a pressure of 2×10^{-4} mbar and a current of 40 mA. The gold was evaporated from a tungsten boat 32 mm \times 7 mm \times 0.1 mm (Umicore, Bödingen, Switzerland) at a rate of 0.45 nm/s according to the inbuilt quartz crystal microbalance. In a next step the substrates covered by gold were spin-coated using PDMS (Elastosil 745 A/B, Wacker Chemie AG, Munich, Germany) mixed in a volume ratio 1:1 (component A and B) with rotation speeds to obtain layer thicknesses ranging from 2 to 5 μm . Before crosslinking the PDMS films at a temperature of 120 $^{\circ}\text{C}$ for a duration of 60 minutes, the coated substrates were partly submerged into ethyl acetate (Fisher Scientific, Reinach, Switzerland) to dissolve and wash off the PDMS to become access to the lower electrode (cp. scheme in Figure 1). After PDMS-crosslinking, a mask to obtain two electrodes with a step-like profile as displayed in Figure 1 covered some parts of the structure. The uncovered PDMS surfaces were then either sputter or thermally coated with a gold film of the same thickness to form the second electrode.

2.2 Cantilever preparation

The 3-inch substrates were cut into rectangular cantilevers with an active area of 3 mm \times 15 mm and the step-like profile at one end to attach the contacts. The cantilevers were fixed using photo-curable resin (Sensationail, Fing'rs, Dübendorf, Switzerland) cured with an adequate UV-light source providing radiation with a wavelength of 400 to 505 nm. Mounted on a PTFE support, the sample including support was put into an airtight box with feed through for wiring the DEA-structure as presented in Figure 2.

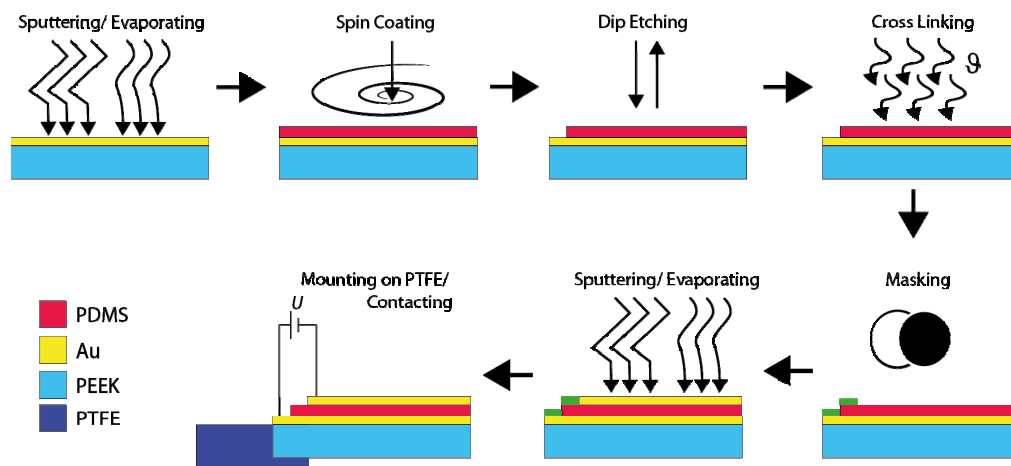


Figure 1. Schematic representation of the manufacturing steps of an asymmetric planar EAP structure. In a first step, the 3-inch PEEK substrates are coated with gold by either magnetron sputtering or thermal evaporation followed by spin-coating of the PDMS. Subsequently the layered structure is submerged into ethyl acetate in order to obtain silicone free access to the first layer of gold. Next the PDMS is thermally polymerized and covered with a second Au layer. The picture on the bottom left shows the asymmetric EAP cantilever structure.

2.3 Cantilever bending measurement

The system to measure the cantilever bending is built on a rotatable frame that holds the laser (He-Ne, 10 mW, Uniphase, Mantca, CA, USA), the cantilever on its holder and the position-sensitive detection unit (PSD, Spotcom, Duma Optronics Ltd, Neshar, Israel). The entire system is placed on an air-damped table (Stada, Vilnius, Lithuania) to reduce the impact of vibrations. To keep the measured samples from moving induced by air convection the PTFE holder is placed in an air-tight box containing a window transparent to the incident and reflected laser beam as shown in Figure 2. The deflection of the vertically oriented cantilever was measured during the step-wise increase of the applied voltage provided from a Stanford Research System high-voltage power supply (PS310, GMP SA, Lausanne, Switzerland). Vertical arrangement was chosen to avoid cantilever bending by gravity.

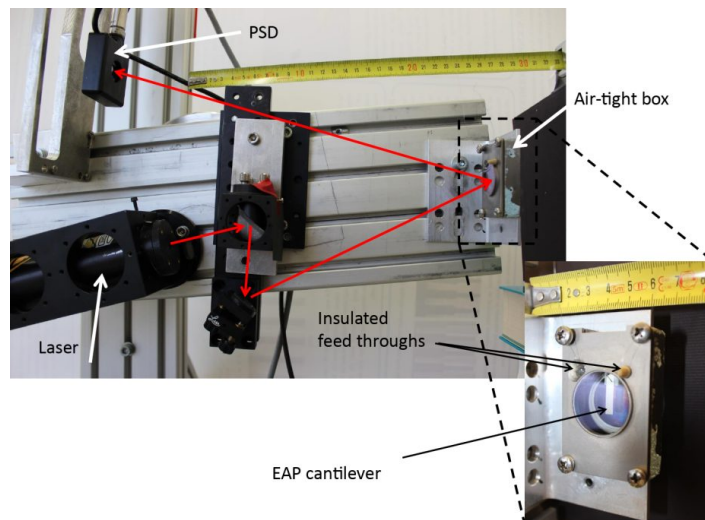


Figure 2. Image of the set-up to measure the bending of asymmetric planar EAP structures. The inset shows the air-tight box containing the EAP cantilever with a window for the incident and reflected laser beams. The electrical contacts are made wiring the gold electrodes.

2.4 Imaging the morphology of the prepared electrodes

The atomic force microscope used was a Bruker Dimension 3100 (Karlsruhe, Germany) operating in tapping mode with a Si cantilever. This cantilever (BudgetSensors, Tap190Al-G) had a spring constant of 190 N/m and a 10 nm tip radius. We applied a scanning speed of 1.19 $\mu\text{m/s}$.

In addition to the atomic force microscope, a scanning electron microscope (Zeiss, Leo Supra 35, Kloten, Switzerland) provided images of the electrode's morphology.

3. RESULTS

3.1 Performance of DEA's with thermally evaporated and magnetron sputtered Au electrodes

Figure 3 shows the experimental data, meaning the bending of the asymmetric EAP microstructures as the function of the applied voltage. Here, the thermal and sputtered electrodes each with the nominal thicknesses of 25 and 50 nm were selected. The PDMS thickness was set to a value of 5 μm , i.e. it is a factor of 100 or 200 thicker than the electrodes. We normalized the displacement of the laser spot on the PSD d by the cantilever length L . The strain in z direction s_z results from the Maxwell pressure p divided by the Young's modulus E , which can be written as

$$s_z = -\frac{p}{E} = -\frac{1}{E} \varepsilon_r \varepsilon_0 \left(\frac{U}{z} \right)^2 \quad (1)$$

with the applied voltage U , the layer thickness of the elastomer z and the relative dielectric constants of the elastomer and of the vacuum ϵ_r and ϵ_0 , respectively [25].

Figure 3 demonstrates the impact of electrode preparation on the actuation. We observe that the thermally evaporated electrodes are less compliant. As a consequence the actuators with thermal electrodes exhibit smaller bending than the sputtered ones at the same voltage.

For voltages below 100 V the actuators show a linear behavior for the bending-strain relation, see fitted curves in Figure 3, as expected according to Equation 1.

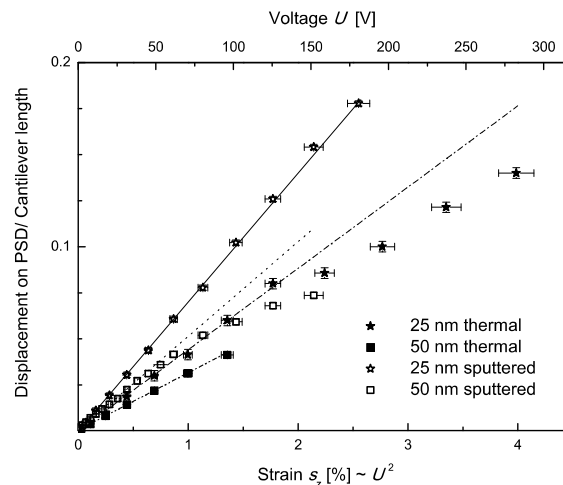


Figure 3. The relation between the applied voltage and the bending of the asymmetric EAP structure demonstrates that the sputtered gold electrodes are better suited than the thermal ones. The solid lines correspond to the fits of the displacement on the PSD as the function of the square of the applied voltages.

3.2 Morphology of the thermally evaporated and magnetron sputtered Au electrodes

Since one can reasonably expect that the defect structures of the electrodes influences the bending behavior of the actuators, the morphology of the thermally evaporated and sputtered gold electrodes was investigated using atomic force microscopy (AFM), see Figure 4, and scanning electron microscopy, data not shown.

The left image of Figure 4 shows the surface of a 15 nm-thin Au layer on a 5 μm -thin PDMS film. Its morphology notably differs from the morphology of the 15 nm-thin sputtered Au film shown in the right image of Figure 4. The AFM image of the thermally prepared Au electrode consists of circularly shaped clusters several 10 nm in diameter, which gives rise to a root mean square roughness of 3.4 nm. The magnetron sputtered Au films are rather flat with a root mean square roughness of 2.2 nm. They show a characteristic defect structure consisting of a few 100 nm-long and 10 to 20 nm-wide cracks. Around each crack one finds an increased height (protrusions), which indicates materials transport from the crack to the surrounding area. Nevertheless, these magnetron sputtered Au films are much more homogeneous than the thermally evaporated ones.

To approve the morphologies of the electrodes prepared by thermal evaporation and magnetron sputtering visualized by AFM, scanning electron microscopy was performed. Both techniques reveal the same morphological features.

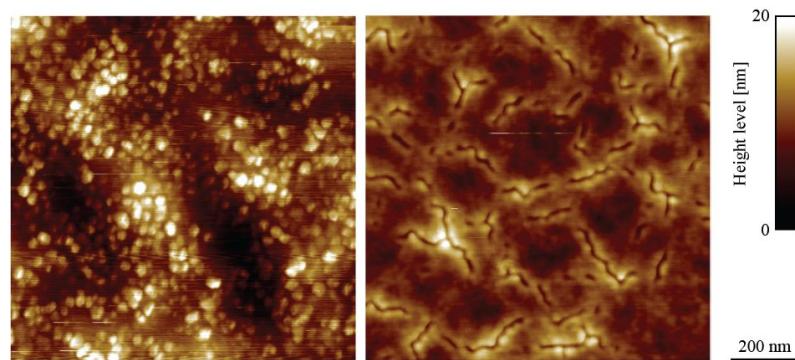


Figure 4. The AFM images of 15 nm-thin thermally evaporated Au films (a) and 15 nm-thin magnetron sputtered Au films (b) deposited on a 5 μm -thick PDMS layer exhibit distinct morphologies on the nanometer scale. Because the thermally evaporated films are coarse with respect to the sputtered ones it is not surprising that the related actuators show minor bending. The root mean square roughness of the thermally evaporated Au film corresponds to 3.4 nm. The related value for the sputtered Au film is 2.2 nm.

3.3 Actuator performance versus film thickness of magnetron sputtered Au electrodes

Figure 5 displays the experimental results of the actuation by the change of the magnetron sputtered Au film thickness from 5 to 70 nm. Again for voltages U below 100 V, one finds the behaviour predicted in Equation (1). For the film thicknesses of 5, 25 and 35 nm the differences are marginal, whereas the thicker films clearly show the expected stiffness increase of the entire DEA structure.

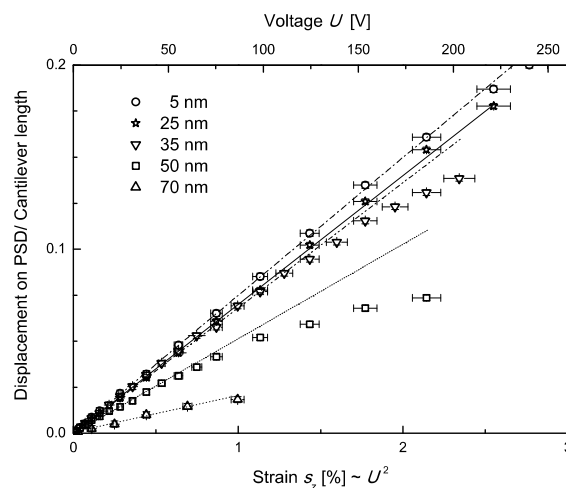


Figure 5. The actuation of an asymmetric DEA structure, which consists of a 25 μm -thick PEEK substrate and a 5 μm -thick PDMS layer with magnetron sputtered Au electrodes with the thicknesses indicated on both sides, shows a behavior as predicted by Equation (1). The diagram also demonstrates that the film thickness of the Au electrodes significantly determines the stiffness of the asymmetric DEA.

In order to evaluate the influence of PDMS-layer thickness on the actuation we prepared further DEA structures. Figure 6 contains data of DEA structures of PDMS layers with thicknesses of 2.1, 2.9, and 5.0 μm sandwiched between 35 and 70 nm-thin Au electrodes, respectively. Figure 6 consists of two parts to present the voltage dependence as well as the strain dependence of actuation. The fits included demonstrate that the data can reasonably be described using Equation 1. The actuators with the 35 nm-thin electrodes exhibit a better performance than the ones with 70 nm-thin Au layers. This phenomenon is more pronounced for the asymmetric structures with 5 μm -thick PDMS films than that with 2.9 μm -thick PDMS layers.

Plotting the normalized bending as the function of the strain s_z , as given in Figure 6(b), one realizes for the measured ranges that the impact of the electrode thickness is dominating the impact of the elastomer thickness. These normalized experimental data further indicate that the thickness ratio between electrode and elastomer is important, which is reflected in the effective Young's modulus of the EAP structure. The data further show the linear dependence up to 2% strain with slopes depending on PDMS- and Au-layer thicknesses.

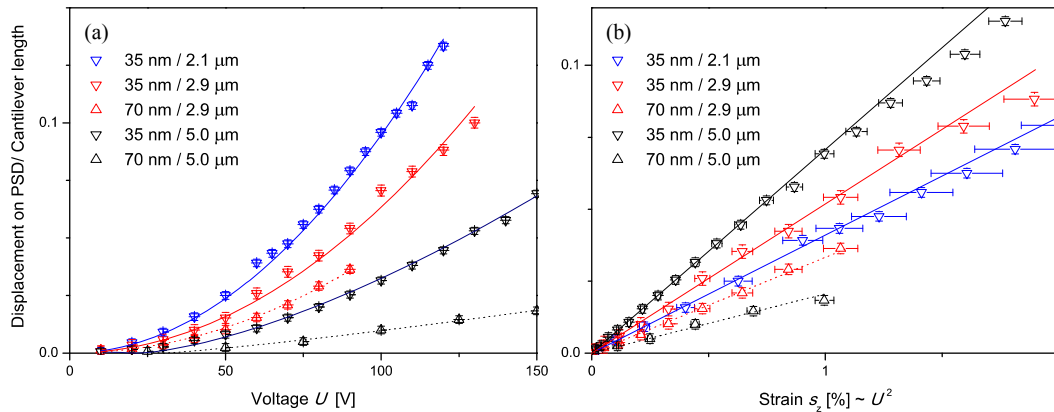


Figure 6. The behavior as predicted by Equation (1) is also found for asymmetric EAP-structures with 2 to 5 μm -thick PDMS layers. The data are represented as the function of applied voltage U in the left diagram (a) and as the function of strain s_z in the right diagram (b).

3.4 Low-voltage behavior and accuracy of the cantilever bending method

In order to demonstrate the improvement of the experimental setup used in previous studies [23, 24], we focus on the low voltage behavior. Figure 7 elucidates first that Equation 1 perfectly predicts the bending behavior as the function of the applied voltage between 10 and 50 V and second that changes in the applied voltages as low as 2 V and the related strain can be reliably detected by means of the current experimental bending measurement. For this purpose, we used again a 25 μm -thick PEEK substrate to build an asymmetric structure. After sputtering a 35 nm-thin Au layer, the 2.1 and 2.9 μm -thick PDMS film, respectively, was spin-coated before the 35 nm-thin counter electrode was sputtered.

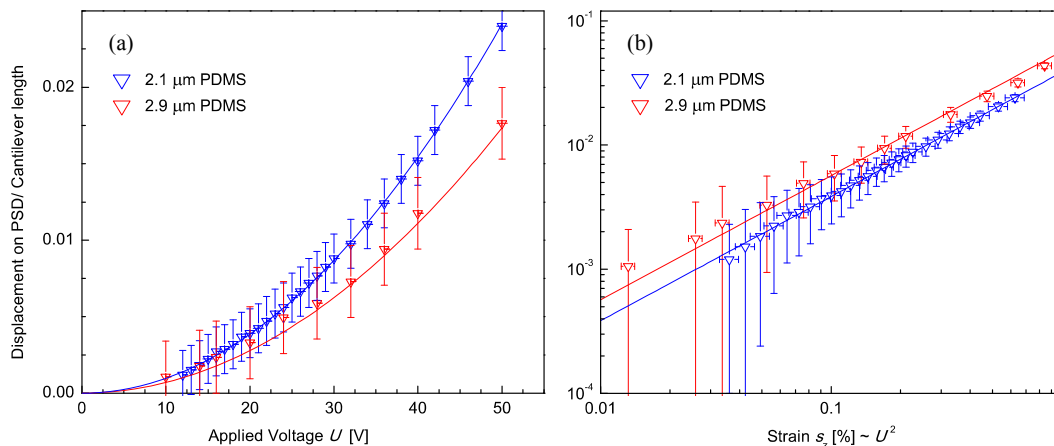


Figure 7. Equation 1 perfectly describes the bending of asymmetric structures consisting of a 25 μm -thick PEEK substrate with 2.1 and 2.5 μm -thick PDMS sandwiched between 35 nm-thin Au films on top, if voltages from 10 to 50 V are applied. In this range, the current experimental setup allow detecting changes of the bending radius through voltage increases as low as 2 V and through strains as low as 10^{-5} .

4. DISCUSSION

The preparation of the electrodes determines the performance of the anisotropic actuator structure. As for both the magnetron sputtering and the thermal evaporation Au has been used, we have to conclude that the defect structure characteristic for the electrode preparation causes the difference represented in Figure 3. The related surface morphology presented in the AFM images of Figure 4 depicts these characteristics. These characteristics have been shown [3]. V. Švorčík *et al.* [3] claimed that the mechanisms of sputtering and evaporation caused the differences in morphology. Apparently the sputtering produces single atoms deposited on to the polymer surface, whereas the thermal evaporation produces atomic clusters leading to the formation of rounded Au islands. This explanation, however, is somehow questionable, as the atomic cluster formation is not clearly demonstrated. In all probability, the three-dimensional islands are the result of the restricted migration length of Au at substrate temperatures of about 20 °C [26]. As the sputtered Au carries higher kinetic energies, they might heat the substrate surface leading to improved surface migration. The cracks are an obvious indication, because one may interpret them as the result of cooling-down process of materials with different thermal expansion.

Nevertheless, one can only speculate about the physical reason behind the performance differences between the thermally evaporated Au and the magnetron sputtered Au electrodes. The experimental data on the bending of the asymmetric structure, however, allow a detailed comparison and thereby provide a method to optimize the electrode preparation.

If asymmetric EAP structures are stretched or bent the characteristic defects in the electrodes with nanometer extensions can significantly reduce the conductivity of the nanometer-thin layers. It seems to be that the defect structure of the thermally evaporated film causes a gradual reduction of charging, whereas for the sputtered Au films the phenomenon is much less pronounced at the same strain. The related dependence of the electrical conductance on the grain and crack size, respectively, was for example described by F. Habrard *et al.* [14].

It should be noted and not surprising that the defect-morphology-related performance difference is more distinctive for thinner Au layers. The deviation of the experimental data from the prediction given by Equation 1 starting at certain strain thresholds is attributed to the defects within the rigid electrodes. Therefore, Au is suboptimal and maybe replaced by softer electrodes or even liquid metals [27]. The thickness of the electrodes by L. R. Finkenauer and C. Majidi is with 60 μm, however, by far too thick for the foreseen application and to be reduced by three to four orders of magnitude. The electrode film, however, has to be thick enough to realize a confluent layer with reasonable conductivity along the entire actuator structure.

Besides the defect structure, the mechanical properties of the entire structure determine the performance of the actuator. There is a significant stiffening of the EAP structure arising from the comprised materials easily derived from the thickness ratios of PDMS and Au layers. Their Young's moduli differ by five orders of magnitude: $E_{\text{PDMS}} = 200 \text{ kPa}$ and $E_{\text{Au}} = 78 \text{ GPa}$ [28]. For example, S. Rosset *et al.* [15] described the stiffening and estimated the mechanical properties for a single polymer layer sandwich structure applying the Voigt model. This behavior is also found in the experimental data of the present study, as displayed in the right diagrams of Figures 6 and 7. As a consequence, the ratio between electrode layer and polymer thickness can be optimized. Considering the data of Figure 6, the actuator structure with 35 nm-thin electrodes and 5 μm-thick PDMS provides the best performance.

The strain resolution shown in Figure 7 can be improved applying an optimized substrate. If the material, here PEEK, is selected and therefore the mechanical properties including the Young's modulus of the substrate given, one can adjust the film thickness. For example, the replacement of a 25 μm-thick PEEK film, used in the present study, by a 6 μm-thick PEEK substrate, which is also commercially available, an increased bending will be observed. This means that it is important to choose the appropriate thicknesses of substrate and electrodes for the pre-selected PDMS layer thickness.

5. CONCLUSION

The present communication reveals that for the bending of an asymmetric dielectric EAP structure the preparation of the electrodes is of prominent importance. The bending of comparable EAP structures, consisting of a 25 μm-thick PEEK substrate and a 5 μm-thick PDMS film sandwiched between 25 nm-thin Au electrodes, with thermally evaporated and magnetron sputtered Au electrodes differ by up to 39 %. For the manufacturing of multi-stack actuators this difference is more than critical, since the stiffening from metal electrodes is regarded as killer criteria. In addition, the preparation of the electrodes determines the optimization of layer thicknesses for the envisioned nanometer-thin multi-layer actuators in

medical implants. The selection of the electrode materials and their preparation procedure affect the conductivity in the multiple operation stages. The conductivity, in turn, dictates the response time, a critical parameter of an artificial sphincter to treat stress incontinence. The quantification both using simulations and experimental approaches, however, is challenging as one observes a nonlinear behavior below thicknesses of 5 to 10 nm [2-4, 13]. The bending bar method [23, 24] is an invaluable experimental tool to optimize EAP micro- and nanostructures.

6. ACKNOWLEDGMENTS

The technical assistance of Monica Schönerberger (Nanotech Service Lab) before and during the AFM imaging and Yves Pellmont (Physics Department University of Basel) for the thermal Au evaporation is appreciated. The financial support of the Swiss National Science Foundation (project 200021-135496) and the nano-tera.ch initiative (SmartSphincter) is gratefully acknowledged. Furthermore, the authors thank VICTREX for supporting us with PEEK films.

REFERENCES

- [1] Svorcik, V., Zehentner, J., Rybka, V., Slepicka, P., and Hnatowicz, V., "Characterization of thin gold layers on polyethyleneterephthalate: transition from discontinuous to continuous, homogenous layer," *Applied Physics A*, 75(4), 541-544 (2002).
- [2] Panchuk, D. A., Bazhenov, S. L., Bol'shakova, A. V., Yarysheva, L. M., Volynskii, A. L., and Bakeev, N. F., "Correlation between structure and stress-strain characteristics of metallic coatings deposited onto a polymer by the method of ionic plasma sputtering," *Polymer Science Series A*, 53(3), 211-216 (2011).
- [3] Švorčík, V., Slepíčka, P., Švorčíková, J., Špírková, M., Zehentner, J., and Hnatowicz, V., "Characterization of evaporated and sputtered thin Au layers on poly(ethylene terephthalate)," *Journal of Applied Polymer Science*, 99(4), 1698-1704 (2006).
- [4] Volynskii, A. L., Panchuk, D. A., Moiseeva, S. V., Abramchuk, S. S., Lebedeva, O. V., Yarysheva, L. M., and Bakeev, N. F., "On the effect of the nature and physical state of a polymer support on the stress-strain characteristics of metallic coatings," *Polymer Science Series A*, 51(3), 302-310 (2009).
- [5] Gupta, D., Faupel, F., Zaporojtchenko, V., Thran, A., Strunskus, T., and Kiene, M., [Metal Diffusion in Polymers and on Polymer Surfaces], Springer Berlin Heidelberg, (2005).
- [6] Svorcik, V., Efimenko, K., Rybka, V., and Hnatowicz, V., "Ga penetration into polymers," *Applied Physics A*, 68(3), 357-358 (1999).
- [7] Thran, A., Strunskus, T., Zaporojtchenko, V., and Faupel, F., "Evidence of noble metal diffusion in polymers at room temperature and its retardation by a chromium barrier," *Applied Physics Letters*, 81(2), 244-246 (2002).
- [8] Feng, J.-T., and Zhao, Y.-P., "Influence of different amount of Au on the wetting behavior of PDMS membrane," *Biomedical Microdevices*, 10(1), 65-72 (2008).
- [9] Panchuk, D. A., Puklina, E. A., Bol'shakova, A. V., Abramchuk, S. S., Grokhovskaya, T. E., Yablokov, M. Y., Gil'man, A. B., Yarysheva, L. M., Volynskii, A. L., and Bakeev, N. F., "Structural aspects of the deposition of metal coatings on polymer films," *Polymer Science Series A*, 52(8), 801-805 (2010).
- [10] Panchuk, D. A., Sadakbaeva, Z. K., Bagrov, D. V., Kechek'yan, A. S., Bol'shakova, A. V., Abramchuk, S. S., Yarysheva, L. M., Volynskii, A. L., and Bakeev, N. F., "Specific features of surface structuring during deformation of plasma-treated polymer films," *Polymer Science Series A*, 52(8), 794-800 (2010).
- [11] Volynskii, A. L., Bazhenov, S., Lebedeva, O. V., and Bakeev, N. F., "Mechanical buckling instability of thin coatings deposited on soft polymer substrates," *Journal of Materials Science*, 35(3), 547-554 (2000).
- [12] Volynskii, A. L., Moiseeva, S. V., Dement'ev, A. I., Panchuk, D. A., Lebedeva, O. V., Yarysheva, L. M., and Bakeev, N. F., "The structure and properties of polymer-metallic coating interphase," *Polymer Science Series A*, 48(7), 731-737 (2006).
- [13] Volynskii, A. L., Panchuk, D. A., Bol'shakova, A. V., Yarysheva, L. M., and Bakeev, N. F., "Structure and properties of nanosized coatings deposited onto polymers," *Colloid Journal*, 73(5), 587-604 (2011).
- [14] Habrard, F., Patscheider, J., and Kovacs, G., "Super-compliant metallic electrodes for electroactive polymer actuators," *Proc. of SPIE* 8340, 834013 (2012).
- [15] Rosset, S., and Shea, H., "Flexible and stretchable electrodes for dielectric elastomer actuators," *Applied Physics A*, 110(2), 281-307 (2013).

- [16] Binnig, G., Quate, C. F., and Gerber, C., "Atomic Force Microscope," *Physical Review Letters*, 56(9), 930-933 (1986).
- [17] Gimzewski, J. K., Gerber, C., Meyer, E., and Schlittler, R. R., "Observation of a chemical reaction using a micromechanical sensor," *Chemical Physics Letters*, 217, 589-594 (1994).
- [18] J. Köser, S. Gaiser, and B. Müller "Contractile cell forces exerted on rigid substrates," *European Cells and Materials*, 21, 479 - 487 (2011).
- [19] Meyer, G., and Amer, N. M., "Novel optical approach to atomic force microscopy," *Applied Physics Letters*, 53(12), 1045-1047 (1988).
- [20] Urwyler, P., Häfeli, O., Schiff, H., Gobrecht, J., Battiston, F., and Müller, B., "Disposable polymeric micro-cantilever arrays for sensing," *Procedia Engineering*, 5(0), 347-350 (2012).
- [21] Urwyler, P., Köser, J., Schiff, H., Gobrecht, J., and Müller, B., "Nano-Mechanical Transduction of Polymer Micro-Cantilevers to Detect Bio-Molecular Interactions," *Biointerphases*, 7, 6 (2012).
- [22] Urwyler, P., Schiff, H., Gobrecht, J., Häfeli, O., Altana, M., Battiston, F., and Müller, B., "Surface patterned polymer micro-cantilever arrays for sensing," *Sensors and Actuators A: Physical*, 172(1), 2-8 (2011).
- [23] Weiss, F. M., Deyhle, H., Kovacs, G., and Müller, B., "Designing micro- and nanostructures for artificial urinary sphincters," *Proc. of SPIE 8340*, 83400A (2012).
- [24] Weiss, F. M., Zhao, X., Thalmann, P., Deyhle, H., Urwyler, P., Kovacs, G., and Müller, B., "Measuring the bending of asymmetric planar EAP structures," *Proc. of SPIE 8687*, 86871X (2013).
- [25] Pelrine, R. E., Kornbluh, R. D., and Joseph, J. P., "Electrostriction of polymer dielectrics with compliant electrodes as a means of actuation," *Sensors and Actuators A: Physical*, 64(1), 77-85 (1998).
- [26] Müller, B., "Natural formation of nanostructures: from fundamentals in metal heteroepitaxy to applications in optics and biomaterials science," *Surf. Rev. Lett.*, 8, 169 (2001).
- [27] Finkenauer, L. R., and Majid, C., "Compliant liquid metal electrodes for dielectric elastomer actuators," *Proc. of SPIE*, 9056, this issue.
- [28] Pamula, V. K., Jog, A., and Fair, R. B., "Mechanical property measurement of thin-film gold using thermally actuated bimetallic cantilever beams," *Proc. MSM*, 1, 410-413(2001).

2.2 Electro-spraying nanometer-thin elastomer films for low-voltage dielectric actuators

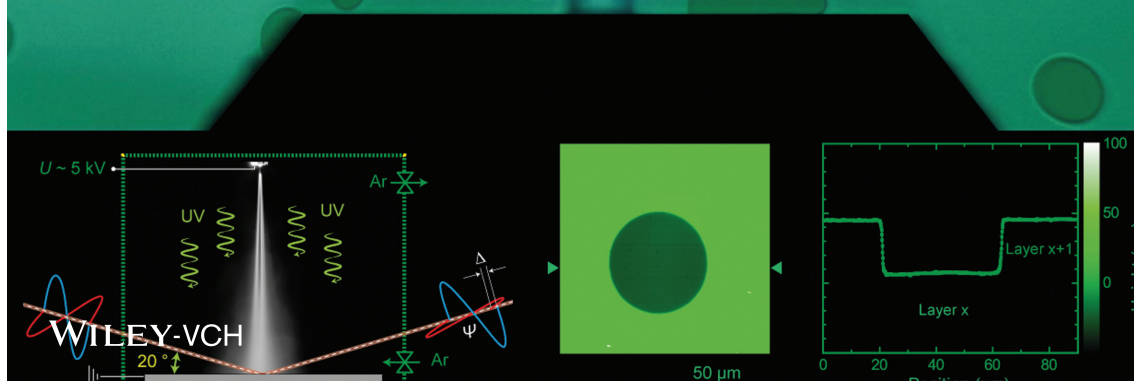
In this work real-time spectroscopic ellipsometry is used to determine deposition rates of electro-sprayed polydimethylsiloxane applying varying flow rates. Furthermore, the surface morphologies of deposited and cured thin films are compared to evaluate the influence of the flow rate.

Published in Advanced Electronic Materials

ADVANCED ELECTRONIC MATERIALS

THIN ELASTOMER FILMS

In article number 1500476, F. M. Weiss et al. describe the preparation of submicrometer-thin polydimethylsiloxane films with a subnanometer root-mean-square surface roughness using alternating current electrospinning. This frontispiece shows an optical micrograph of the electrospayed silicone after UV light curing. The film formation and the flattening during UV-light treatment are in situ observed by means of spectroscopic ellipsometry.



Electrospraying Nanometer-Thin Elastomer Films for Low-Voltage Dielectric Actuators

Florian M. Weiss, Tino Töpfer, Bekim Osmani, Sven Peters, Gabor Kovacs, and Bert Müller*

Micrometer-thin polymer films are often prepared using spin coating. In applications such as low-voltage dielectric elastomer actuators (DEAs), however, nanometer-thin polymer layers are required. In this paper, it is demonstrated that alternating current electro-spray deposition allows for the fabrication of high-quality nanometer-thin polydimethylsiloxane (PDMS) films. The growth of the PDMS with an average molecular weight of 6000 g mol^{-1} at rates of $0.02\text{--}5.54 \text{ nm s}^{-1}$ was in situ monitored by means of spectroscopic ellipsometry. The Cauchy layer model performs above a deposition-rate-dependent average film thickness, which is associated with a confluent film. The droplet size measurements as the function of deposition rate show that inertia and polarization forces dominate in liquid PDMS electro-spraying. The roughness of the deposited films increases with the spray rate. After UV-light curing under Ar atmosphere, however, the films smoothen to root-mean-square roughness values between 0.20 and 0.28 nm determined by atomic force microscopy on areas of $5 \mu\text{m} \times 5 \mu\text{m}$ and between 2 and 20 nm determined by interferometry on an area of 0.72 mm^2 . Such electro-sprayed PDMS films with (sub-)nanometer roughness qualify for the fabrication of low-voltage DEAs.

1. Introduction

Dielectric elastomer actuators (DEAs) are relevant for a wide variety of applications including robotics,^[1,2] haptics,^[3] sound generation,^[4] and lens systems^[5,6] as well as in research of medical implants or artificial muscles.^[7] The actual design depends on the specific application.^[4,8,9] Most frequently, multistack DEAs^[10,11] are fabricated to take advantage of reduced operating voltages. Nevertheless, the DEA microstructures require voltages of several hundred volts or above. For medical and other applications, however, the operating voltages have to be further

reduced, but strain values of the order of 10% should be achieved. Therefore, suitable techniques to prepare nanometer-thin, multistack DEAs consisting of silicone or other relevant polymers have to be developed. Spin-coated elastomer films that were reported to be thinner than that of casting, blading, and roll-to-sheet procedures are usually not thinner than $5 \mu\text{m}$.^[11] Because of the limited adhesion forces between the elastomer and the underlying microstructure, spin coating only allows manufacturing multistack DEAs with a restricted number of layers on a finite area.

Electrospraying comprises a group of methods to build parts of products, which include ceramics,^[12] carbon nanotubes,^[13] polymers,^[14–16] and composite materials.^[17] Whereas the direct current mode is well established,^[18–21] the alternate mode is still in the phase of development, as some recent studies on morphology control^[22] and frequency behavior^[23–25] illustrate. We hypothesize that alternate current electro-spraying is also appropriate to prepare smooth submicrometer-thin polydimethylsiloxane (PDMS) films for DEAs.

We expect that ellipsometry allows for the in situ characterization of the growing PDMS film as previously carried out for direct current electro-spraying.^[26] In situ ellipsometry not only enables the film thickness measurement^[27–29] but also the phenomenological evaluation of the film surface roughness during deposition.^[30–32] As the currently available models to be applied to the experimental ellipsometry data rely on serious assumptions, the extracted quantities must be validated with other methods after the termination of the deposition experiment.

In this paper, we not only deal with the deposition via alternate current electro-spraying but also with the subsequent curing by means of UV radiation. We presume to gain PDMS films with a root-mean-square roughness well below 1 nm .

2. Characterizing Electro-sprayed PDMS Films by Means of Ellipsometry

Figure 1A shows the experimental setup to monitor the electro-spray deposition by means of spectroscopic ellipsometry in situ. The data analysis was restricted to a spectral range of

F. M. Weiss, T. Töpfer, B. Osmani, Prof. B. Müller
Biomaterials Science Center
University of Basel
4123 Allschwil, Switzerland
E-mail: bert.mueller@unibas.ch
F. M. Weiss, Dr. G. Kovacs
Federal Laboratories for
Materials Science and Technology
8600 Dübendorf, Switzerland
S. Peters
SENTECH Instruments GmbH
12489 Berlin, Germany



DOI: 10.1002/aelm.201500476

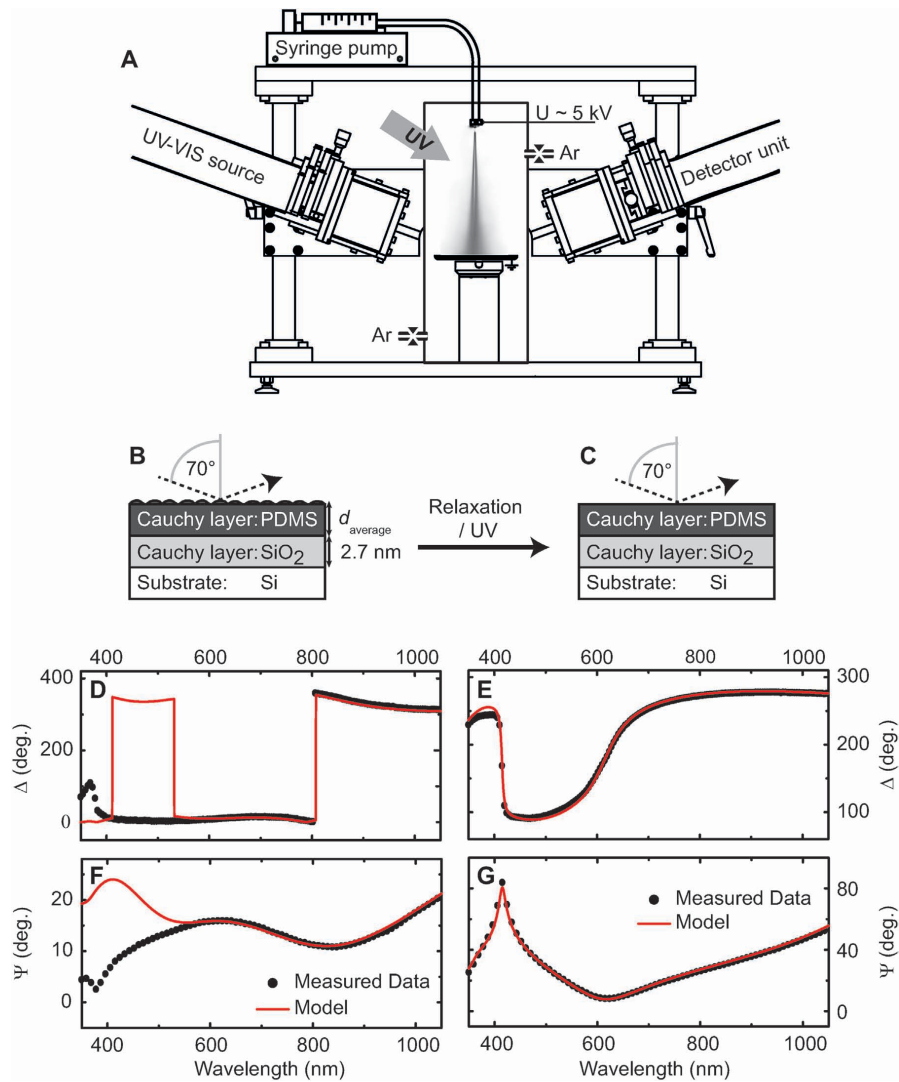


Figure 1. Electro spraying and in situ thin-film characterization using ellipsometry. A) Applying an alternating current, the electric field between nozzle and silicon substrate creates a spray of micrometer-size PDMS/solvent droplets traveling toward the substrate. The spectroscopic ellipsometer monitors the deposition and the subsequent UV curing under 1 bar Ar atmosphere. The schemes labeled B) and C) show the as-sprayed and the cured state of deposited thin films. Whereas the model according to these schemes only partly describes the Ψ - and Δ -wavelength dependencies for the PDMS deposited with a mean rate of 0.02 nm s^{-1} (cf. diagrams (D) and (F)), the data recorded after curing can be perfectly fitted (cf. diagrams (E) and (G)). The PDMS film thickness, the lateral thickness gradient due to the spray profile and the extinction coefficient k_0 for the deposited film and the UV-cured film result in $(387 \pm 2) \text{ nm}$, $(24 \pm 2) \text{ nm per mm}$, 0.072 ± 0.006 , and $(316.0 \pm 0.3) \text{ nm}$, $(8 \pm 1) \text{ nm per mm}$, and 0.005 ± 0.001 , respectively.

300 to 1050 nm, as the absorption of PDMS is increasingly pronounced for wavelengths lower than 300 nm.^[33] As baseline, we collected the ellipsometry data of the bare Si(100) substrate with its 2 to 3 nm thin, native oxide layer. We considered both

the native oxide and the sprayed PDMS as Cauchy layers (cf. Figure 1B,C) to extract the optical properties and the thickness of the growing film. The recorded Ψ - and Δ -data depicted in Figure 1D–G correlate with the complex Fresnel reflection

Materials
Views

www.MaterialsViews.com

ADVANCED
ELECTRONIC
MATERIALS
www.advelectronicmat.de

FULL PAPER

coefficients r_p and r_s of p- and s-polarized light and their ratio ρ , described by the Fresnel equation

$$\rho = r_p/r_s = \tan \Psi \times e^{i\alpha} \quad (1)$$

The wavelength-dependent dielectric function $\bar{n}(\lambda)$ is extracted applying

$$\begin{aligned} \langle \bar{n} \rangle^2 &= ((n) + i(k))^2 \\ &= \sin(\varphi_0)^2 \times \left(1 + \tan(\varphi_0)^2 \left(\frac{1-\rho}{1+\rho} \right)^2 \right) \end{aligned} \quad (2)$$

with φ_0 representing the angle of the incident beam, $n(\lambda)$ the real and $k(\lambda)$ the complex parts of the refractive index. One of the simplest approximations according to the Cauchy series is the usage of a wavelength-independent, constant extinction coefficient

$$k(\lambda) = k_0 \quad (3)$$

and to reduce the wavelength dependence of the refractive index to

$$n(\lambda) = n_0 + c_1 n_1 / \lambda^2 \quad (4)$$

with $c_1 = 100 \text{ nm}^2$. This model is appropriate for the PDMS film in the wavelength range considered, as found in the present study. The agreement between the model and the experimental Ψ - and Δ -data is quantified using the mean square error (MSE)

$$\frac{1}{N} \sqrt{\sum_{i=1}^N \left[\left(\frac{\Psi_i^m - \Psi_i^h}{\delta \Psi} \right)^2 + \left(\frac{\Delta_i^m - \Delta_i^h}{\delta \Psi} \right)^2 \right]} \quad (5)$$

During the initial stages of growth, however, neither the fitting according to the Cauchy layer model nor the fitted data by the effective medium layer model^[34] were reasonable, presumably because of the droplets present on the substrate. At advanced stages of growth, the fitting according to the Cauchy layer model becomes possible as displayed in the diagrams of Figure 1D,F. Here, we assume that the droplets start to form a confluent layer with a rough morphology reflected in the fitted constant extinction coefficient k_0 . Here, k_0 simulates the scattering of light at the protrusions on the growing surface. In this context, however, k_0 is rather a phenomenological parameter to describe the damping of the Ψ - and Δ -amplitudes by light scattering at rough surfaces. Thus, the wavelength dependency of k was neglected.

In order to corroborate the applicability of the fitting procedure described above, we have characterized the films after the termination of the deposition and the curing using UV radiation. The diagrams of Figure 1E,G clearly point the much better fitting according to the Cauchy layer model.

The optical properties of the deposit DMS-V21 resulted from ellipsometry measurements on a 2 μm thick film spin-coated with a smooth morphology. The root-mean-square roughness value corresponds to $(0.85 \pm 0.01) \text{ nm}$. The Cauchy coefficients

were determined to $n_0 = 1.396 \pm 0.005$ and $n_1 = 37 \pm 1$, and $k_0 = 0$.

Using this approximation, the fitting of the data represented in Figure 1D–G gives rise to a film thickness of $(387 \pm 2) \text{ nm}$. The lateral thickness gradients as the result of the spray profile are not considered.

The combined fits of the experimental data given in the diagrams of Figure 1D,F using a constant extinction coefficient results in a k_0 -value of 0.19 ± 0.06 . It indicates a rough surface. One detects major discrepancies between model and experimental data below 600 nm, which leads to the MSE of 53. After UV light curing, the extinction coefficient k_0 equals to 0.010 ± 0.002 and the MSE to 3.5 (see fit in the diagrams of Figure 1E,G). This experimentally observed reduction of light scattering is interpreted as surface smoothing through reordering and relaxation of the polymer chains mediated by the UV light.

3. Ellipsometry Measurements During Electro-spraying

Above, we demonstrated that the Cauchy model is sufficient to extract the film thickness after the termination of film growth. During the initial stages of film growth, however, the determination of the average PDMS thickness is complex, since the individual droplets form islands and lead to a rough surface morphology. Nevertheless, the Ψ - and Δ -data are acquired even during the early stages of electro-spray deposition. The diagram in Figure 2A displays the Ψ - and Δ -data obtained at a wavelength of 632 nm for the selected flow rate of 267 nL s^{-1} . The angles Ψ and Δ start from 160° and 10°, before they oscillate with decreasing amplitudes between 80° and 90° and between 27° and 37°, respectively. Table S1 (Supporting Information) lists the data to show the temporal evolution in detail. The observed oscillations are the consequence of interferences at the selected wavelength. After the termination of deposition, the film thickness was determined to $(1420 \pm 1) \text{ nm}$ taking advantage of the Cauchy coefficients derived above. It is reasonable to assume a constant growth rate over the spray period of 1250 s. This knowledge is applied to derive both the refractive index and the extinction coefficient as the function of the average film thickness (see Figure 2B). For average film thicknesses below 300 nm, the fit does not converge and the related data cannot be obtained. Above that threshold, the fit converges, and the two optical parameters are derived. The refractive index $n(\lambda = 632 \text{ nm})$ starts above 1.13, a superposition of PDMS/solvent droplets and air, and asymptotically reaches the bulk value of PDMS, which corresponds to 1.396 in agreement with published data.^[35] Similarly, the extinction coefficient k_0 exponentially converges to 0.08 ± 0.02 . The surface roughness decreasing as the deposition proceeds explains this asymptotic behavior of the two optical constants.

A constant refractive index simplifies the determination of the film thickness on the basis of the ellipsometry data. One may, therefore, consider regimes, where the refractive index deviates from the bulk value by less than 5%, i.e., it is within the interval $1.325 < n < 1.396$, suitable for such an approximation. As shown by the gray-shaded area in Figure 2B, such an

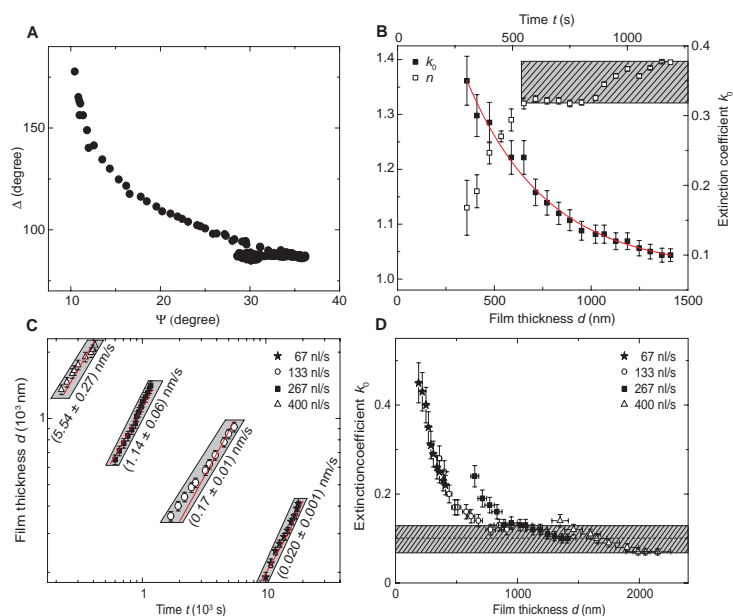


Figure 2. Ellipsometry measurements during electrospaying. A) Ψ - and Δ -values were ellipsometrically measured using a wavelength of 632 nm during the PDMS/solvent deposition with a flow rate of 267 nL s^{-1} . The damped oscillatory behavior comes from interferences of the monochromatic light with the surface structures corresponding in size to the applied wavelength. Table S1 (Supporting Information) lists the data to present the time lapse. B) At the deposition rate of 1.2 nm s^{-1} , the refractive index n and the extinction coefficient k_0 cannot be reasonably fitted for films thinner than 300 nm. For larger film thicknesses, the values asymptotically approach their limits. For films thicker than 520 nm, one may assume a constant refractive index (cf. gray-shaded area). C) The measurement of the PDMS film thickness for the flow rates 67, 133, 267, and 400 nL s^{-1} allows for the determination of the growth rates from the slopes, which correspond to (0.020 ± 0.001) , (0.17 ± 0.01) , (1.14 ± 0.06) , $(5.54 \pm 0.27) \text{ nm s}^{-1}$, respectively. There is a flow-rate-dependent critical thickness below which no reasonable fit of the ellipsometry data is obtained. D) The extinction coefficient k_0 reduces as the growth proceeds. For films thicker than 1000 nm, the extinction coefficient k_0 stays within a well-defined range indicated by the gray-shaded area and may be regarded as constant.

approximation is reasonable for film thicknesses above 650 nm and deposition times exceeding 550 s. For these regimes, however, the experimentally derived extinction coefficient k_0 shows a significant decrease associated with the light scattering at the rough surface. Nevertheless, for the in situ monitoring of electrospayed films, a critical thickness should be selected to work with a constant refractive index of the Cauchy layer.

The validity of this approach can be checked measuring the film thickness as the function of the deposition time. Providing a constant deposition rate, a linear dependence is expected. Figure 2C validates this behavior for the selected flow rates of 67, 133, 267, and 400 nL s^{-1} . The slopes of the related fits (see red-colored full lines) lead to the growth rates of PDMS and correspond to 0.02, 0.17, 1.2, and 5.5 nm s^{-1} , respectively. It should be noted that the film thicknesses at growth termination are in agreement with the results of 3D laser microscopy.

The films are sprayed in the multicone jet mode (cf. photographs of Figure S1, Supporting Information).^[36] Thus, the deposition rate locally varies. This variation is not necessarily fully taken into account in the ellipsometric measurements and the related error bars of the derived film thicknesses.

For this reason, the estimations are included into the diagram of Figure 2C using the gray-shaded areas.

Figure 2C allows reading the critical thicknesses for the selected deposition rates. This thickness increases from 170 via 360 and 520 to 1030 nm for the four selected rates between 67 and 400 nL s^{-1} . This behavior presumably reflects the flow-rate-dependent droplet size. According to scaling laws with dominating inertia and polarization forces valid for ethyl acetate,^[37] the droplet diameter D depends on the square root of the flow rate Q . Admixing 5 vol% of PDMS to ethyl acetate obviously does not remarkably change the physical properties responsible for the electrospay process. This behavior is in line with the data represented in Figure 2D. At a certain film thickness, the extinction coefficient was found to be higher with increasing flow rate. Nonetheless, for films thicker than 1000 nm and the flow rates investigated, the extinction coefficient stays within the range indicated by the gray-shaded area. To simplify matters, it may be regarded as constant. For these thicknesses, the influence of a droplet surface is smaller compared to the compact part of the PDMS film.

Materials
Views

www.MaterialsViews.com

ADVANCED
ELECTRONIC
MATERIALS
www.advelectronicmat.de

FULL PAPER

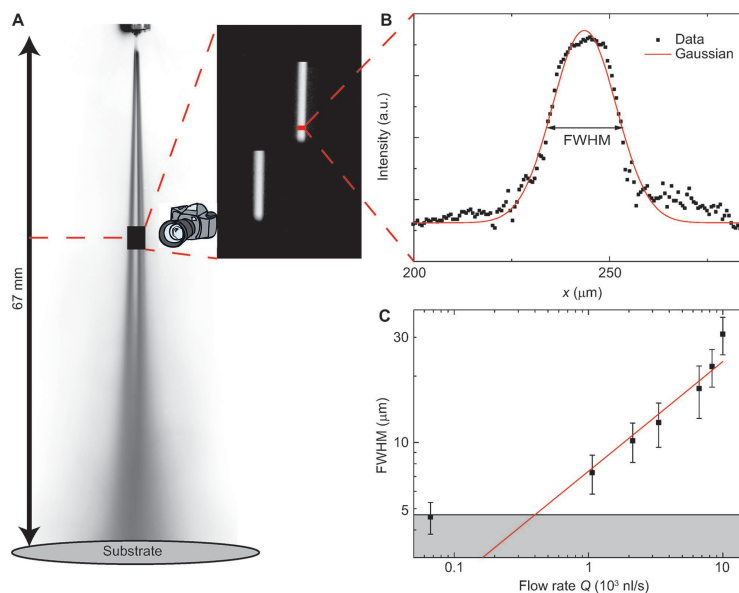


Figure 3. Flow-rate-dependent droplet size. A) Scheme of the experimental setup to determine the droplet diameter as the function of the flow rate. The photograph shows the path of two droplets during the 125 μs exposure time. B) The droplet diameter can be characterized by the FWHM values derived from a Gaussian fit. C) The FWHM depends on the square root of the flow rate. The experimental setup does not permit reliably measuring FWHM values below 5 μm because of the limited spatial resolution.

4. Determination of the Drop Sizes in the Jet

The ellipsometric results are corroborated using optical images of the droplets and looking for the scaling law proposed by Gañán-Calvo.^[37] The exemplary photograph of the droplet's trajectory in **Figure 3A** gives rise to a cross-section that follows a Gaussian distribution (cf. **Figure 3B**). Integrating the data along the droplet path and fitting them, one can easily access the full-width at half-maximum (FWHM). **Figure 3C** shows a double-logarithmic plot of FWHM values derived from at least six trajectories per flow rate as the function of the flow rate. The slope exactly corresponds to the predicted behavior with the exception of the value for 67 nL s^{-1} . The exception is explained by the limited spatial resolution of the experimental setup. Data located in the gray-shaded area are therefore overestimated.

5. UV Curing of Electrospayed PDMS Films

The spectroscopic ellipsometer was also applied to in situ study the alteration of the PDMS film during curing. During this treatment, the extinction coefficient is obviously decreasing. After a treatment period of 1000 s, the extinction coefficient k_0 reaches values between 0.04 and 0.08 for the applied flow rates (see **Figure 4A**). It should be mentioned that this phenomenon could also be represented by a lateral gradient converging k_0 to zero. The decrease of the extinction coefficient can be understood as surface smoothening. Optical interferometry studies

on an area of $982 \mu\text{m} \times 739 \mu\text{m}$, i.e., about six times smaller than the spot size of the ellipsometer, support this description. The root-mean-square roughness values, measured after the curing, correspond to $(15.1 \pm 3.1) \text{ nm}$. The variation of the roughness values is therefore well comparable with the variation of the extinction coefficient.

The as-sprayed film flattens due to its well-known viscoelastic behavior, which is particularly valid for the PDMS with the relatively smaller molecular weight of 6000 g mol^{-1} . The use of UV light accelerates the flattening. Therefore, it is stated that the UV light mediates the smoothening of the electrospayed thin films.

Surprisingly, the surface roughness after curing is independent on the applied flow for deposition rates between 0.02 and 5.5 nm s^{-1} . In order to verify this experimental result, we investigated the surface morphology by means of atomic force microscopy (AFM). The images with a size of $5 \mu\text{m} \times 5 \mu\text{m}$ displayed in **Figure 4B–E** support our conclusion and provide a homogeneous film with a root-mean-square roughness between 0.20 and 0.28 nm.

Preliminary data concerning the deposition of PDMS with larger molecular weights show a similar behavior but as expected a rougher surface morphology.

The atomic force microscope used in the present study allows not only measuring the morphology but also determining the mechanical properties of the PDMS films. The electrospayed films exhibit an elastic modulus of $(1.5 \pm 0.3) \text{ MPa}$ after curing. The elastic modulus of the spin-coated film

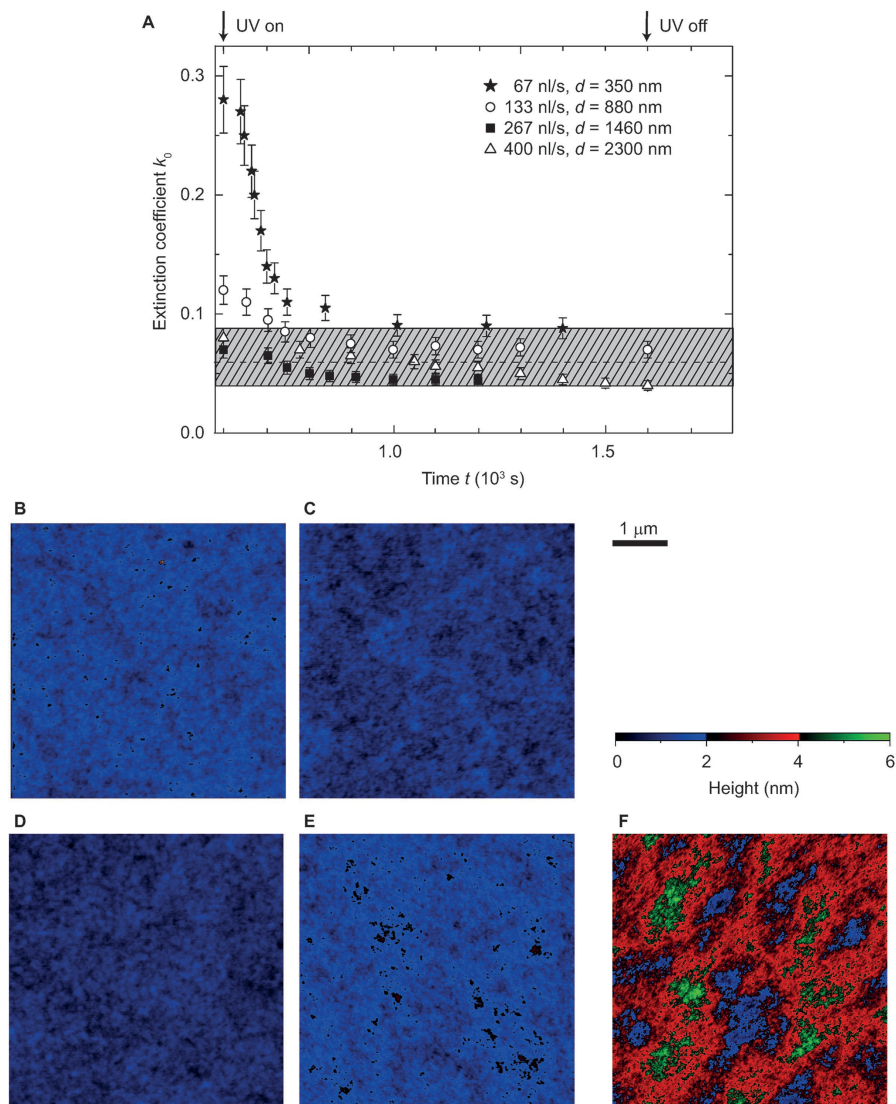


Figure 4. Deposition-rate-independent surface roughness after UV curing. A) During UV irradiation the extinction coefficient of the PDMS thin film becomes smaller. It approaches values between 0.04 and 0.08 for the deposition rates applied for thin-film formation, as shown by the gray-shaded area. B–E) The AFM images compare the surface morphology of UV-light-cured PDMS films for flow rates between 67 and 400 nL s⁻¹ with an average film thickness of 340 nm. As one cannot identify significant differences between the images and their root-mean-square roughness values, the results support the statement that the final surface morphology is independent of the deposition rate. F) The AFM image of the 2 μ m thick spin-coated PDMS film exhibits about three times larger roughness than the electrospayed thin films. The color bar for the height information and the 1 μ m length bar apply for the five AFM images presented.

corresponds to (4.7 ± 0.3) MPa after curing. Hence, one can conclude that the electrospayed films are stable enough for actuator applications.

Since the present study restricts to the PDMS film preparation and characterization, the electronic application in a DEA system will be presented in a forthcoming communication.



www.MaterialsViews.com

**ADVANCED
ELECTRONIC
MATERIALS**
www.advelectronicmat.de

FULL PAPER

6. Conclusion

Alternating current electro-spray deposition of micrometer-size ethyl acetate droplets containing 5% vinyl-terminated PDMS allows preparing PDMS films with deposition rates as currently used in micro- and optoelectronics but with a root-mean-square roughness for the surface three times smaller than advanced spin-coating applying rotation speeds as high as 5000 revolutions per minute. Whereas spin coating results in PDMS films that are very few micrometers thick or slightly below one micrometer, the electro-spraying enables us to fabricate PDMS films well below one micrometer with smaller roughness. As the operation voltage of a DEA—to reach a constant strain—quadratically follows the elastomer thickness, this moderate improvement is an essential step toward low-voltage DEA with reasonable breakdown voltage.

7. Experimental Section

Materials and Setup: In a first step, the liquid vinyl-terminated PDMS polymers (DMS-V21, M_w 6 kDa, Gelest, USA) were dissolved in ethyl acetate (Laboratory reagent grade, Fisher Scientific UK, Brunschwig, Basel, Switzerland) to obtain a 5 vol% concentration. This solution was stirred for 1 h and left for 3 d to make sure that the chains are no longer entangled. Chemicals were used as purchased without any further purification. The polymer solution was then drawn up into a 2 mL glass syringe with metallic Leur-lock (Eternal-Matic, Sanitex, HUBERLAB, Aesch, Switzerland) and connected to a metallic nozzle (26 s, Hamilton, Bonaduz, Switzerland) with an inner diameter of 0.13 mm. The syringe itself was mounted on a syringe pump (Aladdin six syringe pump, World Precision Instruments Germany GmbH, Berlin, Germany) to vary the flow rate between 0.13 and 660 000 nL s⁻¹. The nozzle is connected to the voltage source (TREK, 5/80, Lockport, NY, USA) and coupled with the function generator (Model 119M, Max Meier Elektronik, Zurich, Switzerland) in order to apply a rectangular voltage function of ± 5 kV with a frequency of 18 Hz, which was monitored by an Tektronix oscilloscope (TDS 210, Computer Control AG, Zurich, Switzerland) throughout all experiments of this study. The distance from the nozzle to the Si substrate (SiMat, Silicon Materials, Kaufering, Germany) was kept constant to 67 mm. For cleaning purposes, the Si wafers were rinsed with acetone (Merck KGaA, Darmstadt, Germany) and ethyl acetate. The UV cure was accomplished in Ar (Messer Schweiz AG, Lenzburg, Switzerland) atmosphere of 1 bar applying radiation of a deuterium broad-band UV lamp (Yuyu Lightning, China) covering a spectral range between 180 and 450 nm with its maximum intensity at a wavelength of 210 nm with a distance of 2 cm.

Real-Time Spectroscopic Ellipsometry: Ellipsometry was used to monitor the film growth, its relaxation, and the UV light curing process. Utilizing the spectroscopic ellipsometer SE801 from SENTECH (Berlin, Germany), controlled by the SpectraRay3 software, either Ψ and Δ or the Fourier coefficients S_1 and S_2 were determined as a function of the wavelength between 300 and 1050 nm. The incident beam angle, 70° from the normal, with a beam diameter of 2 mm gave rise to a spot size of 2 mm \times 5 mm on the wafer's surface. The in situ measurement period was set to 1 s steps. The linear and first order nonlinear refractive indices of the DMS-V21 were determined by a static measurement of a spin-coated, 2 μ m thick film and had values of $n_0 = 1.396 \pm 0.005$ and $n_1 = 37 \pm 0.7$, respectively. The wavelength-independent extinction coefficient k_0 was utilized to simulate the scattering at the surface.

Spin-Coating: For a reference of the optical properties of PDMS, a sample of DMS-V21 was spin-coated (WS-400B-6NPP/LITE/AS, Laurell Technologies Corporation, North Wales, PA, USA) on a Si wafer with 5000 rpm for a period of 150 s to obtain a 2 μ m thick film, which was subsequently measured by ellipsometry as described above.

3D Laser Scanning Microscopy: By cutting the cured PDMS layer, a step edge was generated to obtain the layer thickness with optical profilometry by means of a 3D laser scanning microscopy (Keyence VK-X200, Keyence International, Belgium).^[38]

Image SXM 139: Evaluation of the drop size was done by taking pictures (Canon 60D) of the spray with an exposure time of 125 μ s with a magnification of 2.5 (Sterni DV4 SPOT, Carl Zeiss AG, Feldbach, Switzerland). Using Image SXM, the diameter was determined integrating over the width from single cross-sections of the traces obtained in the photograph and taking their mean value. The error was estimated by the FWHM values of the integrated trace widths distribution.

Atomic Force Microscopy: AFM measurements ($5 \times 5 \mu\text{m}^2$, tapping mode, vibration amplitude 500 mV, set point 20%) were performed using a FlexAFM System (Nanosurf AG, Liestal, Switzerland). 2048 lines at a speed of 768 ms were acquired for each image using a noncontact soft tapping AFM probe (PPP-NCSTR probe, tip radius < 7.0 nm, NanoAndMore GmbH, Wetzlar, Germany). The raw data were leveled removing a polynomial background of the second degree and fixing the color range from zero to 2 nm. Root-mean-square values were calculated using the Gwyddion 2.41 software (Gwyddion: an open-source software for scanning probe microscopy (SPM) data analysis, <http://gwyddion.net>).

The mechanical properties of the spin-coated and electro-sprayed films were assessed by atomic force microscopy (FlexAFM C3000, Nanosurf AG, Switzerland). To this end, 100 indentations on 90 μ m \times 90 μ m arrays were acquired with a spherical tip with a radius of 150 nm (B150_FMR, Nanotools GmbH, Germany) at a load of 50 nN. The mean elastic moduli of the cured PDMS films were calculated using the FLEX-ANA (Automated Nanomechanical Analysis) software from Nanosurf. Potential substrate effects can be neglected since the indentation depths were well below 100 nm.

Interferometry: In order to obtain the surface morphology of the UV light-cured films in a spot size of 982 μ m \times 739 μ m, a 3D Optical Surface Metrology System (DCM8, Leica Microsystems AG, Heerbrugg, Switzerland) with a Leica Interferential Mirau SR 50 \times objective was used. The number of points in x- and y-directions was 3808 and 2866 with 258 nm spacing.

Supporting Information

Supporting Information is available from the Wiley Online Library or from the author.

Acknowledgements

The financial support of the Swiss National Science Foundation (project 200021-135496) and the nano-tera.ch initiative (project SmartSphincter) as well as the Swiss Nanoscience Institute (SNI) for the financial contribution to the AFM is gratefully acknowledged. The authors thank Thomas Geiger for supporting the interferometric measurements at the Federal Laboratories for Materials Science and Technology (Empa) and Monica Schönenberger from the Nanotech Service Lab for assistance at the 3D Laser microscope.

Received: December 23, 2015

Revised: January 19, 2016

Published online:

[1] Y. Bar-Cohen, *Proc. SPIE* **2002**, 4695, 1.

[2] Q. Pei, R. Pelrine, S. Stanford, R. Kornbluh, M. Rosenthal, *Synth. Met.* **2003**, 135, 129.

[3] M. Y. Ozsecen, M. Sivak, C. Mavroidis, *Proc. SPIE* **2010**, 7647, 764737.

- [4] R. Heydt, R. Kornbluh, J. Eckerle, R. Pelrine, *Dielectric Elastomers as Electromechanical Transducers: Fundamentals, Materials, Devices, Models and Applications of an Emerging Electroactive Polymer Technology*, Elsevier Science, Oxford **2008**.
- [5] F. Carpi, G. Frediani, S. Turco, D. De Rossi, *Adv. Funct. Mater.* **2011**, *21*, 4152.
- [6] S. Shian, R. M. Diebold, D. R. Clarke, *Opt. Express* **2013**, *21*, 8669.
- [7] B. Müller, H. Deyhle, S. Mushkolaj, M. Wieland, *Swiss Med. Wkly.* **2009**, *139*, 591.
- [8] G. Kofod, M. Paajanen, S. Bauer, *Proc. SPIE* **2006**, *6168*, 61682.
- [9] P. Lochmatter, *Ph.D. Thesis*, ETH Zürich, Zürich **2006**, 330.
- [10] F. Carpi, C. Salaris, D. De Rossi, *Smart Mater. Struct.* **2007**, *16*, S300.
- [11] P. Lotz, M. Matysek, H. F. Schlaak, *IEEE/ASME Trans. Mechatronics* **2011**, *16*, 58.
- [12] A. Jaworek, *J. Mater. Sci.* **2007**, *42*, 266.
- [13] J. N. O'Shea, J. B. Taylor, J. C. Swarbrick, G. Magnano, L. C. Mayor, K. Schulte, *Nanotechnology* **2007**, *18*, 035707.
- [14] K. Altmann, R. D. Schulze, G. Hidde, J. Friedrich, *J. Adhes. Sci. Technol.* **2012**, *27*, 988.
- [15] K. Morota, H. Matsumoto, T. Mizukoshi, Y. Konosu, M. Minagawa, A. Tanioka, Y. Yamagata, K. Inoue, *J. Colloid Interface Sci.* **2004**, *279*, 484.
- [16] I. B. Rietveld, K. Kobayashi, H. Yamada, K. Matsushige, *J. Colloid Interface Sci.* **2006**, *298*, 639.
- [17] Y. S. Kim, *Sens. Actuators B* **2010**, *147*, 137.
- [18] A. C. Sullivan, S. N. Jayasinghe, *Biomicrofluidics* **2007**, *1*, 034103.
- [19] J. Ju, Y. Yamagata, T. Higuchi, *Adv. Mater.* **2009**, *21*, 4343.
- [20] G. Xin, H. Sun, T. Hu, H. R. Fard, X. Sun, N. Koratkar, T. Borca-Tasciuc, J. Lian, *Adv. Mater.* **2014**, *26*, 4521.
- [21] S. M. Mirvakili, J. E. Slota, A. R. Usugaocar, A. Mahmoudzadeh, D. Jun, M. N. Mirvakili, J. T. Beatty, J. D. W. Madden, *Adv. Funct. Mater.* **2014**, *24*, 4789.
- [22] L. Y. Yeo, Z. Gagnon, H.-C. Chang, *Biomaterials* **2005**, *26*, 6122.
- [23] R. Kessick, J. Fenn, G. Tepper, *Polymer* **2004**, *45*, 2981.
- [24] S. Maheshwari, H.-C. Chang, *Appl. Phys. Lett.* **2006**, *89*, 234103.
- [25] L. Y. Yeo, D. Lastochkin, S.-C. Wang, H.-C. Chang, *Phys. Rev. Lett.* **2004**, *92*, 133902.
- [26] T. Ino, T. Hiata, T. Fukuda, K. Ueno, H. Shirai, *J. Non-Cryst. Solids* **2012**, *358*, 2520.
- [27] C. Cai, M. M. Bösch, B. Müller, Y. Tao, A. Kündig, C. Bosshard, Z. Gan, I. Biaggio, I. Liakatas, M. Jäger, *Adv. Mater.* **1999**, *11*, 745.
- [28] B. Müller, M. Jäger, Y. Tao, A. Kündig, C. Chengzhi, C. Bosshard, P. Günter, *Opt. Mater.* **1999**, *12*, 345.
- [29] R. P. Netterfield, P. J. Martin, W. G. Sainty, R. M. Duffy, C. G. Pacey, *Rev. Sci. Instrum.* **1985**, *56*, 1995.
- [30] D. Lehmann, F. Seidel, D. Zahn, *SpringerPlus* **2014**, *3*, 1.
- [31] T. A. Mykhaylyk, N. L. Dmitruk, S. D. Evans, I. W. Hamley, J. R. Henderson, *Surf. Interface Anal.* **2007**, *39*, 575.
- [32] X. Ziang, L. Shifeng, Q. Laixiang, P. Shuping, W. Wei, Y. Yu, Y. Li, C. Zhijian, W. Shufeng, D. Honglin, Y. Minghui, G. G. Qin, *Opt. Mater. Express* **2014**, *5*, 29.
- [33] J. Lee, J. Kim, H. Kim, Y. M. Bae, K.-H. Lee, H. J. Cho, *J. Micromech. Microeng.* **2013**, *23*, 035007.
- [34] D. A. G. Bruggeman, *Ann. Phys.* **1935**, *416*, 665.
- [35] B. Schnyder, T. Lippert, R. Kötz, A. Wokaun, V.-M. Graubner, O. Nuyken, *Surf. Sci.* **2003**, *532–535*, 1067.
- [36] M. Cloupeau, B. Prunet-Foch, *J. Electrostat.* **1990**, *25*, 165.
- [37] A. M. Ganan-Calvo, *J. Fluid Mech.* **2004**, *507*, 203.
- [38] M. Conroy, J. Armstrong, *J. Phys.: Conf. Ser.* **2005**, *13*, 458.

Copyright WILEY-VCH Verlag GmbH & Co. KGaA, 69469 Weinheim, Germany, 2016.

ADVANCED ELECTRONIC MATERIALS

Supporting Information

for *Adv. Electron. Mater.*, DOI: 10.1002/aelm.201500476

Electrospraying Nanometer-Thin Elastomer Films for Low-Voltage Dielectric Actuators

*Florian M. Weiss, Tino Töpfer, Bekim Osmani, Sven Peters, Gabor Kovacs, and Bert Müller**

Supporting information

Electro-Spraying Nanometer-Thin Elastomer Films for Low-Voltage Dielectric Actuators

*Florian M. Weiss, Tino Töpfer, Bekim Osmani, Sven Peters, Gabor Kovacs, and Bert Müller**

Table S1: Representation of the temporal progression of the measured Ψ and Δ values shown in figure 2 A measured *in-situ* during the electro-spray deposition of a 5 % (vol.) PDMS solution in ethyl acetate with a flow rate of 267 nl/s by spectroscopic ellipsometry (SE801, Sentech, Berlin, Germany).

Time t (s)	Ψ (degree)	Δ (degree)
603.9	30.0	87.9
607.2	29.9	87.8
610.7	29.9	88.0
616.7	30.1	87.7
620.0	30.2	87.9
623.5	30.4	87.5
627.0	30.6	88.0
630.3	30.7	88.1
633.6	30.8	88.3
637.1	31.0	88.4
640.6	31.0	88.3
643.9	31.0	88.4
647.2	31.1	88.3
650.7	31.2	88.4
654.2	31.2	88.3
657.5	31.2	88.3
660.8	31.2	88.1
664.4	31.3	88.0
667.8	31.4	87.9
671.1	31.4	87.9
674.4	31.4	87.9
678.0	31.4	87.8
681.4	31.5	87.6
684.7	31.5	87.4
688.0	31.6	87.2
691.6	31.6	87.0
695.0	31.7	87.3
698.3	31.6	87.3
701.6	31.6	87.5
705.2	31.7	87.8
708.6	31.8	86.8
711.9	31.5	88.2
715.3	31.6	88.1
718.8	31.7	88.2
722.3	31.6	88.9
725.6	31.5	89.1
728.9	31.6	89.1
732.4	31.6	89.0
735.9	31.5	89.0
739.2	31.5	89.2
742.5	31.4	89.6
746.0	31.4	89.7

749.5	31.2	90.0
752.8	31.1	90.1
756.2	31.1	90.1
759.7	31.0	89.8
763.1	31.1	89.9
766.5	31.1	90.7
769.8	30.8	91.2
773.3	30.8	90.4
776.8	30.5	90.3
780.1	30.4	90.1
783.4	30.4	90.4
786.9	30.3	90.3
790.4	30.6	89.8
793.7	30.0	90.6
797.0	30.0	90.3
800.6	30.0	90.7
804.0	29.9	90.9
807.3	29.7	91.1
810.6	29.7	91.2
814.2	29.8	91.6
817.7	29.8	91.6
821.0	29.9	91.9
824.3	29.9	92.0
827.8	29.7	91.0
831.3	30.0	92.0
834.6	30.2	92.3
837.9	30.2	91.7
841.4	30.2	91.9
844.9	30.5	92.4
848.2	30.2	92.5
851.5	30.2	91.9
855.1	29.9	91.6
858.5	30.1	93.0
861.8	30.3	91.1
865.1	30.2	92.7
868.7	30.0	92.6
872.1	30.0	92.7
875.5	30.1	92.7
878.8	30.4	93.3
882.3	30.7	92.5
885.8	30.6	92.0
889.1	31.2	91.6
892.4	31.1	91.9
896.0	31.8	91.0
899.4	31.6	91.1
902.7	31.8	92.1
906.0	32.1	90.4
909.6	31.9	90.7
913.0	31.9	91.3
916.3	31.9	91.7
922.4	31.9	91.7
925.8	31.8	92.1
929.1	31.9	92.1
932.4	31.6	91.3
936.0	31.9	91.9
939.4	31.9	91.3

942.7	31.9	91.8
946.0	31.9	91.8
949.6	32.0	92.0
953.0	32.0	92.6
956.3	32.1	92.6
959.7	31.9	92.9
963.2	31.9	92.8
966.7	31.9	92.9
970.0	31.5	92.7
973.3	31.2	93.0
976.8	31.2	93.4
980.3	31.2	93.5
983.6	31.1	93.6
986.9	31.0	93.8
990.4	31.0	93.8
993.9	31.0	93.9
997.2	30.9	93.8
1000.5	31.0	93.7
1004.1	30.7	93.9
1007.5	30.7	93.9
1010.8	30.8	93.7
1014.1	30.5	93.8
1017.7	30.5	93.8
1021.1	30.6	93.7
1024.4	30.6	93.2
1027.7	30.8	93.4
1031.3	30.9	93.8
1034.7	30.9	93.5
1038.0	30.7	92.8
1041.3	30.7	93.8
1044.9	30.6	93.6
1048.3	30.8	94.4
1051.6	31.0	92.9
1054.9	30.9	94.7
1058.5	31.5	94.0
1061.9	31.0	94.9
1065.2	30.8	94.1
1068.6	30.8	94.7
1072.1	30.9	94.0
1075.5	30.8	94.4
1078.9	30.7	93.3
1082.2	30.8	94.2
1085.7	31.0	93.7
1089.2	31.2	93.9
1092.5	31.3	93.4
1095.8	31.3	93.7
1099.3	31.4	93.6
1102.8	31.8	93.5
1106.1	32.2	92.9
1109.4	31.9	93.6
1112.9	31.9	93.4
1116.4	32.1	93.3
1119.8	32.0	93.2
1123.1	32.0	93.3
1126.6	32.0	93.4
1130.1	31.9	93.6

1133.4	32.0	93.8
1136.7	31.9	93.7
1140.2	32.1	93.6
1143.7	31.9	92.8
1147.0	32.0	93.0
1150.3	32.0	92.9
1153.8	31.8	92.8
1157.3	31.7	93.9
1160.6	31.5	93.6
1163.9	31.4	93.4
1167.5	31.6	93.8
1170.9	31.9	93.8
1174.2	31.6	93.8
1177.5	31.5	93.6
1181.1	31.6	93.4
1184.5	31.6	93.9

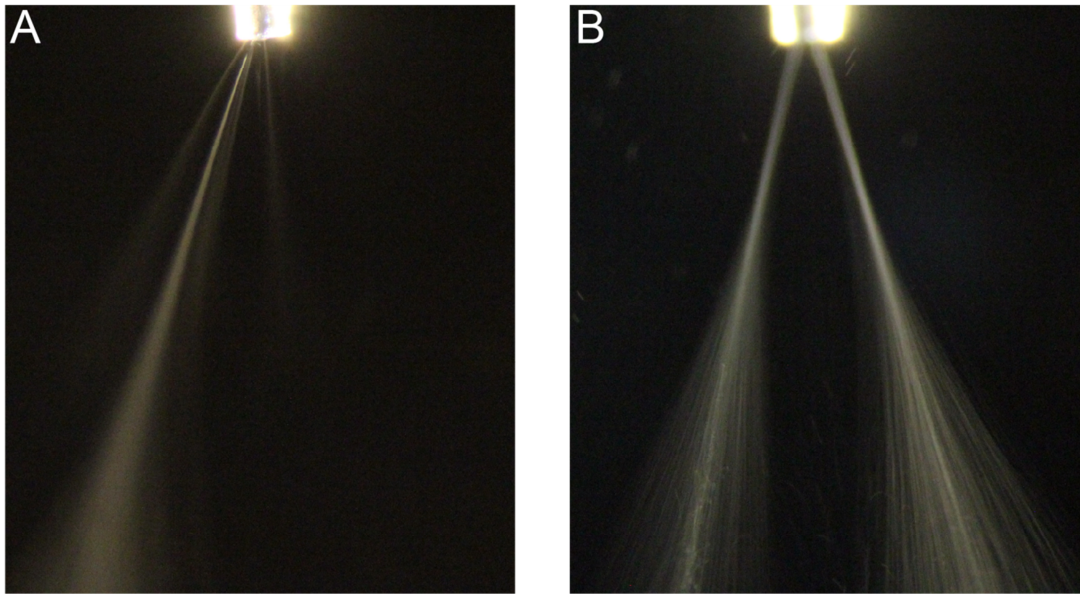


Figure S1. The optical images shown verify the multi-cone jet mode observed with the constant nozzle to substrate distance of 67 mm and an applied voltage of ± 5 kV. A represents the spray at a flow rate of 267 nl/s whereas B 400 nl/s respectively.

2.3 Thin film formation and morphology of electro-sprayed polydimethylsiloxane

Based on quasi-dynamic observations the island morphology as well as the film formation mode are determined using atomic force microscopy, segmentation of optical micrographs and spectroscopic ellipsometry.

Published in Langmuir

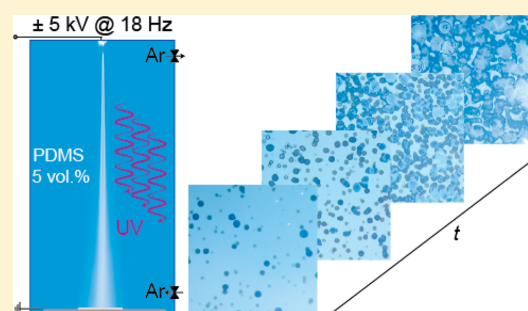
Thin Film Formation and Morphology of Electrospayed Polydimethylsiloxane

Florian M. Weiss,^{†,‡} Tino Töpfer,[†] Bekim Osmani,[†] Hans Deyhle,[†] Gabor Kovacs,[‡] and Bert Müller^{*,†}

[†]Biomaterials Science Center, Department of Biomedical Engineering, University of Basel, Gewerbestrasse 14, 4123 Allschwil, Switzerland

[‡]Federal Laboratories for Materials Science and Technology, Überlandstrasse 129, 8600 Dübendorf, Switzerland

ABSTRACT: Low-voltage dielectric actuators (DEAs) can be fabricated using submicrometer-thin polydimethylsiloxane (PDMS) films. The two established techniques, namely spin coating and molecular beam deposition, however, are inappropriate to produce multistack DEAs in an efficient way. Therefore, we propose an alternative deposition technique, i.e., the alternating current electro-spray deposition (ACESD) of 5 vol % PDMS in ethyl acetate solution and subsequent ultraviolet light curing. Atomic force microscopy makes possible the three-dimensional analysis of cured droplet-like islands. These circular islands, prepared on 2 in. Si(100) wafers from four polymers with molecular masses between 800 and 62 700 g/mol, reveal a characteristic morphology with an increasing height-to-diameter ratio. Using the 6000 g/mol polymer for ACESD, the film morphology evolution was tracked by applying conventional optical microscopy and spectroscopic ellipsometry. When the deposition was terminated after 13 s, circular islands with a mean height of 30 nm were found, while terminating the deposition after about 155 s led to a confluent layer with a mean height of 91 ± 10 nm. Potential electrostatic interactions between the droplets could not be identified through the analysis of spatial island distribution. Nevertheless, ACESD is a budget-priced and competitive deposition technique that can be employed to fabricate submicrometer-thin PDMS films with true nanometer roughness.



1. INTRODUCTION

Molecular beams enable the formation of organic thin films with monolayer precision, as required for applications in (opto)electronics.¹ These flexible but rather expensive deposition techniques are limited to comparably small molecules. Organic molecule deposition is a growing field, although a variety of materials cannot be evaporated because of their limited thermal stability.² Furthermore, the deposition rates are restricted to less than one monolayer per second, which corresponds to about one micrometer per hour. For example, the fabrication of a stacked dielectric elastomer actuator (DEA) requires about 10 000 h to reach a thickness of several millimeters. This simple estimation shows that alternative methods have to be identified, for example, to fabricate low-voltage DEAs.

Currently, DEAs, which find their application in robotics,^{3,4} haptics,⁵ lens systems,^{6,7} sound generation systems,⁸ and sensors,^{9,10} are built from elastomers purchased as films from well-established suppliers or prepared using spin-coating. These elastomer films are thicker than one micrometer and hence require operation voltages of several hundred volts to reach strains of about 10%. As the operation voltage of a DEA increases with the square of the elastomer thickness, even a moderate thickness reduction by less than 1 order of magnitude

is an essential step toward low-voltage DEAs as required for medical implants, including artificial muscles.¹¹ In this paper, we pursue electro-spraying to fabricate nanometer-thin silicone films. The application of a static electric field for the electro-spraying process, however, may be problematic because the charges will accumulate on the isolating substrate. To avoid substrate charging, we propose to employ an alternating current (ac) source.

At first glance, one might expect a film morphology that represents the arbitrary droplet-by-droplet deposition, i.e., a rough film surface. Nonetheless, since the spray droplets not only contain the polymers but also consist mainly of the wetting solvent, one can reasonably expect flat islands with a high aspect ratio between diameter and height. With a PDMS–solvent ratio of 1:20, droplet diffidence on the Si(100) wafer, and the coalescence of islands, we may reasonably expect the formation of a homogeneous, confluent layer. Because of the evaporation of the solvent at a moderate rate, and energy input via ultraviolet light curing, nanometer-thin silicone films with a uniform thickness and low surface roughness might be created.

Received: February 6, 2016

Revised: March 14, 2016

Published: March 15, 2016

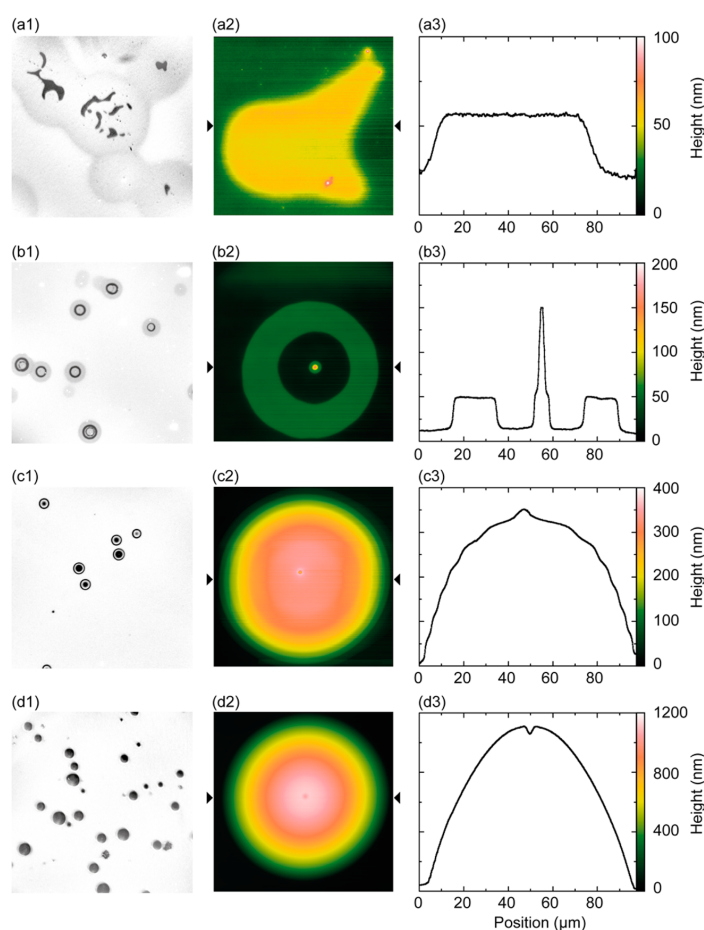


Figure 1. Characteristic morphology of UV-cured PDMS islands electro-sprayed at a flow rate of 267 nL/s by applying a voltage of ± 5 kV and a frequency of 18 Hz, revealed by means of (1) optical microscopy, image size: 2.34 mm \times 2.34 mm; (2) AFM images, size: 97.5 μm \times 97.5 μm ; and (3) AFM profiles with locations indicated by the arrow heads. The polymer chain lengths correspond to number-average molecular weights of (a) 800, (b) 6000, (c) 28 000, and (d) 62 700 g/mol.

Homogeneity may even be enhanced, since the process includes the charging of the droplets, which in turn leads to repulsive electrostatic interactions between them.

We hypothesize that the choice of polymer size determines the islands' height-to diameter ratio, as their mobility depends on molecular mass.¹² Atomic force microscopy (AFM) is perfectly suited for measuring surface morphology and is especially sensitive for island heights. Thus, AFM studies will assist in the search for the optimized size of PDMS molecules to be deposited.

Once the polymer size has been selected, the evolution of film morphology with the advancement of deposition from the early stages of deposition, i.e., the formation of individual islands, to the advanced stages of film growth, i.e., the development of a confluent layer, should be investigated. The spatial distribution of the individual islands can be derived from optical micrographs. Here, island distribution will shed light on the interactions between the charged droplets during and after deposition. This analysis, however, becomes challenging when the individual islands merge and form a confluent layer.

Therefore, for the advanced stages of film growth, we propose characterizing the film by means of spectroscopic ellipsometry, which reveals the wavelength-dependent refractive index, film thickness, surface morphology, and film porosity.¹³

The application of these characterization techniques and the related analysis of the experimental data allow for the enhancement of the electro-spraying process for elastomer thin films that can be exploited for low-voltage DEA nanostructures.

2. EXPERIMENTAL SECTION

2.1. Material and Electro-spray Deposition. Vinyl-terminated PDMS polymers (Gelest, USA) with number-average molecular weights M_n of 800, 6000, 28 000, and 62 700 g/mol (DMS-V05, DMS-V21, DMS-V31, and DMS-V41, respectively) were dissolved in ethyl acetate (Laboratory reagent grade, Fisher Scientific UK, Brunschwig, Basel, Switzerland) to obtain the 5 vol % solution. PDMS samples and solvent were used as purchased. The polymer solution was then drawn up into a 3 mL glass syringe with a metallic Leur-lock (Eternal-Matic, Sanitex, HUBERLAB, Aesch, Switzerland) and connected to a metallic nozzle (26s, Hamilton, Bonaduz,

Switzerland) with an inner diameter of 0.13 mm. The flow rate of the syringe pump (Aladdin six-syringe pump, World Precision Instruments Germany GmbH, Berlin, Germany) was set to 267 nL/s. The applied voltage on the nozzle originates from a voltage source (TREK, 5/80, Lockport, NY). It is coupled with a function generator (Model 119M, Max Meier Elektronik, Zurich, Switzerland) in order to apply a rectangular voltage function of ± 5 kV with a frequency of 18 Hz, monitored by an Tektronix oscilloscope (TDS 210, Computer Controll AG, Zurich, Switzerland). A distance of 67 mm from the Si substrate (SiMat, Silicon Materials, Kaufering, Germany) to the nozzle was chosen. UV-curing was performed without any photoinitiator in an Ar (Carbagas AG, Basel, Switzerland) atmosphere of 1 bar, applying UV radiation from a deuterium broad-band UV lamp (Yuyu Lightning, China) and covering a spectral range between 180 and 450 nm, with its maximum intensity at a wavelength of 210 nm at a distance of 2 cm.

2.2. Atomic Force Microscopy. AFM measurements ($97.5 \times 97.5 \mu\text{m}^2$, tapping mode, vibration amplitude 3000 mV, set point 35%) were performed using a FlexAFM system (Nanosurf AG, Liestal, Switzerland). Using a noncontact soft tapping AFM probe (PPP-NCSTR-10 probe, tip height 10–15 μm , force constant 1.2–29 N/m, NANOSENSORS, Neuchatel, Switzerland), 512 lines at a speed of 5.08 s per line were acquired for the image. The raw data were leveled removing a second-degree polynomial background. Root-mean-square values were calculated using the Gwyddion 2.41 software package (Gwyddion: an open-source software for SPM data analysis, <http://gwyddion.net>).¹⁴

2.3. Optical Micrographs. Images of the PDMS islands and layers at preselected deposition periods after curing were taken with a Canon EOS 600D camera mounted on a Stemi DV4 SPOT microscope (Carl Zeiss AG, Feldbach, Switzerland) with a magnification of 13.

2.4. Island Segmentation. The acquired color images were converted to grayscale using MATLAB (The MathWorks, Inc., Natick, United States). To account for inhomogeneous illumination, the images were leveled by means of second-degree polynomial background subtraction. A 2D Frangi filter implemented in MATLAB (The MathWorks, Inc., Natick, United States)¹⁵ was used to identify the borders of the PDMS islands. The borders' open ends were closed manually in order to generate a binary mask representing the segmented PDMS islands on the Si(100) substrate.

2.5. Spectroscopic Ellipsometry. The SE801 spectroscopic ellipsometer from SENTECH (Berlin, Germany), controlled by SpectraRay3 software, was applied after deposition and curing. As a function of the wavelength between 190 and 1050 nm, angles Ψ and Δ were measured. The Fresnel equation

$$\rho = r_p/r_s = \tan \Psi e^{i\Delta}$$

provides the relation between the recorded Ψ and Δ data and the complex Fresnel reflection coefficients r_p and r_s of p- and s-polarized light and their ratio ρ . This approach helps extract the wavelength-dependent dielectric function $\tilde{n}(\lambda)$

$$\langle \tilde{n} \rangle^2 = (\langle n \rangle + i\langle k \rangle)^2 = \sin(\phi_0)^2 \left(1 + \tan(\phi_0)^2 \left(\frac{1 - \rho}{1 + \rho} \right)^2 \right)$$

with ϕ_0 being the angle of the incident beam and $n(\lambda)$ the real and $k(\lambda)$ the complex parts of the refractive index. The incident beam with a diameter of 4 mm and an angle of incidence of $\phi_0 = 70^\circ$ from the normal results in a measured area of 4 mm \times 10 mm on the Si(100) wafer. During the step scan mode eight polarizer positions with fixed integration times of 0.1 s were monitored. To determine the linear and first-order nonlinear refractive index of the cured DMS-V21, a spin-coated, 2 μm thick film was measured. The analysis provided $n_0 = 1.396 \pm 0.005$, $n_1 = 30.0 \pm 0.7$, and $n_2 = 7.0 \pm 0.2$. These values are based on the Cauchy series approximation¹⁶ with the refractive index $n(\lambda) = n_0 + c_1 n_1/\lambda^2 + c_2 n_2/\lambda^4$ with $c_1 = 10^2 \text{ nm}^2$ and $c_2 = 10^4 \text{ nm}^2$. The extinction coefficient k was set to zero.

3. RESULTS AND DISCUSSION

3.1. Selection of the Polymer Chain Length. In order to find an optimized starting material size or polymer length for the formation of nanometer-thin elastomer films, the morphology of four ac electrospayed PDMS islands was investigated after UV curing. The characteristic morphology is recognized in optical micrographs, as displayed in Figure 1, panels (a1), (b1), (c1), and (d1). The vinyl-terminated PDMS islands, prepared using polymers with molecular weights of 800 and 6000 g/mol, DMS-V05 and DMS-V21, exhibit a shape that reflects the spreading out of the sprayed droplets, as indicated in the optical micrographs of Figure 1, panels (a1) and (b1), by the light-gray area with the darker rings. The diameter of the PDMS islands shrinks with increasing molecular weight. For islands prepared from the polymers with the higher molecular weight, i.e., 28 000 and 62 700 g/mol, DMS-V31 and DMS-V41, no ring could be identified, as illustrated in Figure 1, panels (c1) and (d1). Compared to optical micrographs the AFM images comprise only a restricted area, but they do provide a precise measure of the islands' heights. Furthermore, the islands' shapes are characteristic for each polymer. Those electrospayed using DMS-V05 have plateau-like features about 30 nm high with an aspect ratio of width-to-height of 2700 (cf. Figure 1, panels (a1)–(a3)). PDMS islands fabricated from DMS-V21 show rings that are also about 30 nm high, and these rings enclose an island. Although the profile in Figure 1(b3) presents a rather sharp peak, this island has a height that is 3 orders of magnitude smaller than its diameter. Islands electrospayed using DMS-V31 also show the rings on the optical micrographs (Figure 1(c1)). However, when investigating them by AFM, steps of about 50 nm in height, concentrically arranged around their center, are found, as best recognized in Figure 1(c3). Islands prepared from the polymer DMS-V41 do not show steps. They increase from the periphery to the center, as given in Figure 1, panels (d1)–(d3). In the center, one finds a notch. The diameter-to-height ratio of the islands corresponds to about 900.

The characteristic morphology of the PDMS islands prepared by electrospaying and subsequent UV curing is not fully understood. Nevertheless, there are several publications that describe selected phenomena related to island formation. For example, Grishaev et al.¹⁷ very recently published a study on the complex drop impact morphology of a series of millimeter-size droplets onto hydrophobic and hydrophilic substrates. The present study, however, restricts its focus to the ethyl acetate solvent and the Si(100) substrate. This means that only the 5 vol % polymer caused the characteristic differences seen in the PDMS island shapes. The chain length of the polymers seems to determine diffluence, which is significantly higher for the low-molecular-weight polymers. It can be reasonably stated that the starting materials from Gelest contain oligomers and residuals from the polymerization process, which may influence the wetting behavior. Furthermore, one can assume that 5.0 vol % is well below the overlap concentration of the used polymers. Entanglement effects, which definitely influence the film morphology on nanometer scale, however, become important for the spray on the route from nozzle to substrate because a significant amount of solvent evaporates.

Because the UV radiation treatment changes the morphology and the mechanical properties of the sprayed liquid PDMS film,¹⁸ one may expect that the UV light induces cross-linking.

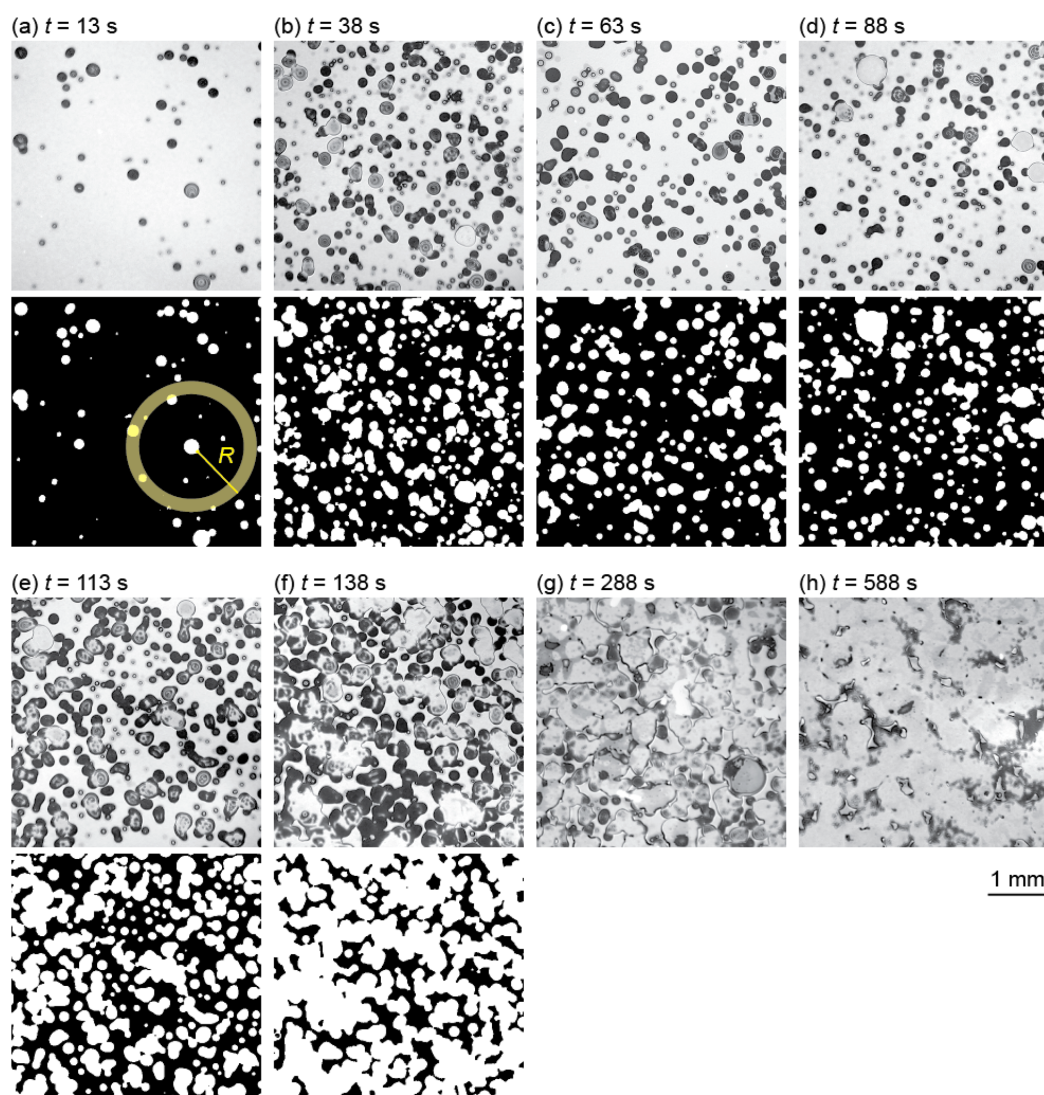


Figure 2. Optical micrographs of electro-sprayed and cured PDMS on Si(100). Deposition time t is indicated. The segmentation of the PDMS islands, white on the black substrate on the images below the micrographs, allows for defining the coverage and analyzing island separation. The yellow scheme in mask (a) elucidates the definition of the radial coverage θ_r . The distance R from each island periphery is calculated according to the distance transform. The radial coverage θ_r for a given R is obtained as the ratio white to black and white at distance R (cf. yellow shaded area). The procedure is repeated for each individual island, and the results are averaged.

The reaction mechanism is associated with a reduced concentration of vinyl functional groups as shown by IR spectroscopy.¹¹ Furthermore, the investigation of UV-irradiated PDMS using wavelengths of about 170 nm revealed scissions of the Si-CH₃ and -CH₂-H bonds.¹⁹ Therefore, a cross-linking mechanism based on the radicalization of these three bonds could lead to a three-dimensional elastomer network.

Contrary to the plateaus, the rings perfectly represented in Figure 1, panels (b1) and (b2), were described two decades ago.²⁰ In the work of Deegan and co-workers, it is explained that once the contact line of an emulsion or a colloidal suspension is pinned to the substrate, the rim of the ring forms.

Solute particles are too large to migrate further in the surrounding solvent, and capillary force drags the solvent toward the contact line, because here the solvent evaporates preferentially. Thus, one may conclude that the more solute molecules in a droplet, the broader the resulting ring. The rather flat island found in the center of the rings featuring an inclination of about 1.5° (cf. Figure 1, panels (b1)–(b3)) may occur as a result of curing, a process which may “freeze” the transport of the solute molecules toward the ring. Consequently, the remaining and mobile solute particles may build up into a heap, thus initiating transport toward the center—again driven by capillary forces due to preferential evaporation.

For the DMS-V31 and DMS-V41 polymers, one has to encounter the entanglement of the chains once they are deposited on substrate. At this stage the concentration of the polymer should have notably increased or even turned into the pure PDMS due to the solvent evaporation in the course of the spraying process. For PDMS the occurrence of entanglements is reported above a critical molecular weight between 10 100 and 12 500 g/mol.²¹

The concentric steps of the PDMS islands prepared from the polymer DMS-V31 resemble PDMS microdroplets described in the literature.²² Whereas the height of the steps reported in the literature corresponds to a few nanometers, we have identified step heights of several tens of nanometers which may originate from smectic ordering of the single polymer chains.²³

The phenomenon observed for DMS-V31, however, can also be explained through the capillary waves which propagate along the surface after the impact of the droplet, as described for water drops.²⁴ As the viscosity of the ethyl acetate solution with PDMS differs from that of water, the temporal evolution of the waves is probably modified. The nonoccurrence of steps on the semispherically shaped PDMS islands made from DMS-V41 droplets indicates that the capillary waves are suppressed because of the changed viscosity.

The notch on top of the PDMS islands prepared using DMS-V41 presumably originates from the droplet impact evolution just before the rebounding process of a secondary droplet starts. Here, viscosity slows down the process.

An investigation into the island morphology shows that DMS-V05 and DMS-V21 are better suited for preparing smooth nanometer-thin PDMS layers than the other two polymers used. Because the longer polymer chains build unimodal films with higher elasticity, DMS-V21 is preferred. Therefore, the present study concentrates on the usage of DMS-V21 dissolved in pure ethyl acetate.

3.2. From Islands to Confluent Film. Figure 2 depicts optical micrographs of PDMS on Si(100), each 4.24 mm × 4.24 mm, after deposition times t ranging from 13 to 588 s. For deposition times up to 90 s, the PDMS islands are well separated, as clearly displayed in the binary data below the optical micrographs. At higher coverage the islands coalesce. Therefore, PDMS films prepared with a deposition time longer than 150 s appear as a confluent layer.

The PDMS islands were automatically segmented to determine their coverage and to analyze island separation. The simultaneously performed manual segmentation validated the appropriate choice of threshold.

Coverage θ arises from the surface fraction covered by the PDMS islands, which is easily derived from the segmented data by dividing the number of pixels belonging to the PDMS by the total number of pixels in the image, as shown in Figure 2. These data are plotted as the function of the deposition time t in Figure 3. The linear fit through the point of origin underlines expected dependence. It should be noted that the entire deposition system had a delay time of about 12 s, which is readily obtained using the linear fit given in Figure 3.

The choice of coverage, however, is somewhat arbitrary. Hence, it makes sense to decode the deposition time by the means of the average film thickness d^* . In a previous study with the same setup, a deposition rate of 1.14 ± 0.06 nm/s was found for a flow rate of 267 nL/s.¹⁸

The diagram in Figure 4 displays mean radial coverage, determined as the distance from each segmented PDMS island surface. Around each island one finds a depletion zone with an

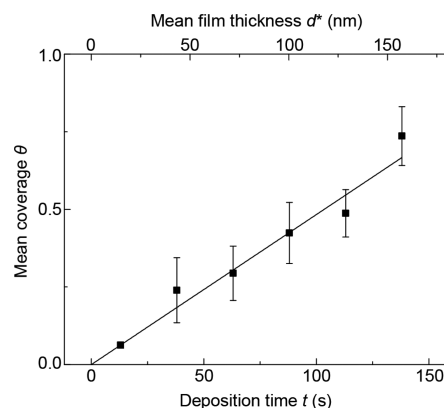


Figure 3. As expected, mean coverage θ is a linear function of deposition time t . Therefore, mean film thickness d^* is obtained from deposition time t via a deposition rate of 1.14 nm/s extracted in a previous study.¹⁸

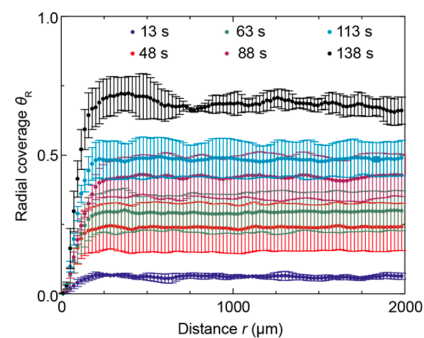


Figure 4. Mean radial coverage θ_r is plotted against the distance of the PDMS islands R . Here, for each segmented island (cf. Figure 2) coverage as a function of radial distance R was calculated. The procedure was repeated for each individual island in one micrograph. The diagram shows the average values of three optical micrographs. The error bars correspond to the related standard deviations.

extension of up to 250 μm , which is independent of deposition time. For larger radial distances, radial coverage reaches a deposition time-dependent plateau. These plateau values correspond to the mean coverage θ represented in Figure 3.

In order to better characterize the depletion zones, slope s is extracted from the data points represented in Figure 4. For this purpose, we use data points in the interval from 20 to 80% between zero and the plateau value of the mean radial coverage θ_r . Furthermore, we introduce intercept i , defined as the distance from the ordinate to the intersection point of the linear fit for slope detection with the plateau value. Intercept i is a lower limit for the depletion zone. Table 1 lists the s and i values obtained for the selected deposition times. It is not surprising that intercept i , and thus the lower limit of the depletion zone, corresponds to about 150 μm and is therefore independent of the deposition time.

The existence of the depletion zone is attributed to repulsive interactions between the charged droplets during deposition. The more dominant effect, though, may originate from the rounded island shape. This geometry gives rise to a depletion

Table 1. Comparison of Slope s and Intercept i Obtained from Radial Coverage Distributions for the Deposition Times Listed

deposition time t (s)	slope s (10^1 m^{-1})	intercept i (μm)
13	2.1 ± 1.0	148 ± 24
38	10 ± 4	127 ± 46
63	11 ± 3	148 ± 37
88	10 ± 6	199 ± 46
113	19 ± 10	145 ± 20
138	25 ± 9	154 ± 18

zone which extends to the mean radius of the isolated PDMS islands. A depletion zone of $150 \mu\text{m}$ agrees well with the mean island radius of $74 \mu\text{m}$ present for two neighboring islands, as derived from the optical micrographs related to a deposition time of 13 s.

Figure 5 contains island size distributions deduced from optical micrographs, as shown in Figure 2a–d. The error bars correspond to the standard deviation of the frequencies received from three images per deposition time. As qualitatively recognized in Figure 2, droplet size is not uniform. We know that the ac multicone jet spray generates droplets with a range of sizes; nevertheless, the characteristic decrease from smaller to larger islands dominates island size distribution, which implies that the majority of spray droplets are relatively small and of a similar size.

During the very early stages of deposition, island density grows in a linear fashion. As deposition proceeds, the probability of island coalescence increases. Therefore, one would expect—as for atomic epitaxial systems such as Cu/Ni(100)²⁵—maximal island density, which is generally termed “saturation island density”. In fact, plotting mean island density ρ versus mean coverage θ , as illustrated in Figure 6, the

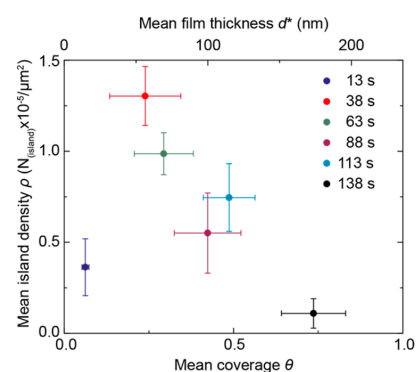


Figure 6. Mean PDMS island density versus mean coverage has a maximal value. Mean film thickness d^* is added to elucidate that for a flow rate of 267 nL/s saturation island density is reached for an average film thickness between 30 and 50 nm. The percolation threshold is found at a mean film thickness of about 150 nm.

expected maximum emerges. For representative epitaxial growth studies the maximum is observed at around 10%.^{25,26} In the present case, the maximum is found at higher coverage, presumably because of statistical growth, i.e., the absence of migrating units.

According to the two-dimensional continuum model for discs with the same radii,²⁷ the percolation threshold is reached at a coverage of 67.6%. For discs with two different radii the threshold depends on the ratio of the two radii and can be as high as 76%.²⁷ In the present case of a 5 vol % solution of DMS-V21 the percolation threshold is found above a coverage of 73.6%, as seen in Figure 6. This observation does not

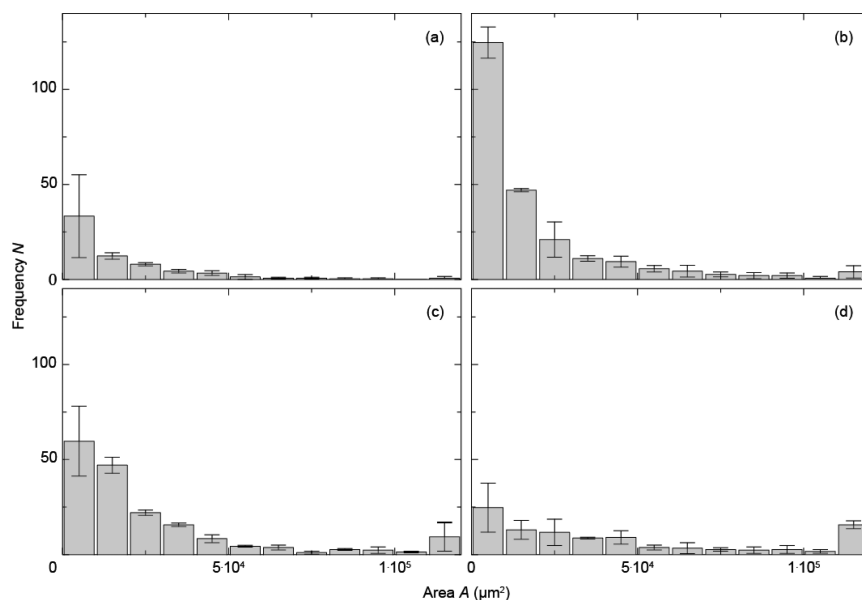


Figure 5. Abundance pattern of electro-sprayed and UV-cured PDMS islands represents characteristic decay. The deposition times are (a) $t = 13 \text{ s}$, (b) $t = 38 \text{ s}$, (c) $t = 63 \text{ s}$, and (d) $t = 88 \text{ s}$.

Langmuir

Article

indicate significant interactions between the droplets en route to or actually on the substrate.

Spectroscopic ellipsometry is a powerful tool for determining the surface morphology of organic films within the illuminated area.¹³ In the present study, we applied this technique to investigate PDMS films after UV curing. To this end, we employed the same experimental conditions for the deposition, i.e., 5 vol % DMS-V21 in ethyl acetate with a flow rate of 267 nL/s and spray times between 13 and 888 s.

The analysis of the experimental ellipsometry data generally requires choosing appropriate models. Here, we assume the validity of the model of nuclei growth within a squared basis, which features width w . Semispherical islands with radius R and height H constitute the UV-cured PDMS. In this model, the corners of the square base are located in the center of the PDMS island. If island size πR^2 equals the cell area of w^2 , a confluent layer is present. In a previous study,¹⁸ Ψ and Δ amplitudes damped by light scattering at the protrusions was simulated using a constant extinction coefficient of the PDMS layer with parameters for the Cauchy equation. In contrast, the nuclei growth model allows for the quantitative description of electrospayed PDMS film morphology. The overlap between model fit and experimentally measured Ψ and Δ data is quantified by the mean-square error (MSE)

$$\frac{1}{N} \sqrt{\sum_{i=1}^N \left\{ \left(\frac{\Psi_i^m - \Psi_i^{th}}{\delta\Psi} \right)^2 + \left(\frac{\Delta_i^m - \Delta_i^{th}}{\delta\Psi} \right)^2 \right\}}$$

As a baseline, ellipsometry data for the Si(100) substrate with the 2–3 nm thin, native oxide layer with parameters for the Cauchy equation were collected.

Figure 7 summarizes the data extracted from the ellipsometer measurements. For the selected deposition times t , mean island height H can be described empirically by using the linear function $H(t) = t/s \times 0.42 \pm 0.03 \text{ nm} + 25.7 \pm 6.4 \text{ nm}$ (cf. Figure 7a). Measurements taken at deposition times of 13 and 38 s reveal mean island heights of 30 ± 5 and 34 ± 5 nm, respectively. Thus, the axis offset $H_0 = 25.7 \pm 6.4$ nm can be interpreted as the minimal island height. This value corresponds to the mean island height measured by means of the AFM (cf. Figure 1, panels (a2) and (a3)).

The coverage shown in the diagram in Figure 7b is the ratio of the area covered by an island and the area of the square unit cell. Linear function $c(t) = t/s \times (0.0064 \pm 0.0013) - (0.0084 \pm 0.056)$ describes the increase in coverage in line with deposition time. The axis intercept related to the setup-specific delay of the spray process matches the delay extracted from the optical micrographs. The coverage extracted from the ellipsometry data corresponds reasonably well to the coverage values derived from the optical micrographs. The differences, especially high for the deposition times 88 and 138 s, are explained by the dissimilarly analyzed areas, which are 4×10 and $4 \times 4 \text{ mm}^2$, respectively.

The linear fit in the diagram in Figure 7b reveals that a spray time of 155 ± 33 s is needed to achieve 100% coverage, which is linked to a mean island height of 91 ± 10 nm.

Instantaneously at spray times above 13 s, the mean island height increases above the minimal island height of about 26 nm. This effect is attributed to a stacking of droplets, and thus the electrospayed film exhibits three-dimensional growth before one single confluent layer occurs.

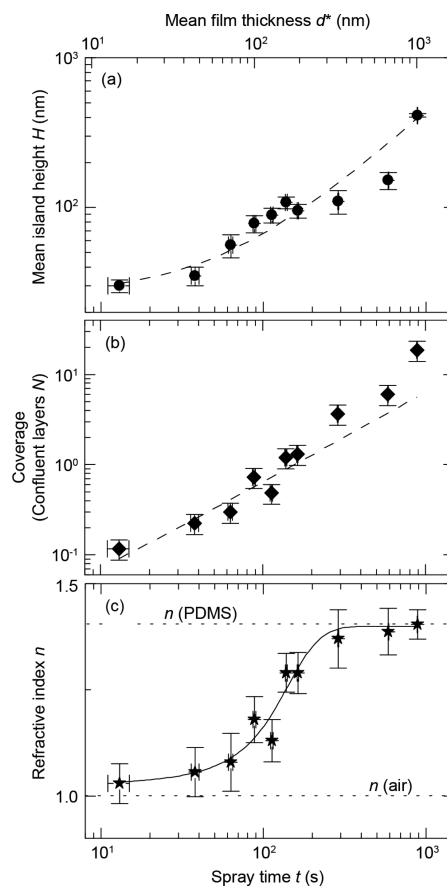


Figure 7. Morphology of the electrospayed and UV-cured PDMS depends on spray duration, as quantified using spectroscopic ellipsometry. Based on the nuclei growth model, mean island height H , diagram (a), the number of confluent PDMS layers N , diagram (b), and the refractive index n , diagram (c), are shown. The dashed lines indicate that island height $H(t)$ and coverage can be described by a linear function of the deposition time. A symmetric step function—similar to the Fermi–Dirac distribution—characterizes changes in the refractive index as the function of deposition time t , which increases from $n_{\text{air}}(632 \text{ nm}) = 1$ to $n_{\text{PDMS}}(632 \text{ nm}) = 1.396$ (both values are indicated by the dotted lines).

Altering the refractive index with the deposition time given in Figure 7c's diagram supports the observation of three-dimensional growth before the confluent layer is formed. The symmetric step-like function $n(t) = 1/\exp(b(t - a) + s_1) + s_2$, with offset constants $s_1 = 2.5$, $s_2 = 1$, and fit parameters $a = (154.7 \pm 10.2) \text{ s}$, $b = (-0.0235 \pm 0.0044) \text{ s}^{-1}$, is utilized to characterize the time dependency of the refractive index between the two extrema $n_{\text{air}}(632 \text{ nm}) = 1$ and $n_{\text{PDMS}}(632 \text{ nm}) = 1.396$. The inflection point at 115 ± 11 s corresponds reasonably well to the deposition time of 155 ± 33 s, at which point the confluent layer forms. For this deposition time the refractive index corresponds to 1.24 ± 0.05 . This value implies the presence of air inclusions and of significant surface roughness. For deposition times above 300 s, however, the refractive index resembles that of PDMS bulk material. Thus,

we state that a compact, nanometer-thin, and smooth PDMS layer of electro-sprayed and cured DMS-V21 is obtained after a deposition time of 300 s. Compact and smooth films of DMS-V21 have also been compared to spin coated films in an earlier investigation for varying flow rates.¹⁸

The advantage of the proposed alternating current source with respect to a static electric field might not only relate to charge accumulation on the substrate but also particularly in the potential to prepare significantly thicker films of comparable smoothness. One might expect that the alternating current mode initially leads to comparably rough films, which heal up as the deposition proceeds.

The value of electro-spraying for the economically efficient preparation of nanometer-thin polymer films is immense, as the technique is the only known alternative to MBD but allows much faster processing in sequential manner. By the use of the alternating voltage mode, one is not restricted to conductive substrates, since charge accumulation is avoided. The parameter space, however, is huge and comprises the molecular weight distribution of the starting material, the choice of the solvent and the concentration of the starting material, the geometrical arrangement of selected nozzles and substrate, and the electrical parameters, namely voltage and frequency. Therefore, much work has to be invested to exploit the method in an industrial environment.

4. CONCLUSIONS

Ac electro-spray deposition and subsequent UV curing allow for fabricating submicrometer-thin, confluent elastomer films on the native oxide of a silicon wafer. For industrial-scale production, multiple nozzle arrangements should be employed, for example to manufacture large-area, multistack DEAs. Using the described experimental setup, which is a prototype for optimizing the parameters for deposition, a rather rough confluent layer about 100 nm thin is obtained. Thicker films made from the polymer DMS-V21 exhibit a smoother surface and are therefore the better choice for DEAs. As a consequence, we conclude that electro-spray deposition with subsequent UV curing is an attractive, fast, and inexpensive alternative to the established techniques currently employed to produce thin PDMS films for low-voltage DEAs.

■ AUTHOR INFORMATION

Corresponding Author

*E-mail bert.mueller@unibas.ch (B.M.).

Funding

The authors gratefully acknowledge the financial support of the Swiss National Science Foundation (project 200021-135496) and the nanotera.ch initiative (project SmartSphincter) as well as the Swiss Nanoscience Institute (SNI) for their financial contribution to the AFM.

Notes

The authors declare no competing financial interest.

■ REFERENCES

- (1) Forrest, S. R. Ultrathin Organic Films Grown by Organic Molecular Beam Deposition and Related Techniques. *Chem. Rev.* **1997**, *97* (6), 1793–1896.
- (2) Johns, I. B.; Smith, J. O.; McElhill, E. A. Thermal Stability of Organic Compounds. *Ind. Eng. Chem. Prod. Res. Dev.* **1962**, *1* (1), 2–6.
- (3) Bar-Cohen, Y. Electroactive Polymers: Current Capabilities and Challenges. *Proc. SPIE* **2002**, *4695*, 1–7.

- (4) Pei, Q.; Pelrine, R.; Stanford, S.; Kornbluh, R.; Rosenthal, M. Electroelastomer Rolls and their Application for Biomimetic Walking Robots. *Synth. Met.* **2003**, *135–136*, 129–131.

- (5) Ozsecen, M. Y.; Sivak, M.; Mavroidis, C. Haptic Interfaces using Dielectric Electroactive Polymers. *Proc. SPIE* **2010**, *7647*, 764737.

- (6) Carpi, F.; Frediani, G.; Turco, S.; De Rossi, D. Bioinspired Tunable Lens with Muscle-like Electroactive Elastomers. *Adv. Funct. Mater.* **2011**, *21*, 4152–4158.

- (7) Shian, S.; Diebold, R. M.; Clarke, D. R. Tunable Lenses using Transparent Dielectric Elastomer Actuators. *Opt. Express* **2013**, *21* (7), 8669–8676.

- (8) Heydt, R.; Kornbluh, R.; Eckerle, J.; Pelrine, R. *Dielectric Elastomers as Electromechanical Transducers: Fundamentals, Materials, Devices, Models and Applications of an Emerging Electroactive Polymer Technology*; Elsevier: Oxford, 2008.

- (9) Rosenthal, M.; Bonwit, N.; Duncheon, C.; Heim, J. Applications of Dielectric Elastomer EPAM Sensors. *Proc. SPIE* **2007**, *6524*, 65241F.

- (10) Jung, K.; Kim, K. J.; Choi, H. R. A Self-sensing Dielectric Elastomer Actuator. *Sens. Actuators, A* **2008**, *143* (2), 343–351.

- (11) Töpfer, T.; Weiss, F.; Osmani, B.; Bippes, C.; Leung, V.; Müller, B. Siloxane-based Thin Films for Biomimetic Low-Voltage Dielectric Actuators. *Sens. Actuators, A* **2015**, *233*, 32–41.

- (12) Valignat, M. P.; Oshanian, G.; Villette, S.; Cazabat, A. M.; Moreau, M. Molecular Weight Dependence of Spreading Rates of Ultrathin Polymeric Films. *Phys. Rev. Lett.* **1998**, *80* (24), 5377–5380.
- (13) Lehmann, D.; Seidel, F.; Zahn, D. R. T. Thin Films with High Surface Roughness: Thickness and Dielectric Function Analysis using Spectroscopic Ellipsometry. *SpringerPlus* **2014**, *3*, 82.

- (14) Nečas, D.; Klapetek, P. Gwyddion: An Open-source Software for SPM Data Analysis. *Open Phys.* **2012**, *10* (1), 181–188.

- (15) Kroon, D.-J. Hessian Based Frangi Vesselness Filter: <http://www.mathworks.com/matlabcentral/fileexchange/24409-hessian-based-frangi-vesselness-filter>.

- (16) Tompkins, H. G.; Irene, E. A. *Handbook of Ellipsometry*; Springer-Verlag GmbH & Co. KG: Heidelberg, 2005.

- (17) Grishaev, V.; Iorio, C. S.; Dubois, F.; Amirfazli, A. Complex Drop Impact Morphology. *Langmuir* **2015**, *31* (36), 9833–9844.

- (18) Weiss, F. M.; Töpfer, T.; Osmani, B.; Deyhle, H.; Kovacs, G.; Müller, B. Electro-Spraying Nanometer-Thin Elastomer for Low Voltage Dielectric Actuators. *Adv. Electron. Mater.* **2016**, DOI: 10.1002/aeml.201500476.

- (19) Vasilets, V. N.; Kovalchuk, A. V.; Ponomarev, A. N. Photooxidation of Siloxane Polymers under Vacuum Ultraviolet Irradiation. *J. Photopolym. Sci. Technol.* **1994**, *7* (1), 165–174.

- (20) Deegan, R. D.; Bakajin, O.; Dupont, T. F.; Huber, G.; Nagel, S. R.; Witten, T. A. Capillary Flow as the Cause of Ring Stains from Dried Liquid Drops. *Nature* **1997**, *389* (6653), 827–829.

- (21) Ladegaard Larsen, A.; Sommer-Larsen, P.; Hassager, O. Some Experimental Results for the End-linked Polydimethylsiloxane Network System. *e-Polym.* **2004**, *4* (1), 548.

- (22) Voué, M.; Valignat, M. P.; Oshanian, G.; Cazabat, A. M.; De Coninck, J. Dynamics of Spreading of Liquid Microdroplets on Substrates of Increasing Surface Energies. *Langmuir* **1998**, *14* (20), 5951–5958.

- (23) Heslot, F.; Fraysse, N.; Cazabat, A. M. Molecular Layering in the Spreading of Wetting Liquid Drops. *Nature* **1989**, *338* (6217), 640–642.

- (24) Bartolo, D.; Josserand, C.; Bonn, D. Singular Jets and Bubbles in Drop Impact. *Phys. Rev. Lett.* **2006**, *96* (12), 124501.

- (25) Müller, B. Natural Formation of Nanostructures: From Fundamentals in Metal Heteroepitaxy to Applications in Optics and Biomaterials Science. *Surf. Rev. Lett.* **2001**, *8*, 169–228.

- (26) Venables, J. A.; Spiller, G. D. T.; Hanbucken, M. Nucleation and Growth of Thin Films. *Rep. Prog. Phys.* **1984**, *47* (4), 399.

- (27) Quintanilla, J. A.; Ziff, R. M. Asymmetry in the Percolation Thresholds of Fully Penetrable Disks with Two Different Radii. *Phys. Rev. E* **2007**, *76* (5), 051115.

2.4 Molecular beam deposition of high-permittivity polydimethylsiloxane for nanometer-thin elastomer films in dielectric actuators

Optimization of a known synthesis allows to obtain a pre-polymer with enhanced electromechanical properties which can be thermally evaporated to form elastomeric nanometer thin films for possible low-voltage dielectric application.

Published in Materials and Design



Contents lists available at ScienceDirect

Materials and Design

journal homepage: www.elsevier.com/locate/matdes

Molecular beam deposition of high-permittivity polydimethylsiloxane for nanometer-thin elastomer films in dielectric actuators

Florian M. Weiss^a, Frederikke B. Madsen^b, Tino Töpfer^a, Bekim Osmani^a, Vanessa Leung^a, Bert Müller^{a,*}^a Biomaterials Science Center, Department of Biomedical Engineering, University of Basel, Gewerbestrasse 14, 4123 Allschwil, Switzerland^b Danish Polymer Centre, Department of Chemical and Biochemical Engineering, Technical University of Denmark, DTU, Søtofts Plads, Bldg. 227, 2800 Kgs. Lyngby, Denmark

ARTICLE INFO

Article history:

Received 12 February 2016
Received in revised form 11 May 2016
Accepted 13 May 2016
Available online 16 May 2016

Keywords:

Dielectric elastomer actuator
Chloropropyl-functional
Vinyl-terminated siloxane co-oligomer
Thermal evaporation
Ultra-violet light curing
Atomic force microscopy
Indentation test
Surface roughness
Spectroscopic ellipsometer

ABSTRACT

To realize low-voltage dielectric elastomer actuators (DEAs) for artificial muscles, a high-permittivity elastomer and a related thin-film deposition technique must be selected. For polydimethylsiloxane, fillers or functionalized crosslinkers have been incorporated into the elastomer to improve dielectric properties. To produce elastomer layers nanometers thin, molecular beam deposition was introduced. We pursue the synthesis of a high-permittivity oligomer, namely a chloropropyl-functional, vinyl-terminated siloxane to be thermally evaporated and subsequent UV curing to form an elastomer. The synthesized oligomer exhibits dielectric permittivity enhanced by 33% and a breakdown increase of 26% with respect to the commercially available oligomer DMS-V05. Films 160 nm thin were fabricated after being evaporated under ultra-high vacuum conditions. Spectroscopic ellipsometry served for film growth monitoring. Using atomic force microscopy, the film surface morphology and mechanics were characterized after growth termination and subsequent curing. The Young's modulus of the elastomer corresponded to (1.8 ± 0.2) MPa and is thus a factor of two lower than that of DMS-V05. Consequently, the properties of the films prepared by the new elastomer can be quantified by the normalized figure of merit, which estimates to 4.6. The presented approach is an essential step toward the realization of low-voltage DEA for medical applications and beyond.

© 2016 Elsevier Ltd. All rights reserved.

1. Introduction

Dielectric elastomer actuators (DEAs) have found a number of applications in tactile displays [1–3], adaptable lenses and gratings [4], sound systems [5], (bio-mimicking) robotics [6–8], and sensors [9,10]. They are well established in research but currently require driving voltages well above 100 V, which makes them unsuitable for use in areas such as medical implants. To expand their potential, a great number of attempts have been made to decrease operating voltages. The most common approach to date in this regard involves enhancing the dielectric properties of the elastomeric material through the use of composite systems or by chemical modification. An alternative, physics-based approach is to reduce the thickness of the elastomer layer to the sub-micrometer level. The resulting ultrathin DEA layers are stacked to provide the required force.

Composite systems containing fillers such as TiO₂ [11,12], BaTiO₃ [13–15], and Al₂O₃ [16] are used to increase the dielectric permittivity of silicone elastomers. Other conducting fillers such as expanded graphite [17], carbon nanotubes [18,19], and encapsulated conducting polymers [20,21] have also been employed. Such composite systems,

however, have the drawback that increased dielectric permittivity is often accompanied by an increased Young's modulus, which in turn reduces achievable strain. Furthermore, composite systems may experience large dielectric losses and reduced breakdown strength, as increases in dielectric permittivity are achieved at loadings near the percolation threshold. Systems near the percolation threshold are prone to filler agglomeration and consequently significant changes in local mechanical properties.

Chemical silicone modifications have been used to create silicone elastomers with increased permittivity, and they lead to a more controlled network structure than composite systems, which depends on the mixing of particles. Furthermore, no free species are present in the networks. Several approaches have been followed to create chemically-modified silicone elastomers with high permittivity. Kussmaul et al. [22], for example, added the synthesized dipolar molecule *N*-allyl-*N*-methyl-*p*-nitroaniline, together with compensating amounts of a hydride-functional cross-linker, to a silicone matrix. Soft silicone elastomers with high permittivity were also prepared by Racles et al. [23], who used cyanopropyl-functional silicones to raise dielectric permittivity, while Madsen et al. used nitrobenzene- and azonitrobenzene-functional cross-linkers [24] and copolymers [25,26]. Very recently, Madsen et al. [27] demonstrated the synthesis and use of chloropropyl-functional, vinyl-terminated siloxane copolymers. The resulting elastomers

* Corresponding author.

E-mail address: bert.mueller@unibas.ch (B. Müller).

were demonstrated to be soft, have a permittivity ϵ' up to 4.7, high breakdown strength, and, very importantly, equally low dielectric loss as the PDMS reference material.

An alternative to changing dielectric properties is lowering the operating voltage by applying thin elastomer layers. As a decrease in thickness leads to a quadratic decrease in the driving voltage required for a given strain, even a small thickness reduction leads to a large payoff. Using molecular beam deposition (MBD), elastomeric polydimethylsiloxane (PDMS) was deposited with film thicknesses in the range of 200 nm [28]. The PDMS thin films could be driven at voltages well below 40 V, marking a promising step forward toward a low-voltage DEA.

Combining elastomers with improved dielectric permittivity with thin-film fabrication in the sub-micrometer range promises to lower the operating voltage more effectively than either of these two approaches can achieve alone. Implementing this combined approach requires a material (i) with high permittivity compared to pure PDMS and (ii) which can be deposited by evaporation under high-vacuum conditions.

Composite systems are inappropriate for fabricating nanometer-thin films via MBD for two reasons. First, there is a high risk of aggregation and imperfections, which will severely influence mechanical and breakdown properties. Second, it is impossible to fabricate films from composite systems by evaporation. Furthermore, as the fabrication of nanometer-thin films by evaporation requires low molecular weight oligomers, materials with bulky and heavy dipolar groups must also be ruled out.

Ideally, the structure of the high-permittivity oligomer should be similar to pure PDMS, since the pure oligomer has previously been deposited successfully by evaporation. Furthermore, it should be possible to produce specific molecular weights of the high-permittivity oligomer, since at a given temperature only oligomers within a narrow molecular weight range can be evaporated. The chloropropyl-functional, vinyl-terminated siloxane copolymers recently synthesized by Madsen et al. [26,27] would satisfy the requirements for application as a high-permittivity nanometer-thin silicone elastomer, provided that their molecular weight can be tailored to the needs of MBD.

In this work we report that we have obtained chloropropyl-functional, vinyl-terminated siloxane co-oligomer with specific molecular weights that are in a suitable range for MBD. Two of these oligomers were characterized and deposited by thermal evaporation under ultra-high vacuum (UHV) conditions. Their film growth was monitored and characterized using *in situ* spectroscopic ellipsometry (SE). Additionally, nanometer-thin films were cured by ultraviolet (UV) radiation, and the resulting films were analyzed using atomic force microscopy (AFM) for nano-indentation and topological measurements.

2. Experimental

2.1. Materials

3-Chloropropylmethyldimethoxysilane, 1,1,3,3,5,5-hexamethyltrisiloxane, dimethoxydimethylsilane, vinyltrimethylsilane, and DMS-V05 were purchased from Gelest Inc. All other chemicals were acquired from Sigma-Aldrich and used as received, unless otherwise stated.

2.2. Synthesis of α,ω -vinyl-poly((chloropropyl)methylsiloxane-co-dimethylsiloxane) (Cl-PDMS)

The synthesis was adapted from a previously described procedure [26] using 3-chloropropylmethyldimethoxysilane (10.00 g, 54.7 mmol) which was dissolved in dry heptane (200 mL) in a 2 L two-neck round-bottomed flask. 1,1,3,3,5,5-hexamethyltrisiloxane (9.36 g, 44.9 mmol) was added, and the mixture was stirred for 5 min. Tris(pentafluorophenyl)borane (7 mL, 0.04 M, 0.2 mol%) in dry toluene

was added and methane gas developed. The mixture was then stirred at room temperature for 1 h, and thereafter excess dimethoxydimethylsilane (23.8 g, 198 mmol) was added in order to quench any potentially remaining hydride groups and to ensure that all oligomers possessed methoxy end groups. The reaction mixture was stirred additionally for a couple of hours. The solvent and excess dimethoxydimethylsilane (bp: 82 °C) were removed *in vacuo* at a temperature of 45 °C with toluene, to make the product a clear oil. The product was thereafter re-dissolved in heptane (75 mL), vinyltrimethylsilane (40 g, 464 mmol) was added, and the mixture was then stirred overnight, after which ¹H NMR was used in order to confirm the removal of methoxy groups and conversion to vinyl groups. Neutral aluminum oxide (20 g) was added to the reaction mixture to remove the tris(pentafluorophenyl)borane catalyst, and the solution was then filtered. The solvent and excess vinyltrimethylsilane reagents were removed *in vacuo*, to make the product a clear oil (16.02 g, 91%). SEC (Toluene): $M_n = 791$ g/mol, $M_w = 1116$ g/mol. IR measurements provided the following vibration modes (wave numbers): 3050 cm^{-1} for the Si–CH=CH₂ stretch, 2960 cm^{-1} for the C–H stretch, 1600 cm^{-1} for the Si–CH=CH₂ stretch, 1410 cm^{-1} for the Si–CH₂ and Si–CH=CH₂ stretches, 1260 cm^{-1} for the Si–CH₃ stretch, and 1055 cm^{-1} for the Si–O stretch. ¹H NMR (CDCl₃, δ_{H} , ppm): 0.08–0.1 (m, ~80H, CH₃–Si), 0.65 (m, ~8H, –Si–CH₂–CH₂–), 1.82 (m, ~8H, –CH₂–CH₂–CH₂), 3.50 (t, ~8H, ³J = 6.9 Hz, Cl–CH₂–CH₂), 5.73 (dd, 2H, ²J = 4.2 Hz, ³J = 20 Hz, CH=CH₂), 5.94 (dd, 2H, ²J = 4.2 Hz, ³J = 15 Hz, CH=CH₂), 6.12 (dd, 2H, ²J = 15 Hz, ³J = 20 Hz, –CH=CH₂). ¹³C NMR (CDCl₃, δ_{C} , ppm): –0.75 to 1.08 (c + d + h), 15.67 (e), 26.71 (f), 47.59 (g), 131.86 (a), 139.10 (b).

2.3. Characterization of DMS-V05 and Cl-PDMS

Fourier transform infrared (FTIR) spectroscopy was performed on a Thermo Scientific iS50 equipped with a diamond crystal attenuated total reflection (ATR) sampling accessory. Spectra were recorded in the range of 4000 to 400 cm^{-1} . ¹H and ¹³C NMR experiments were performed on a Bruker 300 MHz spectrometer in CDCl₃, while size-exclusion chromatography (SEC) was performed on a Tosoh EcoSEC HLC-8320GPC instrument equipped with IR and UV detectors and SDV Linear S columns from PSS. Samples were run in toluene at a temperature of 35 °C at a rate of 1 mL min^{–1}, and molar mass characteristics were calculated using WinGPC Unity 7.4.0 software and linear PDMS standards acquired from PSS. Thermal gravimetric analysis (TGA) was performed on a TA Discovery TGA from TA Instruments, and measurements were carried out in a nitrogen atmosphere at a heating rate of 10 K min^{–1}, from room temperature to 800 °C, while differential scanning calorimetry (DSC) measurements were performed on a TA Discovery DSC from TA Instruments. The DSC thermal analyses were performed at a heating and cooling rate of 10 K min^{–1} from –150 to 200 °C. Dielectric relaxation spectroscopy (DRS) was performed on a Novocontrol Alpha-A high-performance frequency analyzer (Novocontrol Technologies GmbH & Co) operating in the frequency range 10² to 10⁷ Hz at room temperature. The liquid oligomer samples were added to a Teflon ring with a diameter of 25 mm, which was attached to a bottom electrode. Dielectric breakdown strengths were measured on an in-house-built device based on international standards. The liquid oligomers DMS-V05 and Cl-PDMS were dropped into a Teflon ring, which was mounted on the bottom spherical electrode. The top spherical electrode was then adjusted to a distance of 100 μm between the electrodes, and a stepwise increasing voltage was applied until breakdown was observed in the form of a spark and noise between the electrodes. After the breakdown a black breakdown point was seen within the sample.

2.4. Nanometer-thin film preparation by MBD

The PDMS thin films were thermally evaporated and deposited under ultra-high vacuum conditions. The base pressure in the chamber

was 10^{-9} mbar, and the oligomers DMS-V05 and CI-PDMS were filled in a crucible without any purification and then evaporated using low-temperature effusion cells (NTEZ, Dr. Eberl MBE Komponenten GmbH, Weil der Stadt, Germany) with a 25 cm^3 crucible for DMS-V05 and a 2 cm^3 crucible for CI-PDMS. DMS-05 was evaporated at a crucible temperature of $130 \text{ }^\circ\text{C}$ and CI-PDMS at a temperature of $199 \text{ }^\circ\text{C}$. As substrates, 2-in. n-doped Si-wafers (SIEGERT WAFER GmbH, Aachen, Germany) with a thickness of $(279 \pm 25) \mu\text{m}$ were used. They were rotated at a speed of 1.2 rpm and a distance of 30 mm at room temperature. The films were cured during and after deposition by exposing them to UV radiation from an externally mounted source (H2D2 light source L11798, Hamamatsu, Japan) through a CaF window for a period of 20 h 50 min.

2.5. Real-time spectroscopic ellipsometry

To examine real-time deposition, a spectroscopic ellipsometer (SE801, Sentech, Berlin, Germany) with SpectraRay3 software was used. The detected spectrum, monitored at a frequency of 1 Hz and an incident angle of 70° , ranged from 190 to 1050 nm, and an incident beam diameter of 4 mm resulted in a measurement spot of $4 \times 10 \text{ mm}^2$. The obtained wavelength-dependent Ψ and Δ values, or the Fourier coefficients S1 and S2, are related to the complex Fresnel reflection coefficients r_p and r_s of p (parallel) and s (perpendicular) polarized light and their ratio ρ by

$$\rho = r_p/r_s = \tan\Psi \cdot e^{i\Delta}. \tag{1}$$

With the obtained Fresnel reflection coefficient ratio it is possible to extract the wavelength-dependent dielectric function $\tilde{n}(\lambda)$

$$(\tilde{n})^2 = ((n) + i(k))^2 = \sin(\phi_0)^2 \cdot \left(1 + \tan(\phi_0)^2 \left(\frac{1-\rho}{1+\rho} \right)^2 \right). \tag{2}$$

where ϕ_0 represents the angle of the incident beam, $n(\lambda)$ the real and $k(\lambda)$ the imaginary parts of the refractive index, respectively. To determine the linear and first-order non-linear refractive index of DMS-V05 and CI-PDMS a measurement of a spin-coated, 150 nm-thick film of each oligomer was conducted and resulted in $n_0 = 1.384 \pm 0.001$, $n_1 = 22.3 \pm 0.1$, $n_2 = 24.7 \pm 0.1$ for DMS-V05 and $n_0 = 1.418 \pm 0.001$, $n_1 = 22.3 \pm 0.1$, and $n_2 = 20.0 \pm 0.1$ for the CI-PDMS. These values were approximated using the Cauchy series of the refractive index $n(\lambda) = n_0 + c_1 n_1/\lambda^2 + c_2 n_2/\lambda^4$ with $c_1 = 10^2 \text{ nm}^2$ and $c_2 = 10^4 \text{ nm}^2$, whereas the extinction coefficient k was kept at zero.

To determine the growth mechanism, a Cauchy layer and an effective medium approximation (EMA) model were applied. The Cauchy layer model represents the simplest approach and assumes a perfect plane parallel surface and two-dimensional growth. Bruggeman's EMA model [29] includes surface roughness induced by the nucleation centers. The uppermost layer, consisting of clusters and voids (or inclusions), is considered as having an effective dielectric or optical property deduced from equal fractional parts of the deposited and void material, cf. Eq. (3) below.

$$0 = \sum_{i=1}^N f_i \frac{n_{\sim i}^2 - n_{\sim e}^2}{n_{\sim i}^2 + 2n_{\sim e}^2}. \tag{3}$$

Table 1

Number average molecular weights M_n and weight average molecular weights M_w obtained by SEC for the different fractions of the thermally evaporated DMS-V05 under ultra-high vacuum conditions.

	DMS-V05 (original)	DMS-V05 (residue)	DMS-V05 (deposited)
M_n	807 g/mol	1560 g/mol	944 g/mol
M_w	1364 g/mol	1910 g/mol	1033 g/mol

Table 2

SEC results of CI-PDMS and DMS-V05 for comparison.

	DMS-V05 (deposited)	CI-PDMS
M_n	944 g/mol	791 g/mol
M_w	1033 g/mol	1116 g/mol.

The EMA is only applicable if the measured system fulfills two key assumptions: (i) The surface roughness/nucleation centers are smaller than the minimum wavelength, in order to ignore light scattering, and (ii) dielectric function has to be size- and shape-independent. For the thermally evaporated PDMS, both of these key points were fulfilled. For the evaluation of the data the void fraction was set to 0.5, which is reasonable according to Fujiwara et al. [30].

For the evaluation of the models the mean square error (MSE) of the divergence from the obtained fit to the acquired data was compared. The MSE is defined in Eq. (4).

$$\text{MSE} = \frac{1}{N} \sqrt{\sum_{i=1}^N \left\{ \left(\frac{\Psi_i^m - \Psi_i^{th}}{\delta\Psi} \right)^2 + \left(\frac{\Delta_i^m - \Delta_i^{th}}{\delta\Psi} \right)^2 \right\}} \tag{4}$$

2.6. Atomic force microscopy

The mechanical properties of the evaporated and UV cross-linked polymer structures were assessed using AFM spectroscopic methods (FlexAFM C3000, Nanosurf AG, Switzerland). Here, 900 indentation measurements on $30 \mu\text{m} \times 30 \mu\text{m}$ arrays were acquired at loads of 25 and 10 nN, using a soft cantilever with a spherical tip ($R = 150 \text{ nm}$, B150_CONTR, Nanotools GmbH, Germany). Calculations were based on the Johnson-Kendall-Roberts (JKR) model of elastic contact theory incorporating adhesion effects. The software employed in this instance was developed by Nanosurf AG (FLEX-ANA®, Automated Nanomechanical Analysis) to perform calculations for each force distance curve. Potential effects of the Si substrate were neglected, since the indentation depths were below 50 nm.

Surface topology measurements ($5 \times 5 \mu\text{m}^2$, tapping mode, vibration amplitude 370 mV (DMS-V05), and a 1.22 V (CI-PDMS) set point 5%) were performed using a FlexAFM System (Nanosurf AG, Liestal, Switzerland). In total, 1024 lines at speeds of 0.982 s (DMS-V05) and 4.94 s (CI-PDMS) were acquired for each image, using a non-contact soft tapping AFM probe (Tap190Al-G probe, NanoAndMore GmbH, Wetzlar, Germany). The root-mean-squares of the surface values were calculated using Gwyddion 2.41 software (Gwyddion: Open-source software for SPM data analysis, <http://gwyddion.net>).

3. Results and discussion

3.1. Oligomer characterization and comparison

The molecular weight characteristics of DMS-V05 were obtained using size exclusion chromatography (SEC). The oligomer DMS-V05, as purchased, was evaporated under UHV conditions as stated in Section 2.4. Subsequently, the deposited material and the residue in the crucible were harvested for SEC. The experimental data for the molecular weights of these three species are listed in Table 1.

Table 3

Dielectric breakdown strengths of the liquid oligomers DMS-V05 and CI-PDMS.

	Thickness (μm)	Voltage at breakdown (kV)	Breakdown strength (V/ μm)
DMS-V05	100	1.01 ± 0.03	10.1 ± 0.3
CI-PDMS	100	1.27 ± 0.05	12.7 ± 0.5

Table 4
Summary of properties of DMS-V05 and CI-PDMS as well as figure of merit calculations.

	Dielectric permittivity	Breakdown strength	Young's modulus	Normalized figure of merit
	ϵ'	E_B (V/ μm)	Y (MPa)	$F_{om}/F_{om,ref}$
DMS-V05	3	10.1 ± 0.3	3.9 ± 0.3	1
CI-PDMS	4	12.7 ± 0.5	1.8 ± 0.2	4.6

Knowing the weight properties of the commercially available 'standard' oligomer, the target molecular weight should be in the same range as the deposited PDMS. Hence, a siloxane co-oligomer with dielectric permittivity-enhancing chloropropyl groups was synthesized according to the described procedure [26], though this was modified to create a low-molecular weight co-oligomer. The co-oligomer was prepared from commercially available starting materials through the tris(pentafluorophenyl)borane-catalysed Piers-Rubinsztajn condensation reaction of 3-chloropropylmethyldimethoxysilane and the hydride-terminated dimethylsiloxane molecule 1,1,3,3,5,5-hexamethyltrisiloxane, which constituted the spacer unit between the functional chloropropyl groups. The chosen quantities of the precursors resulted in co-oligomers containing approximately four chloropropyl-functional groups. The co-oligomer was then end-functionalized with vinyl groups to allow for UV-initiated cross-linking reactions. The structure and reactive pathway for the resulting co-oligomer, α,ω -vinylpoly((chloropropyl)methylsiloxane-co-dimethylsiloxane) (CI-PDMS), can be seen in Scheme 1.

The aim of the synthesis from a molecular weight point of view was to achieve a molecular weight in the range of 'DMS-V05 deposited', cf. Table 1, since this is the molecular weight that is actually evaporated during sample preparation. As seen in Table 2, oligomer CI-PDMS has a molecular weight comparable to 'DMS-V05 deposited', albeit a slightly higher polydispersity index.

The prepared co-oligomer, CI-PDMS, as well as the commercial oligomer, DMS-V05, were characterized with FTIR and ^1H and ^{13}C NMR. FTIR spectra can be found as supporting information, and, as expected, there are no major differences between DMS-V05 and CI-PDMS in their FTIR spectra. Peaks associated to the chloropropyl group are very weak but can be observed at frequencies of 1310 and 910 cm^{-1} whereas the one at 860 cm^{-1} is invisible due to the overlap of the strong peak from the Si-CH₃ absorption [31]. The results of ^1H NMR measurements of CI-PDMS are summarized in the experimental section. The ^1H NMR spectra of both CI-PDMS and DMS-V05 are furthermore given as supporting information. It is clear that CI-PDMS is structurally different from DMS-V05. Both oligomers possess peaks for Si-CH₃ protons at $\delta_{\text{H}} = 0.08$ –0.1 ppm as well as -CH=CH₂ protons in the form of three distinctive doublets of doublets at $\delta_{\text{H}} = 5.7$ –6.1 ppm. The CI-PDMS oligomers conversely have three distinctive multiplets, representing the protons from each of the -CH₂- groups in the chloropropyl-functionality at $\delta_{\text{H}} = 0.65$, 1.82 and 3.50 ppm, respectively. ^{13}C NMR corroborated these results for CI-PDMS through resonances at $\delta_{\text{C}} = 15.67$, 26.71 and 47.59 ppm, for the -CH₂- carbon atoms in the propyl-chain, and resonances at $\delta_{\text{C}} = 131.86$ and 139.10 ppm for the two carbon atoms in the vinyl groups (-CH=CH₂).

The effect of molecular structure on the thermal behavior of the two oligomers was measured by DSC. The measured thermograms are presented in the supporting information. Both DMS-V05 and CI-PDMS

show glass transition temperatures T_g well below -100 °C, which is characteristic for siloxanes. None of the oligomers exhibit a clear crystallization temperature T_c , but DMS-V05 does show a small melting peak T_m . For CI-PDMS, no T_c or T_m is observed, which means that the oligomer does not crystallize. This behavior points to the successful formation of spatially well-separated chloropropyl-functional groups along the oligomer backbone.

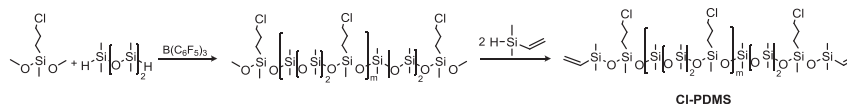
The thermal behavior and stability of the oligomers DMS-V05 and CI-PDMS was measured with TGA. As seen in the thermogram, evaporation for CI-PDMS starts at a lower temperature than for DMS-V05, which may be due to a larger fraction of small molecules such as residual solvent, starting materials, and smaller oligomers. After this initial evaporation, oligomer evaporation starts at approximately 150 °C, which is comparable to DMS-V05. Polysiloxanes are known for their thermal stability. Decomposition phenomena, however, cannot be ruled out. As clear from Fig. 1, the degradation of higher molecular weight fractions starts at temperatures well above 300 °C.

Dielectric permittivity of CI-PDMS oligomer was measured by dielectric relaxation spectroscopy, and the results are shown in the supporting information. At a frequency of 100 Hz the CI-PDMS oligomer gives rise to $\epsilon' = 4.0$ and DMS-V05 to $\epsilon' = 3.0$, which is a 33% increase in permittivity. Furthermore, dielectric losses remain relatively low for the CI-PDMS oligomer.

It was impossible to measure the dielectric breakdown strength of cured samples, using traditional methods [32], due to the nanometer-sized thicknesses of the films, which makes handling too difficult. Furthermore, measured breakdown strength depends strongly on the elastomer's film thickness [33,34]. Instead, the breakdown strengths of the liquid, low-viscosity oligomers, DMS-V05 and CI-PDMS, were measured. The results are presented in Table 3. It can be seen that the dielectric breakdown strength of CI-PDMS is approximately 25% higher than that for DMS-V05. Since the measurements were performed on liquid samples, there is no dependency regarding the stiffness of the samples, which is observed for elastomers [35–37]. Here, the breakdown strength has been found to scale linearly – or even exponentially – with the Young's modulus. Therefore, the results give a clear indication that the breakdown strength of CI-PDMS in the cured state would also be higher than that of DMS-V05 in the cured state at comparable Young's moduli.

3.2. Nanometer-thin film deposition

During deposition under UHV conditions spectroscopic ellipsometry data was acquired, in order to characterize the island and film growth of the oligomers. The successful evaluation of the data, using the Cauchy layer (CL) and the effective medium approximation (EMA), as introduced by Bruggeman, is shown in Fig. 2, where the diagrams in (a) and (b) represent the oligomer layer thicknesses derived from the CL model for DMS-V05 and CI-PDMS, respectively. Diagrams (c) and (d) show EMA layer thicknesses, which are plotted against the deposition time. The time scales differ by a factor of ten. Obviously, the oligomers grow according to the CL model, and during the initial stages of deposition the films grow relatively quickly. The point of inflection, related to the maximal deposition rate, is already reached between 10 and 20 nm, following which deposition time eventually decreases. Applying the EMA model and considering surface roughness, the data reveal that for DMS-V05 the surface is intrinsically flat, thus indicating two-dimensional growth. During the initial growth stages of CI-PDMS, EMA layer



Scheme 1. Synthetic route for chloropropyl-functional siloxane co-oligomer CI-PDMS.

110

F.M. Weiss et al. / Materials and Design 105 (2016) 106–113

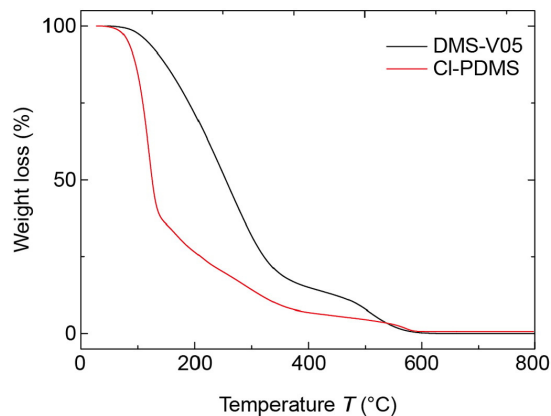


Fig. 1. TGA thermograms of DMS-V05 and Cl-PDMS. The Cl-PDMS shows a first shoulder at a temperature of 140 °C attributed to the loss of precursor and solvent molecules. For both oligomers a shoulder is observed at a temperature of about 350 °C, being a known value for the decomposition of dimethylsiloxane fluids.

thickness seems to fluctuate around a mean value of about 2.5 nm. A maximum EMA thickness of 12 nm is reached at 4800 s, thereby indicating that up to this time three-dimensional growth dominates. Subsequently, film growth switches to the layer-by-layer mode.

The observed three-dimensional growth during the early stages of Cl-PDMS deposition is attributed to the increased polarity of the chloropropyl side chains, as a result of which wettability seems to decrease and therefore islands form. This polarity increase also explains the relatively high evaporation temperature related to the slow deposition rate, which is due to stronger interactions between the molecules. Another source for the deposition rate difference is the crucible size, in

that the larger the crucible, the larger its surface and the related number of molecules that evaporate.

After DMS-V05 deposition the UV curing was continued. During this treatment, the parameters S1 and S2 were monitored to detect the associated changes of the film properties. After a period of 21 h the parameters S1 and S2 continuously acquired could be considered as constant. This behavior was interpreted as termination of the curing process.

3.3. Comparison of UV-cured DMS-V05 and Cl-PDMS

Comparing the wavelength-dependent refractive indices of DMS-V05 and Cl-PDMS, before and after post-deposition curing, see Fig. 3, two observations arise. First, the refractive index of Cl-PDMS exceeds the one of DMS-V05. Second, curing increases the refractive indices of the two oligomers. In the case of DMS-V05 the increase is more pronounced. It is interesting to note that for Cl-PDMS one observes a slight ratio decrease in the refractive indices after-to-before curing in line with increasing wavelength, whereas for DMS-V05 it increases slightly.

The larger refractive index of Cl-PDMS with respect to DMS-V05 originates from the polarity of the chloropropyl-functional co-oligomer. This observation provides further evidence that Cl-PDMS has the higher dielectric permittivity, since the refractive index and permittivity are proportional, linked *via* the complex dielectric function. The increase in the refractive index, owing to cross-linking, is related to the curing reaction mechanism not being fully understood yet. During the UV irradiation, two mechanisms may occur simultaneously. First, IR spectroscopy showed a diminished concentration of the vinyl groups [28]. Second, it has been reported that high-energy radiation cleaves the Si–C and CH₂–H bonds [38]. The cleavage of the Si–C bond eventually induces the formation of SiO₂ [39]. Thus, the refractive index leans more toward SiO₂, which corresponds to 1.460 at 632 nm [40]. The greater increase in the refractive index of DMS-V05 is attributed to the higher number of methyl groups present compared to Cl-PDMS. This finding has been supported by Yahya et al. [41], who investigated the refractive index

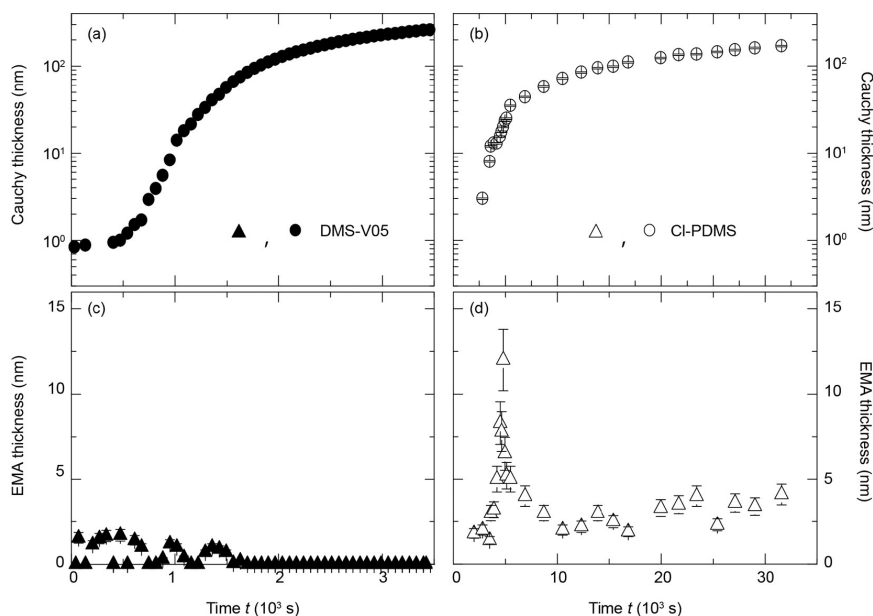


Fig. 2. Deposition data of DMS-V05 and Cl-PDMS acquired *in situ* by spectroscopic ellipsometry. Diagrams (a) DMS-V05 and (b) Cl-PDMS were obtained by applying the Cauchy model. The data in diagrams (c) DMS-V05 and (d) Cl-PDMS correspond to the effective medium approximation.

with respect to cross-link density. Interestingly the Si–C bond of the chloropropyl side chain tends to be more stable against the UV light than the methyl group. This behavior is indicated by the presence of chloride in the energy dispersive X-ray spectra of the film as well as by the FTIR measurements exhibiting the related absorption peak at 1310 cm^{-1} .

Nano indentation, obtained by atomic force microscopy, was not analyzed using the Hertz contact model, since the adhesion forces are in the range of the applied forces. Therefore, the Johnsons-Kandall-Robers model [42], which considers adhesion forces, was applied to evaluate force distance curves, with the goal of extracting the Young's moduli. Fig. 4 displays the histograms of the 900 indentation measurements performed on each polymer film. The indentation depth for DMS-V05 was $(26 \pm 1)\text{ nm}$ and for CI-PDMS $(38 \pm 2)\text{ nm}$. The Young's modulus of 160 nm -thin CI-PDMS films is a 2.2 factor lower than that of DMS-V05, as shown in Fig. 4. This result relates to the cross-link density of CI-PDMS, owing to the lower number of methyl groups and bulky side chains.

By measuring stiffness profiles from the center toward the rim of the substrate, one recognizes that the Young's modulus decreases. This behavior is understandable, because UV radiation determines the degree of curing. Furthermore, we observed a skin effect present at the intermediate curing stages. After indentation the AFM camera shows the impression crater, which vanishes over time. This viscoelastic behavior is presumably due to a liquid phase below the skin layer. As the curing starts from the surface, the formation of a skin layer at intermediate curing stages sounds reasonable.

Fig. 5 presents the characteristic force-distance curves of the nano-indentation measurements. Pull-off force, also termed adhesion force, $F_{\text{adh}2} = (20.5 \pm 0.3)\text{ nN}$ for CI-PDMS is slightly greater than adhesion force $F_{\text{adh}1} = (17.7 \pm 0.2)\text{ nN}$ for DMS-V05. The area below the zero force of retracting curves generally corresponds to the adhesion works $W_{\text{adh}1}$ and $W_{\text{adh}2}$ describing the energy the cantilever has to overcome to get back into the zero-force regime. The work of adhesion W_{adh} per unit area for a spherical tip on a flat surface, according to the JKR model, can be calculated from the tip radius R [43]:

$$W_{\text{adh}} = \frac{2F_{\text{adh}}}{3\pi R} \quad (5)$$

Adhesion force depends on material properties and on surface roughness [43]. AFM measurements allow for determining surface roughness $S_q = (0.898 \pm 0.001)\text{ nm}$ for CI-PDMS and (0.425 ± 0.001)

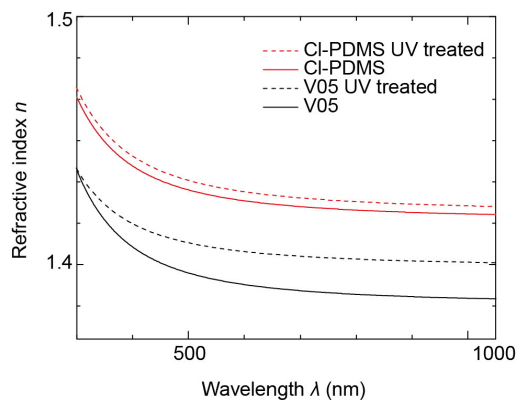


Fig. 3. Refractive indices of DMS-V05 (black) and CI-PDMS (red) measured by means of spectroscopic ellipsometry. The solid lines represent data obtained after deposition, and the dotted lines values after UV curing. (For interpretation of the references to color in this figure legend, the reader is referred to the web version of this article.)

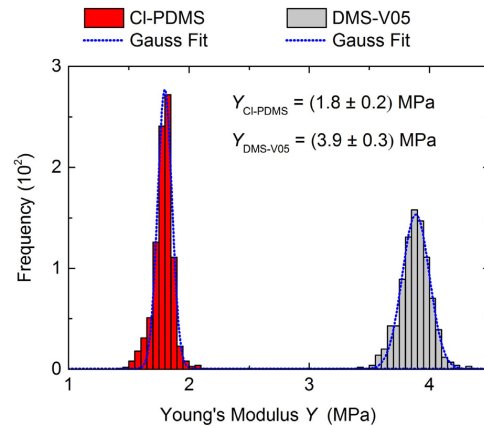


Fig. 4. Young's modulus of cured DMS-V05, in grey, and CI-PDMS, in red, measured by AFM nano-indentation. Both samples have a thickness of 160 nm and were UV irradiated for 20 h and 50 min . (For interpretation of the references to color in this figure legend, the reader is referred to the web version of this article.)

nm for DMS-V05. Differences in surface roughness, cf. Fig. 6, give rise to the value of $W_{\text{adh}}(\text{CI-PDMS}) = 29\text{ mJ/m}^2$ compared to $W_{\text{adh}}(\text{DMS-V05}) = 25\text{ mJ/m}^2$, as described by the adhesion observed on artificially roughened PDMS surfaces [44].

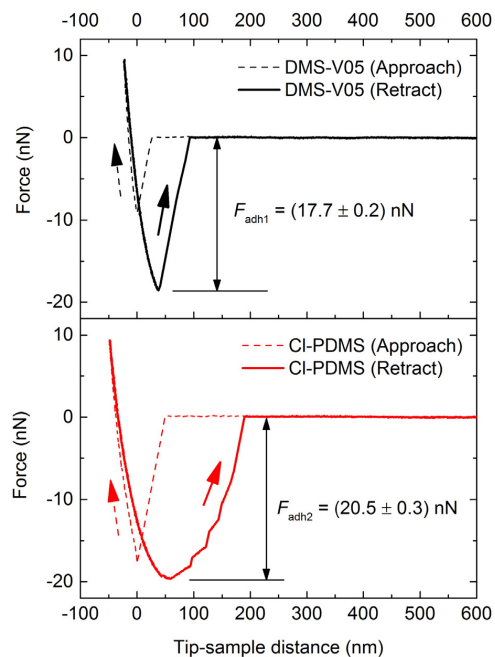


Fig. 5. Force-distance curves are converted from the deflection of the cantilever and the z-piezo position for the deposited and cured films. The black dashed and solid lines represent the approach and the retracting curves of DMS-V05, respectively, whereas the red lines are for CI-PDMS. Negative values indicate the indentation depth of the tip. The error for adhesion forces $F_{\text{adh}1}$ and $F_{\text{adh}2}$ corresponds to the standard deviation of the Gaussian fit applied to the adhesion histograms. (For interpretation of the references to color in this figure legend, the reader is referred to the web version of this article.)

The surface roughness of the cured films, derived from the AFM measurements and depicted in Fig. 6, mirrors the values found by the spectroscopic ellipsometry experiments presented in Section 3.2.

To compare dielectric elastomers, P. Sommer-Larsen and A. Ladegaard Larsen [45] defined a single parameter, namely the *figure of merit* F_{om} , which depends on the dielectric constant, dielectric breakdown strength, and the Young's modulus of the elastomer:

$$F_{om} = \frac{3\epsilon' E_B^2}{Y}$$

The figure of merit is often normalized to a reference material. In the present communication, we take DMS-V05 as a reference and hence obtain 4.6 for CI-PDMS, cf. Table 4. As the figure of merit can be used to optimize elastomer properties for dielectric elastomer actuators [45], it demonstrates that CI-PDMS is a much better choice for fabricating low-voltage DEAs.

4. Conclusion

The chloropropyl-functional co-oligomer CI-PDMS can be synthesized with a molecular weight adapted for thermal evaporation under vacuum conditions. Therefore, it can be readily compared with the

commercially available oligomer DMS-V05. This choice supports the direct comparison with other starting materials for the preparation of polymer films for DEA applications. With a 33% increased dielectric constant and a greater than two-fold reduction in the Young's modulus, the used CI-PDMS is much better suited than the commercially available DMS-V05 for preparing nanometer-thin films for low-voltage DEAs.

The nanometer-thin polymer films are not only difficult to handle for characterization purposes, but need to be significantly improved to reach a defect level that enables their reliable use for the desired sensor and actuator applications.

Acknowledgements

The authors acknowledge helpful discussions with Anne Ladegaard Skov and the active support of Liyun Yu (dielectric spectroscopy and dielectric breakdown measurements on liquid samples). Furthermore, the financial support of the Swiss National Science Foundation (project 200021-135496), the Nano-tera.ch Initiative (project SmartSphincter), the Danish Council for Independent Research, and the Swiss Nanoscience Institute (SNI) for their financial contribution to the AFM is gratefully acknowledged.

References

- [1] P. Chakraborti, H.A.K. Toprakci, P. Yang, N. Di Spigna, P. Franzon, T. Ghosh, A compact dielectric elastomer tubular actuator for refreshable Braille displays, *Sensors Actuators A Phys.* 179 (2012) 151–157.
- [2] R. Heydt, S. Chhokar, Refreshable braille display based on electroactive polymers, *Proc. Int. Disp. Res. Conf.* (2003) 5.
- [3] Z. Yu, W. Yuan, P. Brochu, B. Chen, Z. Liu, Q. Pei, Large-strain, rigid-to-rigid deformation of bistable electroactive polymers, *Appl. Phys. Lett.* 95 (2009) 192904.
- [4] L. Maffli, S. Rosset, M. Ghilardi, F. Carpi, H. Shea, Ultrafast all-polymer electrically tunable silicone lenses, *Adv. Funct. Mater.* 25 (2015) 1656–1665.
- [5] R. Heydt, R. Kornbluh, J. Eckerle, R. Pelrine, Sound radiation properties of dielectric elastomer electroactive polymer loudspeakers, *Proc. SPIE* 6168 (2006) (61681M-M-8).
- [6] I.A. Anderson, T.A. Gisby, T.G. McKay, B.M. O'Brien, E.P. Calius, Multi-functional dielectric elastomer artificial muscles for soft and smart machines, *J. Appl. Phys.* 112 (2012) 041101.
- [7] K. Gabor, L. Patrick, W. Michael, An arm wrestling robot driven by dielectric elastomer actuators, *Smart Mater. Struct.* 16 (2007) S306.
- [8] R. Pelrine, R.D. Kornbluh, Q. Pei, S. Stanford, S. Oh, J. Eckerle, et al., Dielectric elastomer artificial muscle actuators: toward biomimetic motion, *Proc. SPIE* 4695 (2002) 126–137.
- [9] K. Jung, K.J. Kim, H.R. Choi, A self-sensing dielectric elastomer actuator, *Sensors Actuators A Phys.* 143 (2008) 343–351.
- [10] M. Rosenthal, N. Bonwit, C. Duncheon, J. Heim, Applications of dielectric elastomer EPAM sensors, *Proc. SPIE* 6524 (2007) (65241F-F-7).
- [11] F. Carpi, D.D. Rossi, Improvement of electromechanical actuating performances of a silicone dielectric elastomer by dispersion of titanium dioxide powder, *IEEE Trans. Dielectr. Electr. Insul.* 12 (2005) 835–843.
- [12] G. Ouyang, K. Wang, X.Y. Chen, TiO₂ nanoparticles modified polydimethylsiloxane with fast response time and increased dielectric constant, *J. Micromech. Microeng.* 22 (2012) 074002.
- [13] G. Gallone, F. Galantini, F. Carpi, Perspectives for new dielectric elastomers with improved electromechanical actuation performance: composites versus blends, *Polym. Int.* 59 (2010) 400–406.
- [14] Z. Zhang, L. Liu, J. Fan, K. Yu, Y. Liu, L. Shi, et al., New silicone dielectric elastomers with a high dielectric constant, *Proc. SPIE* 6926 (2008) 692610–692618.
- [15] L. Jiang, A. Betts, D. Kennedy, S. Jerrams, Improving the electromechanical performance of dielectric elastomers using silicone rubber and dopamine coated barium titanate, *Mater. Des.* 85 (2015) 733–742.
- [16] P. Lotz, M. Matysek, P. Lechner, M. Hamann, H.F. Schlaak, Dielectric elastomer actuators using improved thin film processing and nanosized particles, *Proc. SPIE* 6927 (2008) (692723–10).
- [17] A. Egede Dagaard, S.S. Hassouneh, M. Kostrzewska, A.G. Bejenariu, A.L. Skov, High-dielectric permittivity elastomers from well-dispersed expanded graphite in low concentrations, *Proc. SPIE* 8687 (2013) (868729–11).
- [18] I. Chen, C. Liu, K. Liu, C. Meng, C. Hu, J. Wang, et al., High-performance, low-voltage, and easy-operable bending actuator based on aligned carbon nanotube/polymer composites, *ACS Nano* 5 (2011) 1588–1593.
- [19] L.Z. Chen, C.H. Liu, C.H. Hu, S.S. Fan, Electrothermal actuation based on carbon nanotube network in silicone elastomer, *Appl. Phys. Lett.* 92 (2008) 263104.
- [20] M. Molberg, D. Crespy, P. Rupper, F. Nüesch, J.-A.E. Månson, C. Löwe, et al., High breakdown field dielectric elastomer actuators using encapsulated polyaniline as high dielectric constant filler, *Adv. Funct. Mater.* 20 (2010) 3280–3291.
- [21] D.M. Opris, M. Molberg, C. Walder, Y.S. Ko, B. Fischer, F.A. Nüesch, New silicone composites for dielectric elastomer actuator applications in competition with acrylic foil, *Adv. Funct. Mater.* 21 (2011) 3531–3539.

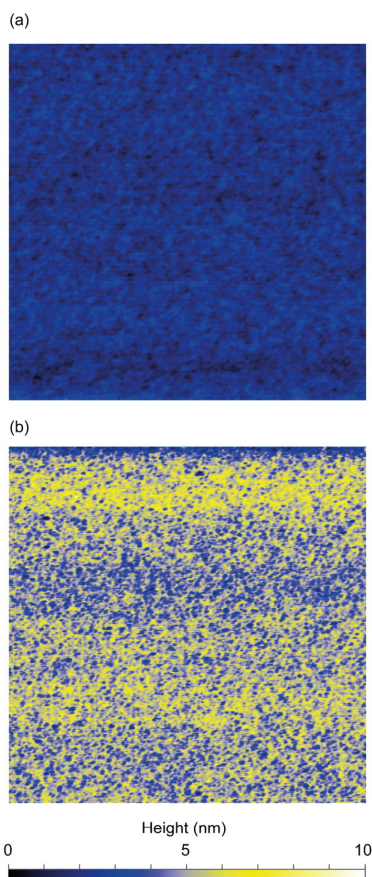


Fig. 6. AFM images of UV-cured surfaces for (a) DMS-V05 and (b) CI-PDMS. The scan size for both images is $5 \times 5 \mu\text{m}^2$. The surface roughness for the CI-PDMS film is more than twice the value of the DMS-V05 film.

- [22] B. Kussmaul, S. Risse, G. Kofod, R. Waché, M. Wegener, D.N. McCarthy, et al., Enhancement of dielectric permittivity and electromechanical response in silicone elastomers: molecular grafting of organic dipoles to the macromolecular network, *Adv. Funct. Mater.* 21 (2011) 4589–4594.
- [23] C. Racles, M. Cazacu, B. Fischer, D.M. Opris, Synthesis and characterization of silicones containing cyanopropyl groups and their use in dielectric elastomer actuators, *Smart Mater. Struct.* 22 (2013) 104004.
- [24] F.B. Madsen, A.E. Daugaard, S. Hvilsted, M.Y. Benslimane, A.L. Skov, Dipolar cross-linkers for PDMS networks with enhanced dielectric permittivity and low dielectric loss, *Smart Mater. Struct.* 22 (2013) 104002.
- [25] F.B. Madsen, L. Yu, A.E. Daugaard, S. Hvilsted, A.L. Skov, Silicone elastomers with high dielectric permittivity and high dielectric breakdown strength based on dipolar copolymers, *Polymer* 55 (2014) 6212–6219.
- [26] F.B. Madsen, I. Javakishvili, R.E. Jensen, A.E. Daugaard, S. Hvilsted, A.L. Skov, Synthesis of telechelic vinyl/allyl functional siloxane copolymers with structural control, *Polym. Chem.* 5 (2014) 7054–7061.
- [27] F.B. Madsen, L. Yu, A.E. Daugaard, S. Hvilsted, A.L. Skov, A new soft dielectric silicone elastomer matrix with high mechanical integrity and low losses, *RSC Adv.* 5 (2015) 10254–10259.
- [28] T. Töpfer, F. Weiss, B. Osmani, C. Bippes, V. Leung, B. Müller, Siloxane-based thin films for biomimetic low-voltage dielectric actuators, *Sensors Actuators A Phys.* 233 (2015) 32–41.
- [29] D.A.G. Bruggeman, Berechnung verschiedener physikalischer Konstanten von heterogenen Substanzen. I. Dielektrizitätskonstanten und Leitfähigkeiten der Mischkörper aus isotropen Substanzen, *Ann. Phys.* 416 (1935) 665–679.
- [30] H. Fujiwara, J. Koh, P.I. Rovira, R.W. Collins, Assessment of effective-medium theories in the analysis of nucleation and microscopic surface roughness evolution for semiconductor thin films, *Phys. Rev. B* 61 (2000) 10832–10844.
- [31] P.J. Launer, Infrared Analysis of Organosilicon Compounds: Spectra-Structure Correlations, *Silicone Compounds Register and Review* 1987, p. 100.
- [32] F. Carpi, I. Anderson, S. Bauer, G. Frediani, G. Gallone, M. Gei, et al., Standards for dielectric elastomer transducers, *Smart Mater. Struct.* 24 (2015) 105025.
- [33] D. Gatti, H. Haus, M. Matysek, B. Frohnapfel, C. Tropea, H.F. Schlaak, The dielectric breakdown limit of silicone dielectric elastomer actuators, *Appl. Phys. Lett.* 104 (2014) 052905.
- [34] J. Huang, S. Shian, R.M. Diebold, Z. Suo, D.R. Clarke, The thickness and stretch dependence of the electrical breakdown strength of an acrylic dielectric elastomer, *Appl. Phys. Lett.* 101 (2012) 122905.
- [35] M. Kollasche, H. Stoyanov, H. Ragusch, S. Risse, A. Becker, G. Kofod, Electrical Breakdown in Soft Elastomers: Stiffness Dependence in Un-pre-stretched Elastomers, 2010 10th IEEE Int. Conf. Solid Dielectr 2010, pp. 1–4.
- [36] S. Vudayagiri, S. Zakaria, L. Yu, S.S. Hassouneh, M. Benslimane, A.L. Skov, High breakdown-strength composites from liquid silicone rubbers, *Smart Mater. Struct.* 23 (2014) 105017.
- [37] L. Yu, S. Vudayagiri, S. Zakaria, M.Y. Benslimane, A.L. Skov, Filled liquid silicone rubbers: possibilities and challenges, *Proc. SPIE* 9056 (2014) (90560S-S-9).
- [38] S.J. Clarson, J.A. Semlyen, *Siloxane Polymers*, Prentice Hall, 1993.
- [39] B. Schnyder, T. Lippert, R. Köttz, A. Wokaun, V.-M. Graubner, O. Nuyken, UV-irradiation induced modification of PDMS films investigated by XPS and spectroscopic ellipsometry, *Surf. Sci.* 532–535 (2003) 1067–1071.
- [40] L.M. Landsberger, W.A. Tiller, Refractive index, relaxation times and the viscoelastic model in dry-grown SiO₂ films on Si, *Appl. Phys. Lett.* 51 (1987) 1416–1418.
- [41] S.N. Yahya, C.K. Lin, M.R. Ramli, M. Jaafar, Z. Ahmad, Effect of cross-link density on optoelectronic properties of thermally cured 1,2-epoxy-5-hexene incorporated polysiloxane, *Mater. Des.* 47 (2012) 416–423.
- [42] K.L. Johnson, K. Kendall, A.D. Roberts, Surface energy and the contact of elastic solids, *Proc. R. Soc. Lond. A* 324 (1971) 301–313.
- [43] H.-J. Butt, B. Cappella, M. Kappl, Force measurements with the atomic force microscope: technique, interpretation and applications, *Surf. Sci. Rep.* 59 (2005) 1–152.
- [44] H.-C. Kim, T.P. Russell, Contact of elastic solids with rough surfaces, *J. Polym. Sci. B Polym. Phys.* 39 (2001) 1848–1854.
- [45] P. Sommer-Larsen, A.L. Larsen, Materials for dielectric elastomer actuators, *Proc. SPIE* 5385 (2004) 68–77.

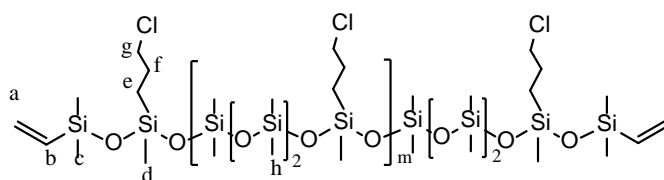
Supporting information:**Molecular beam deposition of high-permittivity polydimethylsiloxane for nanometer-thin elastomer films in dielectric actuators**

Florian M. Weiss,^a Frederikke B. Madsen,^b Tino Töpfer,^a Bekim Osmani,^a Vanessa Leung,^a and Bert Müller^a

^a *Biomaterials Science Center, Department of Biomedical Engineering, University of Basel, Gewerbestrasse 14, 4123 Allschwil Switzerland*

^b *Danish Polymer Centre, Department of Chemical and Biochemical Engineering, Technical University of Denmark, DTU, Søtofts Plads, Bldg. 227, 2800 Kgs. Lyngby, Denmark*

Scheme S1 presents the pre-polymer structure of the synthesized Cl-PDMS (α,ω -vinyl-poly((chloropropyl)methylsiloxane-*co*-dimethylsiloxane)). The small letters (a - h) indicate the carbon atoms detected in ¹³C-NMR.



Scheme S1. Structure of α,ω -vinyl-poly((chloropropyl)methylsiloxane-*co*-dimethylsiloxane) (Cl-PDMS).

The comparison of the FTIR data from the pre-polymers DMS-V05 and Cl-PDMS do not give any information on the structural differences, because the absorption of the Cl-C bond is in the finger print region, where absorption bands overlap. The data was obtained by FTIR measurements in the ATR mode.

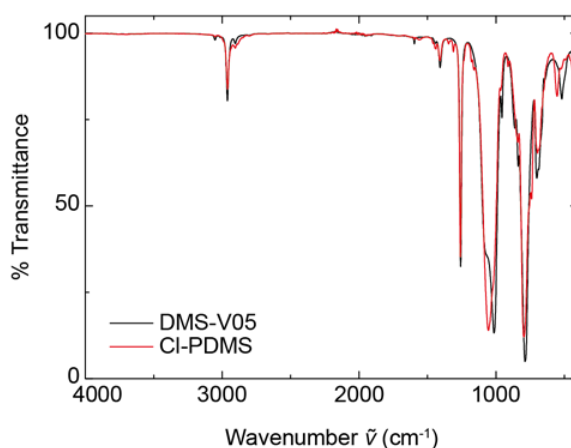


Fig. S1. FTIR-spectra measured in the ATR mode.

Differential scanning calorimetry (DSC) thermograms of DMS-V05 and Cl-PDMS are shown in Figure S2. The black and red lines represent the heating and cooling data of DMS-V05, whereas the blue- and magenta-colored lines show the data of Cl-PDMS. The heating and cooling rates were set to 10 K/min from -150 to 200 °C.

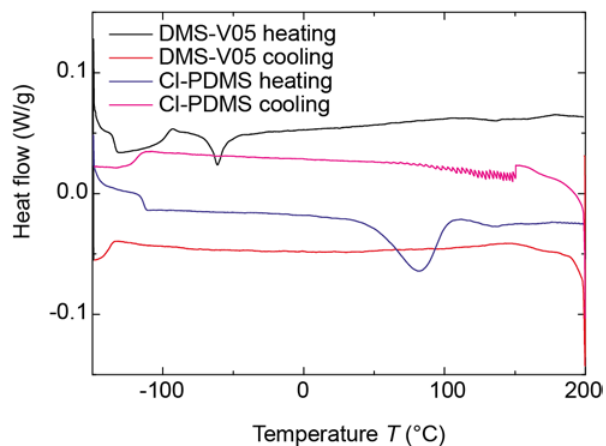


Fig. S1. DSC thermograms of DMS-V05 and Cl-PDMS.

Figure S3 presents the dielectric spectroscopy measurements taken in the liquid state of DMS-V05 and Cl-PDMS. Diagram (a) displays the dielectric constant data obtained for the pre-polymers, whereas diagram (b) represents the measured tangent loss from the two polymers.

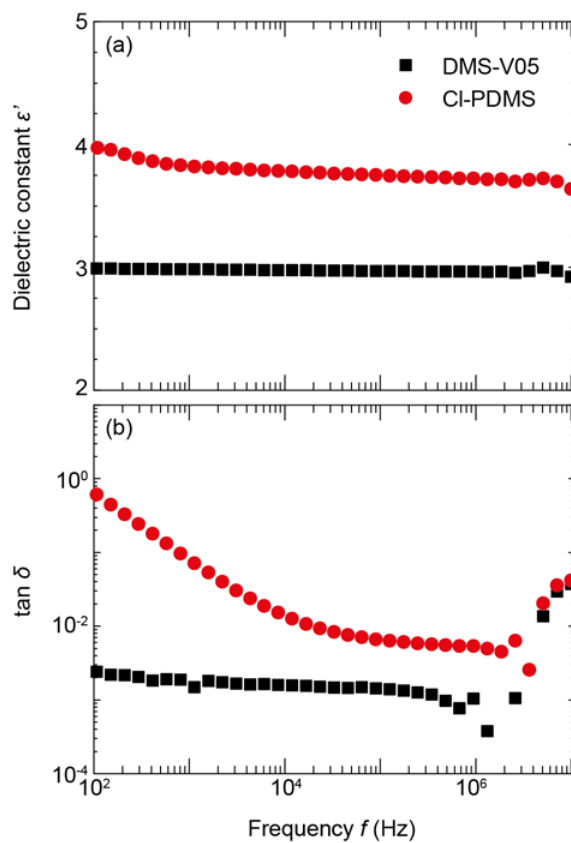


Fig. S3. Dielectric constant (a) and tangent loss (b) spectra of liquid DMS-V05 and Cl-PDMS.

3 Conclusions and Outlook

RF magnetron sputtered nanometer-thin films of gold on 5 micrometer thick polydimethylsiloxane exhibit superior mechanical properties compared to thermally evaporated ones. This is due to the obtained microstructures under the chosen parameters. For future applications in low-voltage DEA technology the significant difference in actuation of 39 % has a major impact on the stiffening effect for multi-stack actuators and has to be considered for fabrication.

Exploring ac electro-spray deposition and organic molecular beam deposition for manufacturing submicrometer thin elastomeric films, it was found that both methods lead to the targeted aim when deposited on Si wafers. Both methods are capable of depositing PDMS pre-polymer molecules which could be subsequently cured applying UV radiation. The resulting films show promising properties for low-voltage dielectric elastomer actuators. There are distinct features of the two methods which have to be considered in future, especially, for production of multi-stack DEAs with thousands of layers or industrial up-scaling.

Alternating current electro-spray deposition (ACESD) has been proved to be a suitable alternative technique to organic molecular beam deposition and spin coating. By depositing charged micrometer droplets of a 5 vol. % vinyl terminated PDMS solution and subsequent UV curing it is possible to manufacture elastic thin films in the scale of 100 nm or greater with higher deposition rates than OMBD. The root-mean-square surface roughness of the cured PDMS films obtained for both deposition methods is in the same subnanometer to nanometer range and is smaller than the one obtained by spin coating as determined by atomic force microscopy. Further advantages of the electro-spray deposition are the inexpensive set up and the possibility to use higher molecular weight pre-polymers compared to OMBD.

At this stage of investigation it has been observed that the deposits may vary locally due to the multi-cone jet mode occurring with the constant parameters in these experiments. It will be crucial in future to find optimized parameters to form a stable single-cone jet spray. Once a stable single cone-jet spray has been established the resulting homogeneity of the films should be much higher over a larger area. Therefore, the frequency and the amplitude of the electric field as well as the flow rate have to be well coordinated for a given solution. Once this draw-back is mastered ACESD has high potential for industrial-scale production, since multiple nozzle arrangements could be employed, for example to manufacture large-area, multi-stack DEAs.

The optimized synthesis of the poly((chloropropyl)methylsiloxane-co-dimethylsiloxane) copolymer yielded a pre-polymer in the range of 1,000 *g/mol*. This is in the same range as the measured molecular weight of the evaporated fraction of the commercially available standard, DMS-V05. Either of them is vinyl terminated and mainly consists of dimethylsiloxane units. The newly synthesized pre-polymer contains three to four chloropropyl side groups per molecule besides the methyl groups, responsible for an increase of the effective dipolar moment of the molecule. As a

consequence of this polarity increase an enhanced dielectric permittivity of 33 % as well as an enlargement of the break down strength of 26 % could be reached. Additionally, a diminished Young's modulus of a factor of 2.2 was obtained for the cured films. All together this results in a figure of merit of 4.6 which is normalized with the standard. Furthermore, the cured film exhibits a surface roughness in the subnanometer scale, qualifying this enhanced material for future low-voltage DEA application prepared by OMBD.

Despite having low deposition rates, OMBD performs a much better areal homogeneity and can deposit the evaporated material as a confluent layer already in the scale of only a few nanometers. Both of these features currently cannot be obtained with ACESD. The down sides of OMBD are the limitation of usable pre-polymers due to thermal stability issues combined with the expensive equipment making this method unattractive for industrial upscale purposes.

For both methods it is of great importance to further investigate the UV irradiation induced curing. The experience showed that this process is rather time consuming and should be optimized. Irradiation from the top evokes skin formation which seems to absorb the radiation and therefore slows down the curing of the liquid phase beneath the skin. Hence, in future more selective and controllable curing paths should be chosen. This could be realized via reactive groups which absorb at specific longer wavelengths in order to use radiation sources which do not emit high energy wavelengths. Additionally, the functional groups should also be present in the side chains so a defined network may be formed. Another approach towards more controlled and more effective curing would be the use of photoinitiators. They are commercially available and have a broad range of absorption bands to initiate curing reactions.

The work done in this thesis was an important step towards nanometer-thin film preparation for the fabrication of low-voltage multi-stack actuators for the application in sensitive environments.

Bibliography

- [1] Khater, U. M., Haddad, G., and Ghoniem, G. M., [*Pelvic Floor Dysfunction: A Multidisciplinary Approach*], ch. Epidemiology of Non-Neurogenic Urinary Dysfunction, 9–13, Springer London, London (2009).
- [2] Chaikin, D. C., Rosenthal, J., and Blaivas, J. G., “Pubovaginal fascial sling for all types of stress urinary incontinence: long-term analysis,” *The Journal of Urology* **160**(4), 1312–1316 (1998).
- [3] Iosif, C. S., “Sling operation for urinary incontinence,” *Acta Obstetrica et Gynecologica Scandinavica* **64**(2), 187–190 (1985).
- [4] Mourtzinou, A., Smith, J. J., and Barrett, D. M., “Treatments for male urinary incontinence: A review,” *AUA Update Series* **24**(15), 122–131 (2005).
- [5] Madsen, F. B., Daugaard, A. E., Hvilsted, S., and Skov, A. L., “The Current State of Silicone-Based Dielectric Elastomer Transducers,” *Macromolecular Rapid Communications* (2016).
- [6] Pelrine, R., Kornbluh, R., Pei, Q., and Joseph, J., “High-Speed Electrically Actuated Elastomers with Strain Greater Than 100%,” *Science* **287**(5454), 836–839 (2000).
- [7] Rosset, S. and Shea, H. R., “Flexible and stretchable electrodes for dielectric elastomer actuators,” *Applied Physics A* **110**(2), 281–307 (2012).
- [8] Hwang, T., Kwon, H.-Y., Oh, J.-S., Hong, J.-P., Hong, S.-C., Lee, Y., Ryeol Choi, H., Jin Kim, K., Hossain Bhuiya, M., and Nam, J.-D., “Transparent actuator made with few layer graphene electrode and dielectric elastomer, for variable focus lens,” *Applied Physics Letters* **103**(2) (2013).
- [9] Watanabe, M., Shirai, H., and Hirai, T., “Wrinkled polypyrrole electrode for electroactive polymer actuators,” *Journal of Applied Physics* **92**(8) (2002).
- [10] Habrard, F., Patscheider, J., and Kovacs, G., “Super-compliant metallic electrodes for electroactive polymer actuators,” (2012).
- [11] Bowden, N., Brittain, S., Evans, A. G., Hutchinson, J. W., and Whitesides, G. M., “Spontaneous formation of ordered structures in thin films of metals supported on an elastomeric polymer,” *Nature* **393**(6681), 146–149 (1998).
- [12] Osmani, B., Töpfer, T., Deschenaux, C., Nohava, J., Weiss, F. M., Leung, V., and Müller, B., “Micro- and nanostructured electro-active polymer actuators as smart muscles for incontinence treatment,” *AIP Conference Proceedings* **1646**(1) (2015).
- [13] Chopra, K. L., “Growth of Sputtered vs Evaporated Metal Films,” *Journal of Applied Physics* **37**(9) (1966).

- [14] Jaworek, A. and Sobczyk, A. T., “Electrospraying route to nanotechnology: An overview,” *Journal of Electrostatics* **66**(3–4), 197–219 (2008).
- [15] Morota, K., Matsumoto, H., Mizukoshi, T., Konosu, Y., Minagawa, M., Tanioka, A., Yamagata, Y., and Inoue, K., “Poly(ethylene oxide) thin films produced by electrospray deposition: morphology control and additive effects of alcohols on nanostructure,” *Journal of Colloid and Interface Science* **279**(2), 484–492 (2004).
- [16] Rietveld, I. B., Kobayashi, K., Yamada, H., and Matsushige, K., “Process parameters for fast production of ultra-thin polymer film with electrospray deposition under ambient conditions,” *Journal of Colloid and Interface Science* **339**(2), 481–488 (2009).
- [17] Xie, J., Jiang, J., Davoodi, P., Srinivasan, M. P., and Wang, C.-H., “Electrohydrodynamic atomization: A two-decade effort to produce and process micro-/nanoparticulate materials,” *Chemical Engineering Science* **125**, 32–57 (2015).
- [18] Rietveld, I. B., Kobayashi, K., Yamada, H., and Matsushige, K., “Electrospray Deposition, Model, and Experiment: Toward General Control of Film Morphology,” *The Journal of Physical Chemistry B* **110**(46), 23351–23364 (2006).
- [19] Cho, A.-Y., “Morphology of Epitaxial Growth of GaAs by a Molecular Beam Method: The Observation of Surface Structures,” *Journal of Applied Physics* **41**, 2780–2786 (jun 1970).
- [20] O’Connor, J., Sexton, B., and Smart, R., eds., [*Surface Analysis Methods in Materials Science*], Springer, Berlin Heidelberg (2013).
- [21] Forrest, S. R., “Ultrathin organic films grown by organic molecular beam deposition and related techniques,” *Chemical Reviews* **97**(6), 1793–1896 (1997). PMID: 11848893.
- [22] Johns, I. B., McElhill, E. A., and Smith, J. O., “Thermal Stability of Organic Compounds,” *IEEC Product Research and Development* **1**(1), 2–6 (1962).
- [23] Töpfer, T., Weiss, F., Osmani, B., Bippes, C., Leung, V., and Müller, B., “Siloxane-based thin films for biomimetic low-voltage dielectric actuators,” *Sensors and Actuators A: Physical* **233**, 32–41 (2015).

Acknowledgments

Now, being almost at the end of a journey which has lasted about 4.5 years I would like to acknowledge many special persons I had the opportunity to meet, connect, work, discuss and share experiences.

For making all this possible I would like to express my gratitude first to Prof. Bert Müller. Due to his supervision I could grow in an interdisciplinary environment which has been very nourishing for my views and approaches to scientific problems. With letting me start up with this new project on artificial sphincter muscles he gave me the freedom to explore many different methods at various institutions. This, I am sure, will provide a solid base for my future. Also I am very grateful to my second supervisor, Dr. Gabor Kovacs. He also contributed a lot to my scientific growth by giving me the opportunity with a collaboration work at Empa Dübendorf where I could build a set up for electro-spray deposition of silicone films, new to the EAP community.

Especially thankful I am to Prof. Anne Ladegaard Skov for being co-referee and taking the time to evaluate my thesis and to come all the way down to Basel from Copenhagen for my defense. Furthermore, for always supporting me whenever I had questions about elastomers and for having me as a guest at DTU. Speaking of DTU I would like to point out the collaboration with Dr. Frederikke Bahrt Madsen which is/has been very fruitful for me and let me dive back into the world of chemistry. I am very happy and grateful for this experience.

At this point I would also like to say thank you to Prof. Ernst Meyer for taking the time to supervise my exam. Also for giving me access to his laboratory and use his equipment for first thermal fractioning experiments of liquid polymers under vacuum conditions and lending a small UHV chamber to us to obtain a proof of concept.

For having me as a guest PhD student for a couple of month at the Forschungszentrum Jülich I would like to thank Prof. Detlev Grützmacher, Dr. Gregor Mussler, Martin Lanius and Dr. Stefan Trelenkamp. I am much obliged to have had the excursion to learn about deposition and processing techniques of semiconducting materials as well as working in the new clean room.

Further I would like to thank Prof. Cathrine Housecroft and Prof. Edwin Constable for letting me work in their labs and using their equipment and of course also their team which always warmly welcomed me in the labs. To point out Dr. Andreas Bünzli, Annika Büttner, Dr. Nik Hostetter, Dr. Ewald Schönhofer and Dr. Sebastian Fürer for their wonderful support whenever I needed help with anything, I am truly thankful.

Prof. Jens Gobrecht and Konrad Vogelsang I would like to thank for supporting me with the preparation of first actuators at the laboratory for micro- and nanotechnology (LMN) at PSI.

Also I am grateful to Prof. Jürg Hulliger, Dr. Matthias Burgener, Dr. Mathias Rech, Dr. Ravish Sankoli, Dr. Mithra Manesh and Bernhard Trusch for support, letting me use their labs and lending me equipment.

Not to forget the valuable support from Sascha Martin for the construction of the test UHV chamber and letting me use his workshop at the physics department of the university Basel as well as the support from Volker Brunner from the workshop at the university hospital Basel and Andreas Tonin from the electric workshop at the physics department in Basel. Thank you guys!

For all the discussions and support about the Electro-spray Deposition I would like to thank Prof. Ivo Rietveld (Universite Paris Descartes) and Dr. Nicolas Lavielle (Empa St. Gallen and University of Strasbourg).

I appreciate the support from Erich Heiniger for drawing the plans and Erwin Pieper for the construction of the ESD System built at Empa Dübendorf.

Further I would like to thank Fredi Schmidli for the excursion into the metallurgy of dental implants and their corrosivity as well as the interesting discussions.

I am also grateful to Prof. Michael de Wild for letting me use his laboratories and equipment as well as Theo Bühler for lending us the sputter deposition system. Also thanks to Dr. Markus Dürrenberg, Marcel Düggelein, Daniel Mathys and Eva Bieler from the Zentrum für Mikroskopie (ZMB) for all the discussions and support concerning electron microscopy analysis.

I would like to thank Dr. Dalin Wu, Dr. Axel Hochstetter and Samuel Lörcher for helping with polymer analysis and Dr. Anatoly Johnson for helping me with the laser induced curing experiments.

Of course I would like to thank all colleagues at the Biomaterials Science Center for the great time and support, especially Tino Töpfer and Bekim Osmani as well as Hans Deyhle for all their input, helpful discussions and data analysis.

Last but not least I would like to thank all my friends and family who were an amazing support throughout all these years.

Curriculum Vitae

Curriculum Vitae**Florian Weiss****Personal Data**

Name Last Name	Florian Micha Weiss
Address	Frobenstrasse 75 4053 Basel
Date of Birth	10 April 1983
Nationality	Swiss
Mobile	+41 79 734 12 05
Email	florian.weiss@bluewin.ch
Languages	Native: German Fluent: English Basics: French

**Education**

02/2016 – present	Biomaterials Science Center, University of Basel, CH <i>PostDoc position, Prof. Bert Müller</i> Electrochemical impedance spectroscopy for corrosion characterization of metallic dental implants
09/2011 – 02/2016	Biomaterials Science Center, University of Basel, CH <i>PhD in Nano-Science, Prof. Bert Müller</i> Thesis: "Fabrication and Characterization of Nanometer Thin Films for Low-Voltage DEAs" Setting up an ultra-high vacuum system to deposit few 100 nanometer PDMS layers used in electroactive polymer actuators for medical implants to treat incontinence Empa - Swiss Federal Laboratories for Materials Science & Technology, CH <i>PhD in Nano-Science, Dr. Gabor Kovacs</i> Setting up an electrospray deposition system to deposit up to 1 micron of PDMS layers for electroactive polymer actuators Research Center Jülich, DE <i>PhD in Nano-Science, Prof. Detlev Grützmacher</i> Manufacturing SiGe nano-springs as an alternative technology to electroactive polymers for artificial muscles
08/2009 – 03/2011	Department of Chemistry and Biochemistry, University of Bern, CH <i>Master Module Type B: Material Science – Physical Chemistry</i> Thesis in the research group of Prof. Jürg Hulliger "Pyroelectric Energy Harvesting by Ceramic Composite Materials"
08/2004 – 06/2009	Department of Chemistry and Biochemistry, University of Bern, CH <i>Bachelor in Chemistry and Molecular science</i> Bachelor Thesis in the research group of Prof. Jürg Hulliger "Modification of the YBCO System"
04/1998 – 06/2003	Ecole d'Humanité, Hasliberg, CH <i>Certificate: GCSE (A-/O-Levels)</i>

Curriculum Vitae**Florian Weiss****Work Experience**

04/2011 – 09/2011	Research Assistant by PD. Dr. P. Broekmann, University of Bern, CH Investigation of Potential Transients in Copper Deposition and the Influence of Additives for the Damascene Process (in collaboration with BASF)
11/2010 – 12/2010	Research Assistant by Prof. Dr. J. Hulliger, University of Bern, CH Literature research
06 - 10/2010	Logistics, Planzer Transport AG
07 – 08/2009	Research internship by Prof. Dr. A. Weidenkaff, EMPA Dübendorf, CH Synthesis and Characterization of Thermoelectric Oxides
01 - 03/2009	Research Assistant by Prof. Dr. J. Hulliger, University of Bern, CH Literature research
07 – 08/2008	Research internship by Dr. R. Eichler, Paul Scherrer Institut (PSI), Villigen, CH Establishing Targets for Super Heavy Elements by Amalgamation and Electrochemical means
07/2007	Research internship by Prof. Dr. J. Hulliger, University of Bern, CH Synthesis and separation of Superconductive particles gained by a combinatorial approach

Laboratory Experience and Skills

Laboratory	Good knowledge in (a) functional ceramic synthesis, (b) electrochemical-, physical vapor and electrospray thin film deposition of metals, semi-conductors and polymers, (c) ultra-high vacuum handling, (d) spin-coating, (e) clean room experience (ISO 2) with semi-conductor materials processing (Lithography, wet- and dry etch, metal deposition), (f) various analysis methods: Atomic force microscopy, Dielectric spectroscopy, Differential scanning calorimetry, Energy-dispersive X-ray spectroscopy, Electrochemical impedance spectroscopy, Gel permeation chromatography/ Size exclusion chromatography, Infrared spectroscopy (ATR, reflection mode, transmittance), Profilometry, Scanning electron microscopy, Spectroscopic Ellipsometry, Thermogravimetric analysis, Ultraviolet/Visible light spectroscopy, X-ray diffraction, 3D Lasermicroscopy
Software	Microsoft Office, OriginPro, EndNote, Adobe Illustrator, Adobe Photoshop, Solidworks (CAD)

Oral- and Poster Presentations

06/09 - 10/2016	Poster Presentation at the 22th Swiss Conference on Biomaterials and Regenerative Medicine <i>Zürich, Schultess Klinik, June 9-11, 2016</i>
06/09 - 10/2015	Poster Presentation at the 21th Swiss Conference on Biomaterials and Regenerative Medicine <i>Lausanne, EPFL, June 9-11, 2015</i>
03/11/2014	Oral Presentation at Electroactive Polymer Actuators and Devices (EAPAD) XVI, Smart Structures/NDE <i>San Diego, USA, March 9-13, 2014</i>
11/13/2012	Poster Presentation at the PhD Student Symposium <i>Dübendorf, EMPA, November 13, 2012</i>

Curriculum Vitae**Florian Weiss**

Memberships

2010 – Present	Member of Swiss Association for Materials Science and Technology (SVMT)
2011 – Present	Member of Swiss Chemical Society (SCS)
2014 – Present	Member of SPIE
2015 – Present	Member of Swiss Society of Biomaterials + Regenerative Medicine

Leisure time activities

Reading, cooking, vita-parcour, traveling

Curriculum Vitae**Florian Weiss**

Publication List

1. Leung, V.; Fattorini, E.; Karapetkova, M.; Osmani, B.; Töpfer, T.; Weiss, F.; Müller, B. Biomimetic Artificial Sphincter Muscles: Status and Challenges. *Proc. SPIE* **2016**, 9797, M1-M7.
2. Osmani, B.; Deyhle, H.; Weiss, F. M.; Töpfer, T.; Karapetkova, M.; Leung, V.; Müller, B. Morphology and Conductivity of Au Electrodes on Polydimethylsiloxane Using (3-Mercaptopropyl)Trimethoxysilane (MPTMS) as an Adhesion Promoter. *Proc. SPIE* **2016**, 9798, 1-11.
3. Töpfer, T.; Lörcher, S.; Weiss, F.; Müller, B. Tailoring the Mass Distribution and Functional Group Density of Dimethylsiloxane-Based Films by Thermal Evaporation. *APL Mater.* **2016**, 4 (5), 056101.
4. Töpfer, T.; Wohlfender, F.; Weiss, F.; Osmani, B.; Müller, B. Characterization of Ultraviolet Light Cured Polydimethylsiloxane Films for Low-Voltage, Dielectric Elastomer Actuators. *Proc. SPIE* **2016**, 9798, 211-2110.
5. Weiss, F. M.; Kovacs, G.; Töpfer, T.; Osmani, B.; Leung, V. Y. F.; Müller, B. Electro-Spraying and Ultra-Violet Light Curing of Polydimethylsiloxane to Fabricate Thin Films for Low-Voltage Dielectric Elastomer Actuators. *Proc. SPIE* **2016**, 9798, C1-C9.
6. Weiss, F. M.; Madsen, F. B.; Töpfer, T.; Osmani, B.; Leung, V.; Müller, B. Molecular Beam Deposition of High-Permittivity Polydimethylsiloxane for Nanometer-Thin Elastomer Films in Dielectric Actuators. *Mater. Des.* **2016**, 105, 106-113.
7. Weiss, F. M.; Töpfer, T.; Osmani, B.; Deyhle, H.; Kovacs, G.; Müller, B. Thin Film Formation and Morphology of Electro sprayed Polydimethylsiloxane. *Langmuir* **2016**, 32, 3276-3283.
8. Weiss, F. M.; Töpfer, T.; Osmani, B.; Peters, S.; Kovacs, G.; Müller, B. Electro spraying Nanometer-Thin Elastomer Films for Low-Voltage Dielectric Actuators. *Adv. Electron. Mater.* **2016**, 1-8.
9. Osmani, B.; Töpfer, T.; Weiss, F. M.; Wohlfender, F.; Leung, V.; Bippes, C.; Müller, B. Nanomechanical Characterization of Polydimethylsiloxane Films. *Eur. Cells Mater.* **2015**, 30, 56.
10. Töpfer, T.; Osmani, B.; Weiss, F. M.; Müller, B. Viscoelastic Properties of Polydimethylsiloxane Studied by Cantilever Bending. *Eur. Cells Mater.* **2015**, 30, 68.
11. Töpfer, T.; Osmani, B.; Weiss, F. M.; Winterhalter, C.; Wohlfender, F.; Leung, V. Y. F.; Müller, B. Strain-Dependent Characterization of Electrode and Polymer Network of Electrically Activated Polymer Actuators. *Proc. SPIE* **2015**, 9430, 0B1-0B11.
12. Töpfer, T.; Weiss, F.; Osmani, B.; Bippes, C.; Leung, V.; Müller, B. Siloxane-Based Thin Films for Biomimetic Low-Voltage Dielectric Actuators. *Sensors Actuat. A-Phys* **2015**, 233, 32-41.
13. Weiss, F. M.; Schmidli, F.; Jungo, M.; Müller, B. Incompatibility of Dental Alloys: Evaluation by Ec-Pen Corrosion Measurements *Eur. Cells Mater.* **2015**, 30, 70.
14. Osmani, B.; Töpfer, T.; Deschenaux, C.; Nohava, J.; Weiss, F. M.; Leung, V.; Müller, B. Micro- and Nanostructured Electro-Active Polymer Actuators as Smart Muscles for Incontinence Treatment. *INTERNATIONAL CONFERENCES AND EXHIBITION ON NANOTECHNOLOGIES AND ORGANIC ELECTRONICS (NANOTEXNOLOGY 2014): Proceedings of NN14 and ISFOE14* **2014**, 1646, 91-100.
15. Weiss, F. M.; Töpfer, T.; Osmani, B.; Winterhalter, C.; Müller, B. Impact of Electrode Preparation on the Bending of Asymmetric Planar Electro-Active Polymer Microstructures. *Proc. SPIE* **2014**, 905607,1-9.
16. Hai, N. T. M.; Furrer, J.; Stricker, F.; Huynh, T. M. T.; Gjuroski, I.; Luedi, N.; Brunner, T.; Weiss, F.; Fluegel, A.; Arnold, M. Polyvinylpyrrolidones (Pvps): Switchable Leveler Additives for Damascene Applications. *J. Electrochem. Soc.* **2013**, 160, D3116-D3125.
17. Huynh, T. M. T.; Weiss, F.; Hai, N. T. M.; Reckien, W.; Bredow, T.; Fluegel, A.; Arnold, M.; Mayer, D.; Keller, H.; Broekmann, P. On the Role of Halides and Thiols in Additive-Assisted Copper Electroplating. *Electrochim. Acta* **2013**, 89, 537-548.
18. Weiss, F. M.; Zhao, X.; Thalmann, P.; Deyhle, H.; Urwyler, P.; Kovacs, G.; Müller, B. Measuring the Bending of Asymmetric Planar EAP Structures. *Proc. SPIE* **2013**, 86871, X1-X6.
19. Weiss, F. M.; Deyhle, H.; Kovacs, G.; Müller, B. Designing Micro- and Nanostructures for Artificial Urinary Sphincters. *Proc. SPIE* **2012**, 83400, A1-A10.

Erklärung

Ich erkläre, dass ich die Dissertation „Fabrication and Characterization of Nanometer Thin Films for Low-Voltage DEAs“ nur mit der darin angegebenen Hilfe verfasst und bei keiner anderen Universität und keiner anderen Fakultät der Universität eingereicht habe.

Basel, den 09.02.2012

Florian M. Weiss